Nalcor Energy

Landsvirkjun Power in collaboration with

EFLA Engineering and

S.M. Fikke Meteorological Consultant – Overhead Lines

Evaluation of in-cloud icing in the Long Range Mountain Ridge

Reykjavík, December 2010

Landsvirkjun POWER

EFLA CONSULTING ENGINEERS

Table of content

1 Introduction

This work was performed by Landsvirkjun Power (LVP) in cooperation with Egil Thorsteins (EFLA Engineering), Svein M. Fikke (Meteorological Consultant – Overhead Lines), Árni Jón Elíasson and Bjørn Egil Kringlebotn Nygaard.

The work involves:

- Evaluation of icing measurements at the test spans 2009-1 and the test span 2009-2 during the period of November 2009 to June 2010
- Modelling historical icing events in the most severe locations in the Long Range Mountains (LRM) using nearby weather observation
- Modeling and simulating icing for selected weather conditions in the area of LRM, using a state-of-the-art meso-scale numerical weather prediction system.
- Comparing the modeled icing to known icing observation in the area
- Evaluating the existing design load for in-cloud icing in the area
- Make first evaluation of the maximum in-cloud ice load in the LRM, i.e. 50 year return period in the most exposed location.
- Classifying the line route in the LRM according to risk of icing
- Make first analysis on the risk of in-cloud icing in the Labrador area
- Propose next steps

2 Icing measurements winter 2009-2010

2.1 Description of test sites

Nalcor Energy installed two test spans for measuring ice load in the area of the Long Range Mountain in the autumn 2009. The test spans are called 2009-1 (Nalcor 1) and 2009-2 (Nalcor 2).

The test span 2009-1 is exposed to moisture from the sea in south westerly direction, and is furthermore perpendicular to the bottom of valley. Therefore, high in-cloud ice load can be frequently expected. In-cloud icing can also be expected from north-easterly and easterly directions. The direction of test span 2009-1 is parallel to the expected line route in this area. This site is believed to be the most exposed part of the Long Range Mountain crossing with respect to in-cloud icing.

The test span 2009-2 is more inland than test span 2009-1 and is not as exposed to in-cloud icing, although in-cloud icing can be expected both from westerly and easterly wind directions. The direction of test span 2009-2 is parallel to expected line route in this area. Figure 2 shows the measuring equipments used at the test sites.

Table 1 gives information on the location of the test spans. Figure 1 shows the test span 2009-1 and Figure 2 shows the measuring equipments used at the test sites.

Table 1. *Test span information.*

Test span	Height above sea level	Direction of span	Lat.	Long.
2009-1	600 m	330°N	50°06.051´N	57°25.444´W
2009-2	530 m	350°N	50°03.786´N	57°23.839´W

Figure 1. *Test span 2009-1.*

Figure 2. *Measuring equipment.*

Figure 3 shows the location of test span 2009-1 and test span 2009-2 with respect to the proposed line route. The location of the weather observation station at Daniel's Harbour is given by a green circle. Cross–sections for possible icing directions are given in Figure 4 for test span 2009-1 and Figure 5 for test span 2009-2. The locations of the cross-sections are shown in Figure 3, blue lines for test span 2009-1 and red lines for test span 2009-2. A solid line is used for sections perpendicular to the span and broken lines for 15° and 30° deviations from the perpendicular.

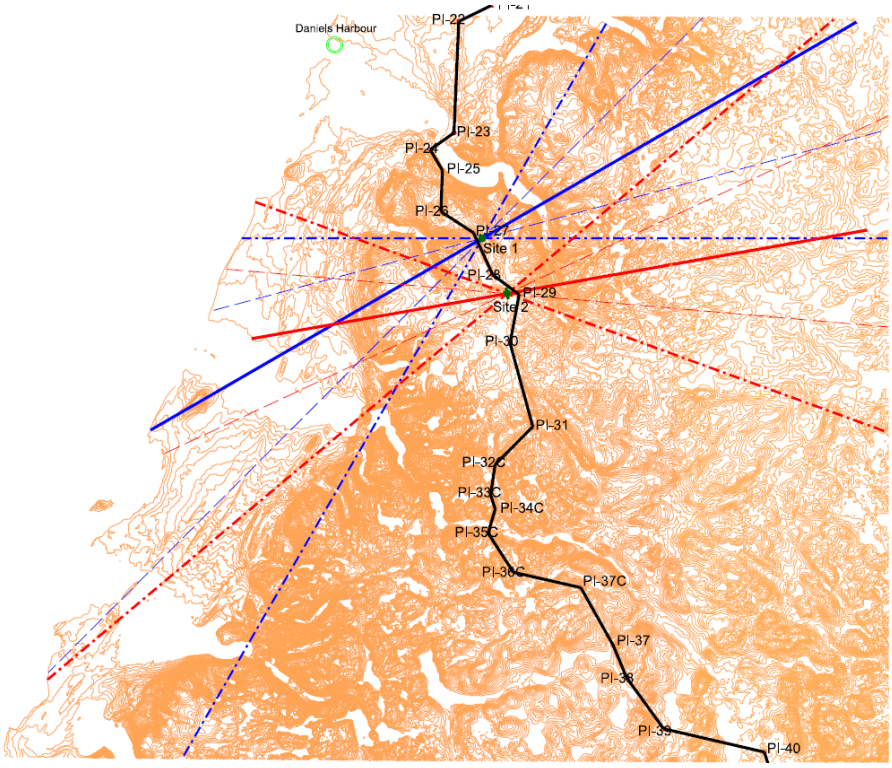

Figure 3. *Location of test sites and directions where cross-section profiles are given.*

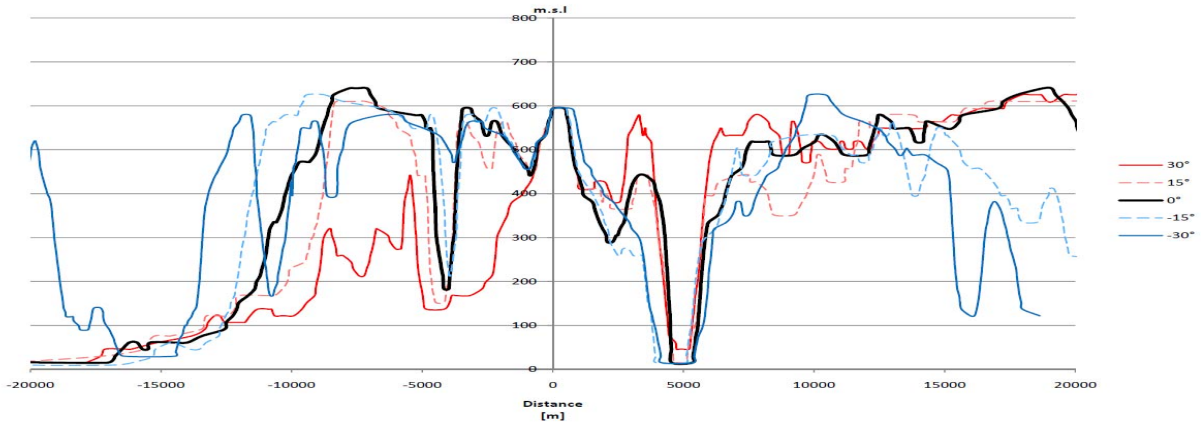

Figure 4. *Cross-section profile from test span 2009-1. Lines are given for the orthogonal direction from span and 15° and 30° angles from it.*

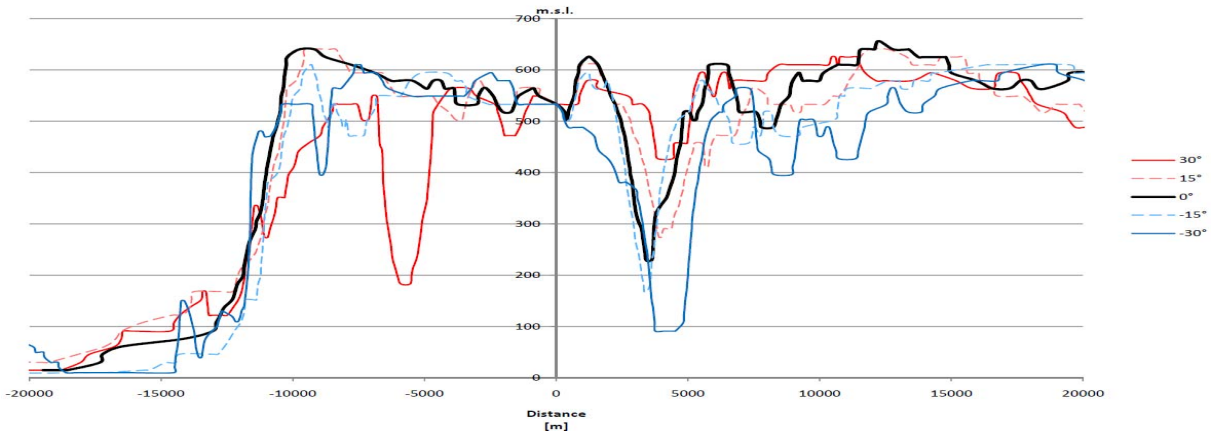

Figure 5. *Cross-section profile from test span 2009-2. Lines are given for the orthogonal direction from the span and 15° and 30° angles from it.*

2.2 Measurements

The test spans are 80 m long and the conductors are strung on wooden poles 10 m above ground. End tension measurements are made with load cells connected with data loggers. The tension recorders measure tension at 0.5-1 Hz and store maximum, minimum and mean values at 10 minute intervals. Mechanical dynamometers are also installed to give maximum value in case of failure of the electronic force recorders. Ambient temperature measurements are obtained every 10 minutes at the same height above ground as the conductors. The temperature can be expected to be slightly biased in icing situations, although experience does not indicate a big influence. Measurements of the conductor's end tension are then converted into an external load per unit length, using the geometry of the test span and mechanical properties of the cable and guys. The underlying assumption is that loading is equally distributed along the span and that guys have same amount of icing as the span. The measurement's horizontal and vertical components cannot accurately be distinguished since wind-speed measurements are not made at the site but are acquired from a nearby weather station. The analyzed load is therefore the conductor's total load, consisting of both vertical and horizontal components. The load can be originated from icing, wind and dynamical conductor motion (vibration, galloping, ice shedding etc.). The part of the loading that is believed to be ice load is evaluated using available data and experience.

Installed conductor tension is somewhat less than is used in similar spans in Iceland. This may lead to more fluctuation in the measured conductor tension.

All the measurement devices are calibrated for GMT +0, therefore all of the data is based on GMT+0.

2.3 Overview of observed icing in test spans 2009-1 and 2009-2

Figure 7 shows the evaluated icing and measured temperature at test span 2009-1 and test span 2009-2 over the measurement period. The two icing sets correlate well together with respect to accumulation time and time of ice shedding but size of the loading is different. Icing events at test span 2009-1 are larger and more frequent than at test span 2009-2. The temperature is very similar at both locations but test span 2009-1 usually has slightly lower temperatures.

Recorded temperatures at test span 2009-1 are in some cases unreliable when the temperature is below -15°C. The temperature recorder at test span 2009-2 works better in such low temperatures.

Test sites were visited on January 19, 2010. Figure 6 shows a photo of test span 2009-1. The highest ice loading was measured a few days before but the ice had fallen off the conductor but remained on the pole and the instruments.

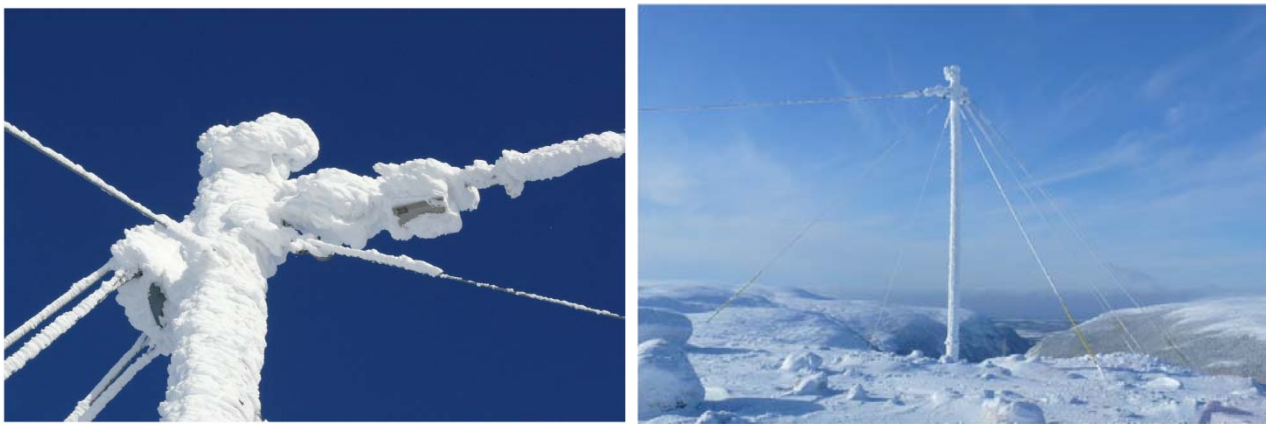

Figure 6. *Icing observed at test site 2009-1 during the visit on January 19, 2010. There was a small amount of icing observed on the conductor, but rime observed on the poles and instruments.*

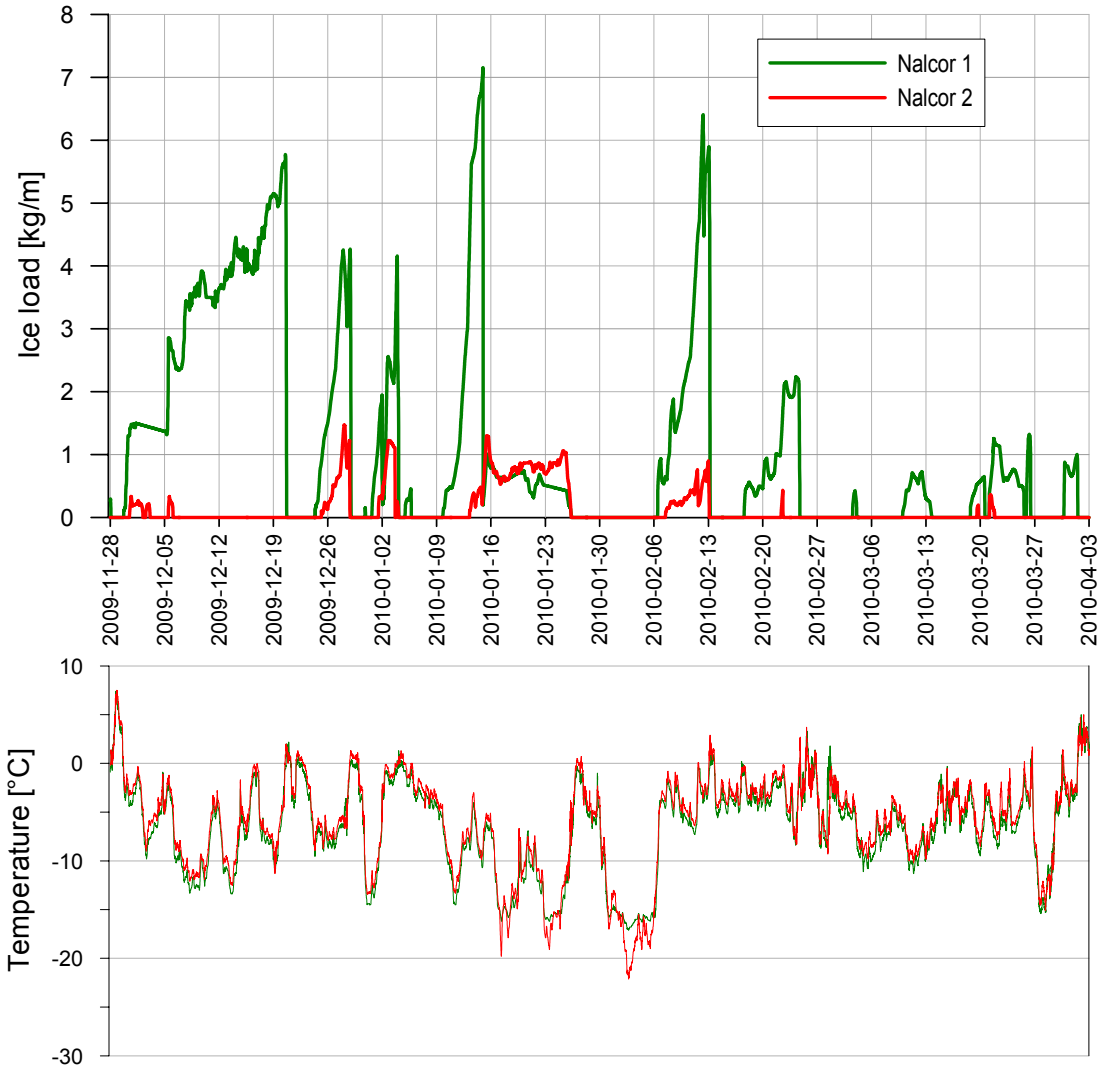

Figure 7. *Evaluated icing and measured temperature in test span 2009-1 (green line) and test span 2009-2 (red line).*

2.4 Measured icing in test span 2009-1

2.4.1 Icing events

During the measurement period for test span 2009-1 (2009-11-23 to 2010-06-14), nine (9) major icing events were recorded. The maximum tension recorded during the period represents an equivalent loading of 112.7 N/m. When the wind and dynamic load are subtracted from the overall load, it is evaluated that the maximum ice load at that time was 4.1 kg/m. The highest ice load occurred in event 4 and was evaluated as 7.2 kg/m.

For the most part of measurement period, the temperature was below zero (for 73.6% of the time). The temperature was between 0 to 2°C, 11.6% of the time. No major gallop events occurred.

The base stringing (no ice or wind) of the test span is estimated as 387 kg, when temperature is -1.1°C.

Figure 8 shows the unit loading and the temperature for the whole measuring period.

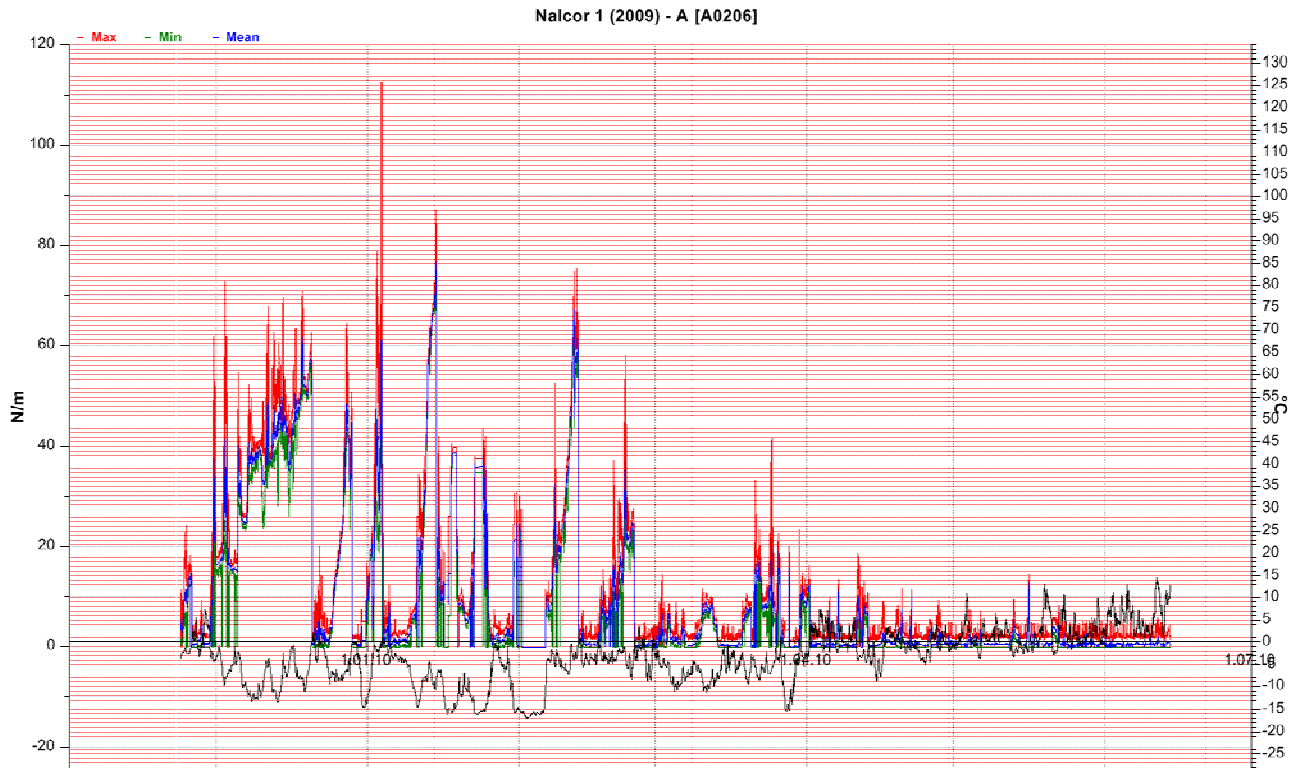

Figure 8. *All measurements at test span 2009-1 in the period of* 2009-11-23 to 2010-06-14*. The red curve is the maximum load; blue is the average load and green is the minimum load, all measured within a 10 minute* interval. The black curve is the temperature.

Most of the dataset for test span 2009-1 is very reliable but a few values were evaluated to be corrupt and editing was needed. The corrupt data seem to occur in short periods when the temperature is below -15°C and it is most likely related to too low voltage in the data logger, for so low temperature. The voltage is adjustable and it is recommended to be adjusted in future measurements. In-cloud icing is very unlikely to accumulate when temperature is below -15°C so it is believed that no major ice load events are missing.

Identified icing events at test site 2009-1 with maximum ice load higher than 1.0 kg/m are given in Table 2.

Table 2. *Icing events measured in test span 2009-1.*

Icing event	From	To	Temperature range			Maximum value of measuring curves			Evaluation of max. ice load
			Max. value	Mean. value	Min. value	Max. curve	Mean. curve	Min. curve	
			[°C]	[°C]	[°C]	[Kg/m]	[Kg/m]	[Kg/m]	[Kg/m]
1	2009-11-30	2009-12-20	1.7	-7.2	-13.4	7.4	6.3	5.8	5.8
2	2009-12-24	2009-12-29	0.2	-6.7	-9.0	6.6	5.0	4.5	4.3
3	2009-12-31	2010-01-04	1.3	-5.2	-13.8	11.5	6.2	4.5	4.2
4	2010-01-09	2010-01-15	-4.0	-9.5	-14.5	8.9	7.8	7.3	7.2
5	2010-02-06	2010-02-13	1.8	-4.2	-11.0	7.7	6.9	6.5	6.4
6	2010-01-04	2010-01-04	-0.6	-3.5	-8.4	5.9	3.8	2.9	2.2
7	2010-03-18	2010-03-20	-2.3	-7.5	-17.1	8.9	7.8	7.3	7.2

2.4.2 Icing events in test span 2009-1

All icing events with an ice load greater than 1.0 kg/m are presented in the following figures. Observations on wind speed, wind direction and lowest ceiling height from the weather station at Daniel's Harbour are also presented. For the icing event, all three observed curves are displayed with red lines i.e. maximum, mean and minimum values, each measured within 10 minute measuring interval. A curve representing what is believed to be the actual ice load is given with a black line.

2.4.2.1 Test span 2009-1, event #1 between 2009-11-29 – 2009-12-21

Two significant accumulations appear in this period, during the early morning of Nov 30th, and one before noon on Dec. 5th. Both occur with winds from west and temperature between -0.5 and -4 °C. During the last couple of weeks, more scattered accretions occur, depending on the advection of humid air towards the test span area.

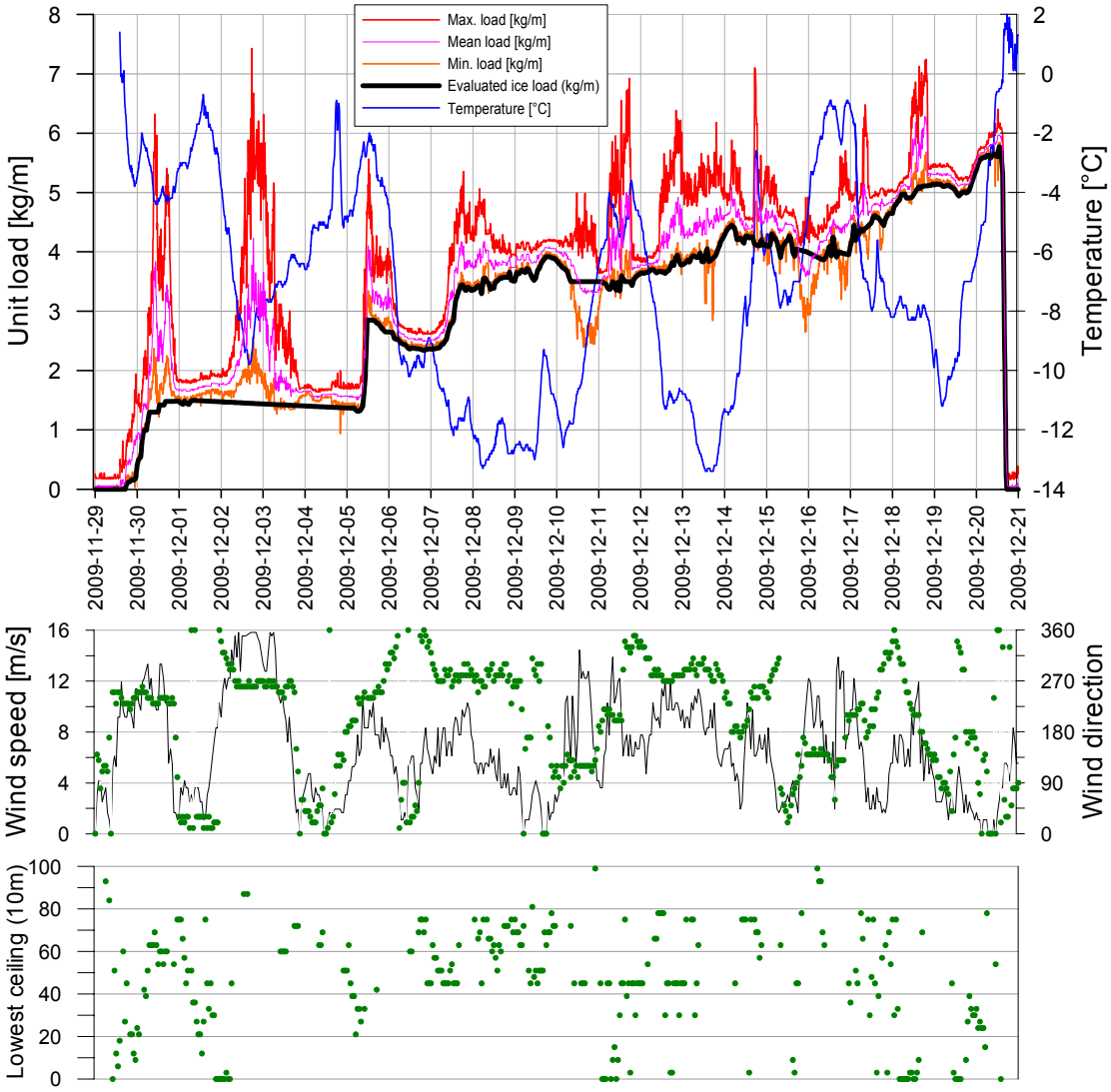

Figure 9. *Icing event 1 in test span 2009-1 and wind and ceiling height measurements at Daniel's Harbour.*

The influence of wind on the measured loading can be identified from the load curves. When the three curves are close to each other the wind speeds are generally low. In cases with strong winds there are large differences between the maximum curve and minimum curves. This scatter is usually a fluctuating wind drag when the curves follow a similar path. Galloping of conductors is identified when the average curve is straight and the minimum curve is an inversed maximum curve. The thick black line represents what is believed to be the actual ice loading. Ice shedding takes place when the temperature passes above 0 C. Icing type is in-cloud icing.

2.4.2.2 Test span 2009-1, event #2 between 2009-12-24 – 2009-12-30

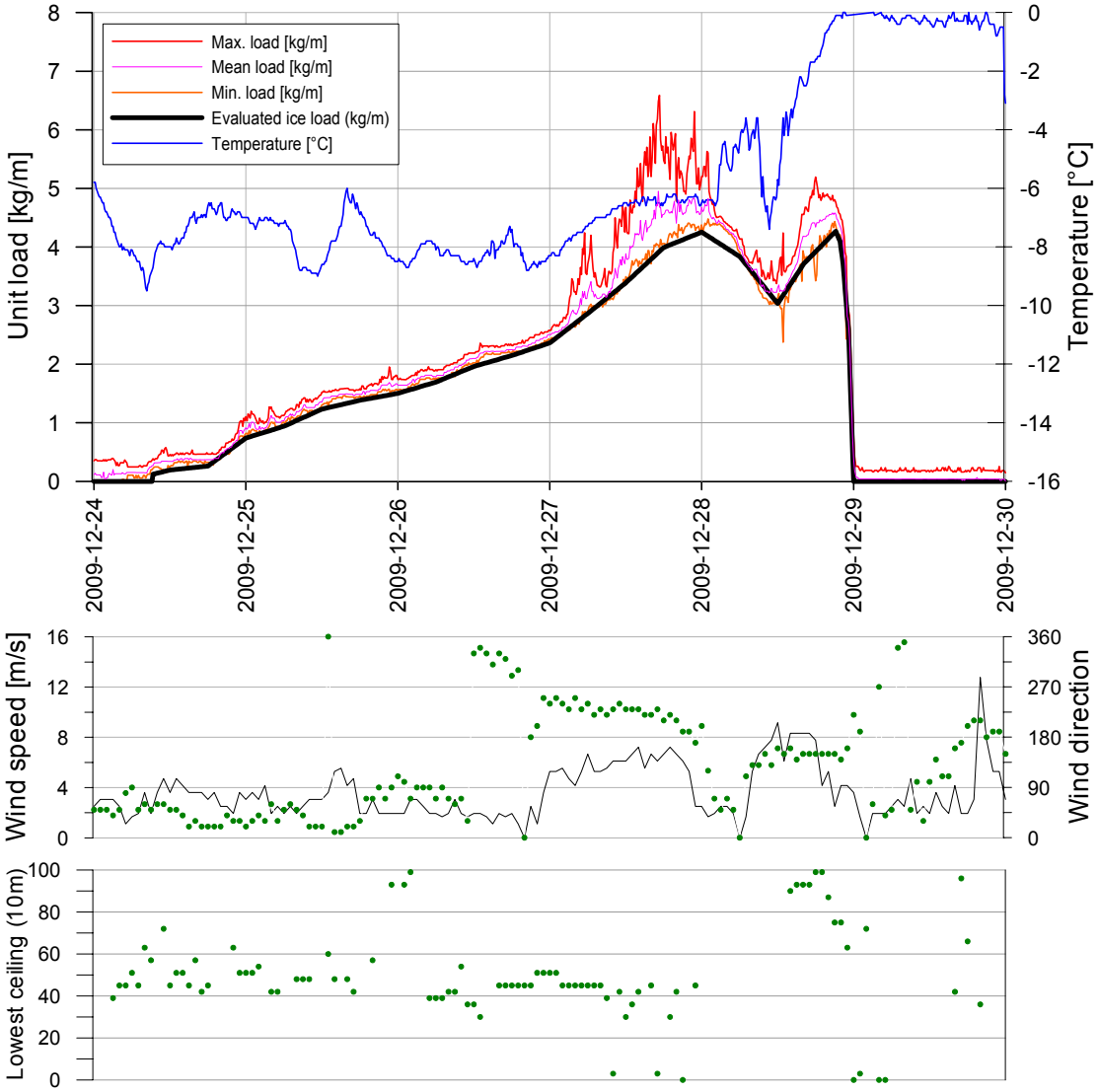

Figure 10. *Icing event 2 in test span 2009-1 and wind and ceiling height measurements at Daniel's Harbour.*

The ice accumulation is gradually building up from 12:00 PM Dec 24th until 12:00 AM Dec 28th. The icing direction begins from NE but changes later to westerly direction. The wind speeds measured at Daniel's Harbour are low and coming from NE. Presumably Daniel's Harbour underestimates winds at test site 2009-1 from this wind direction. The wind speeds at test site 2009-1 are not very high because the load curves are smooth and close together. Ice shedding takes place first due to strong wind and finally when the temperature passes above 0°C. Icing type is in-cloud icing.

2.4.2.3 Test span 2009-1, event #3 betwee 2009-12-31 – 2010-01-05

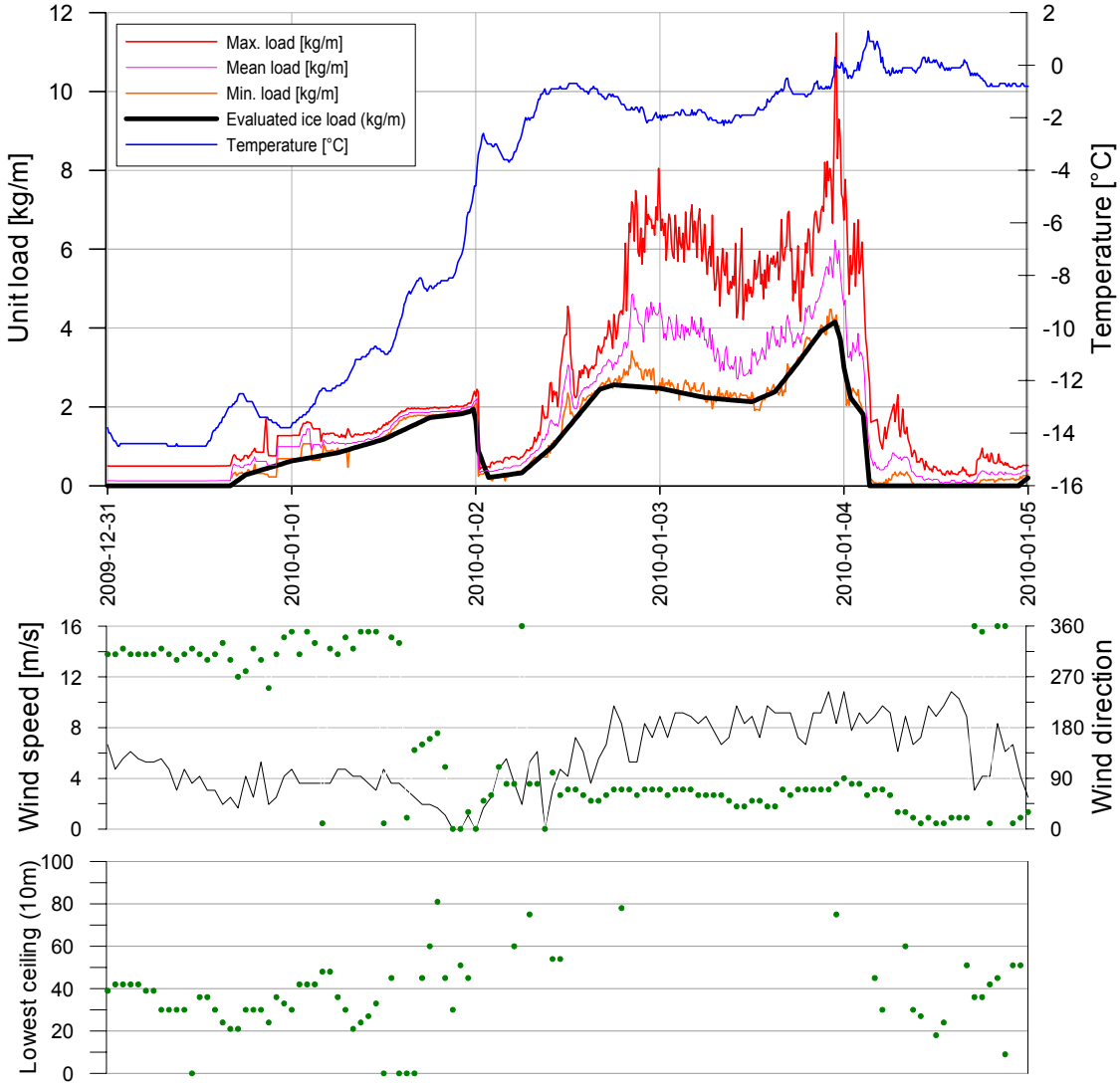

Figure 11. *Icing event 3 in test span 2009-1 and wind and ceiling height measurements at Daniel's Harbour.*

The ice accumulation begins when the temperature is below -8°C, with a rather low wind speed from the westerly direction. Ice shedding takes place on 02 January when the temperature is close to -3°C. Icing continues but from NE-E direction. Wind speed at Daniel's Harbour is in the range of 8-10 m/s, but it is assumed to be considerably higher at the test site. Measurements at the test site shows large difference between the maximum and minimum load curves on 2010-01-03, which indicate high winds.

The ice build-up during 03 January is modeled by WRF, see chapter 5.1. This simulation shows a wind direction from ENE, which is the same as at Daniel's Harbour. The wind speeds at test site are slightly above 20 m/s in this period.

Ice shedding takes place when temperature is around 0°C. Icing type is in-cloud icing.

2.4.2.4 Test span 2009-1, event #4 between 2010-01-09 – 2010-01-16

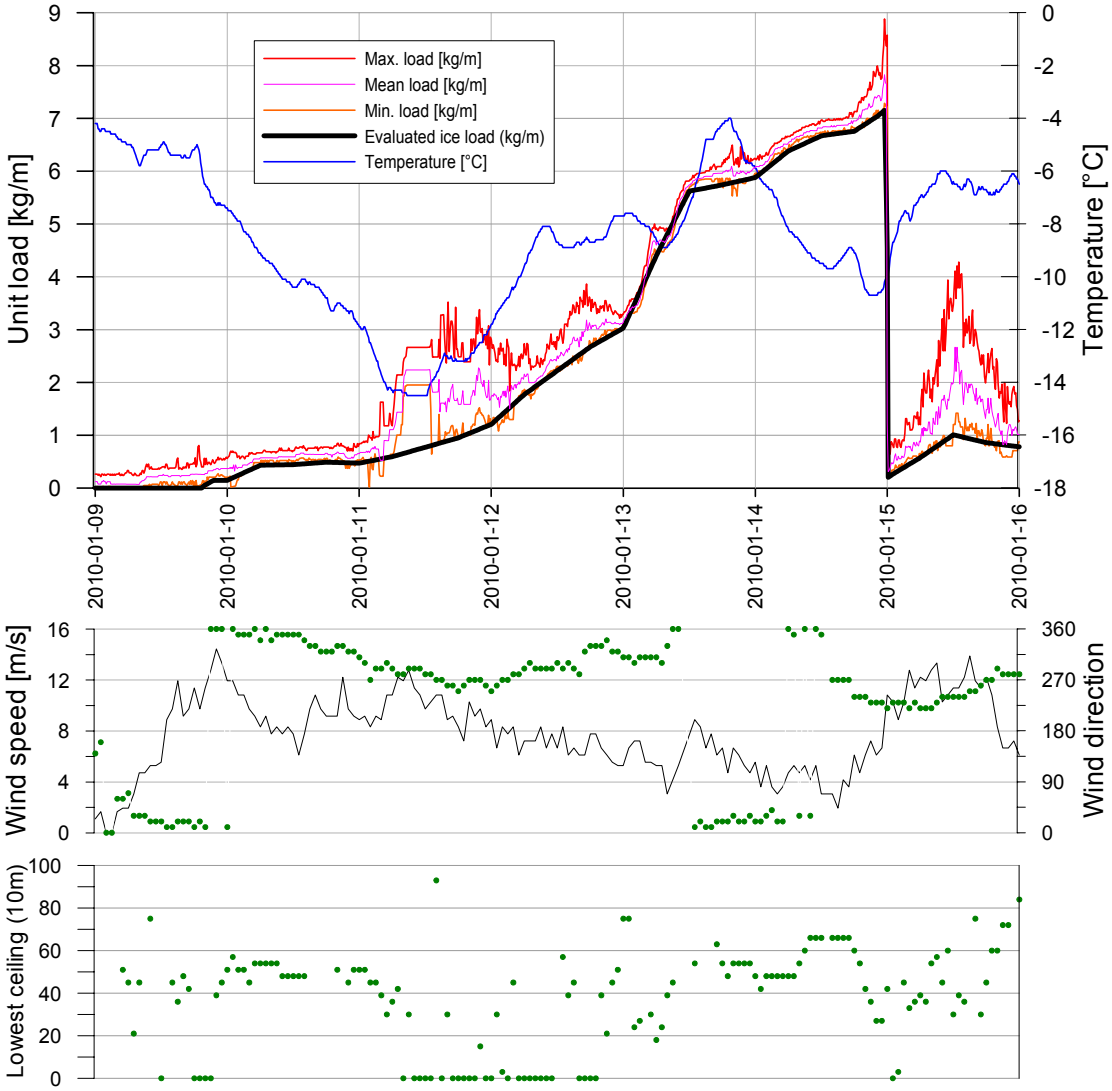

Figure 12. *Icing event 4 in test span 2009-1 and wind and ceiling height measurements at Daniel's Harbour.*

This icing event contains the largest icing measured during the period, an equivalent loading of 7.2 kg/m for the test span.

The ice accumulation begins when the temperature is below -8°C, with a wind speed between 12-15 m/s (estimated from Daniel's Harbour) from the westerly direction. Part of the ice accumulation is from the N to NNE direction.

The ice build-up from January 13th – 16th is modelled by WRF (see chapter 5.3). This simulation shows a wind direction from about N until 12:00 PM on January 19th, and changes to the W, as shown for Daniels's Harbour. Wind speeds are below 10 m/s before early morning (UTC) the 15th but reaches about 22 m/s around noon (UTC).

Ice shedding takes place when the temperature is -10°C. At this time the wind seems to be increasing at the test site. Icing type is in-cloud icing.

2.4.2.5 Test span 2009-1, event #5 between 2010-02-06 – 2010-02-14

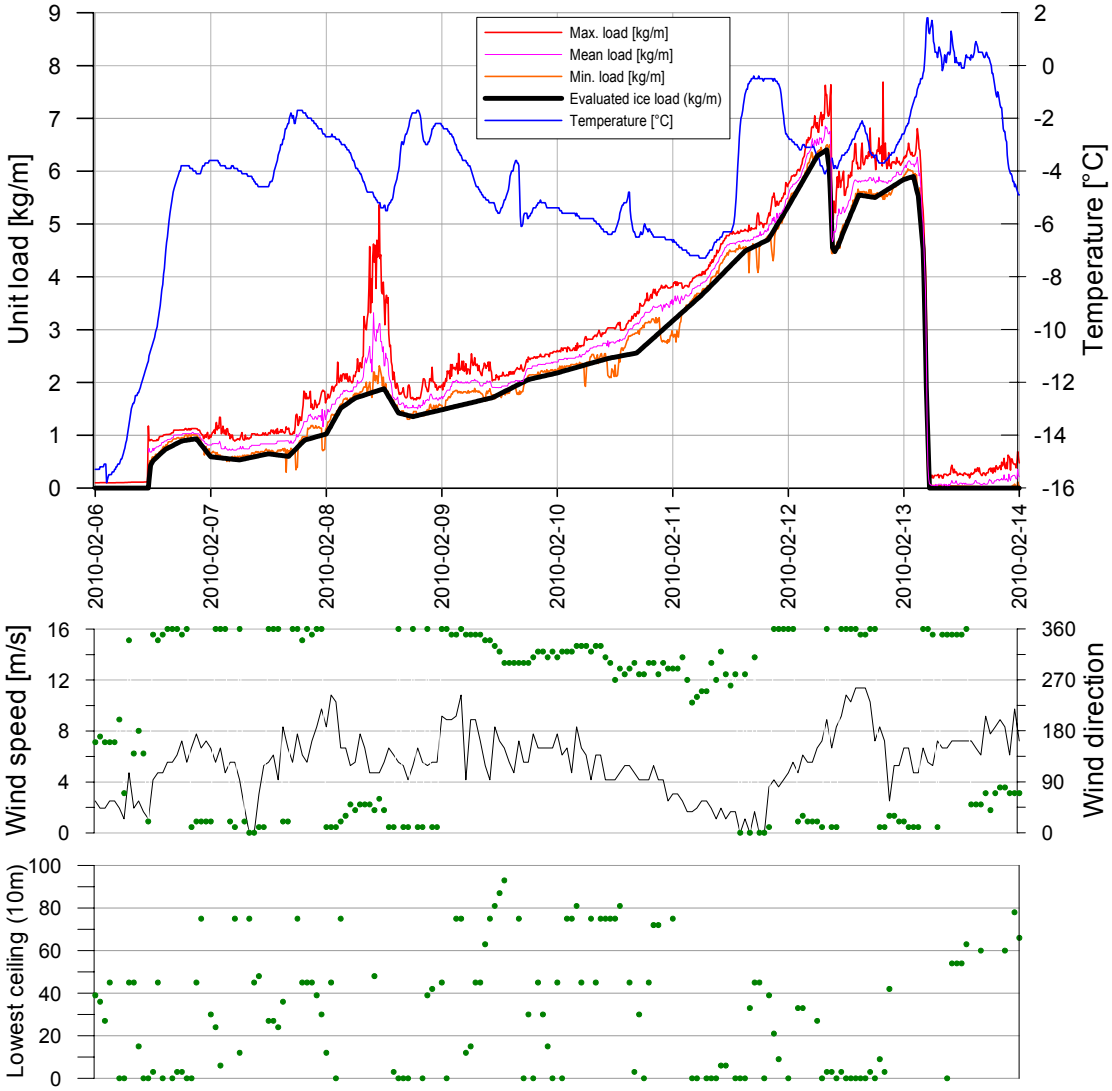

Figure 13. *Icing event 5 in test span 2009-1 and wind and ceiling height measurements at Daniel's Harbour.*

The ice accumulation begins in northerly wind direction. Quite rapid accumulation is for a while from NE direction but main accumulation is from NNW to NW. The temperature at time of accumulation was in range of -1 to -7°C.

The ice build-up from January 10th – 13th is modelled by WRF (see chapter 5.4). This simulation shows a wind direction from about NW until 12:00 PM on January 11th, and changes to the N and NE. Wind speeds are around 10 m/s or less.

Partial ice shedding takes place when the temperature is -3.5°C due to a higher wind speed, but the main ice shedding takes place the when temperature is around 0°C. Icing type is in-cloud icing.

2.4.2.6 Test span 2009-1, event #6 between 2010-02-17 – 2010-02-25

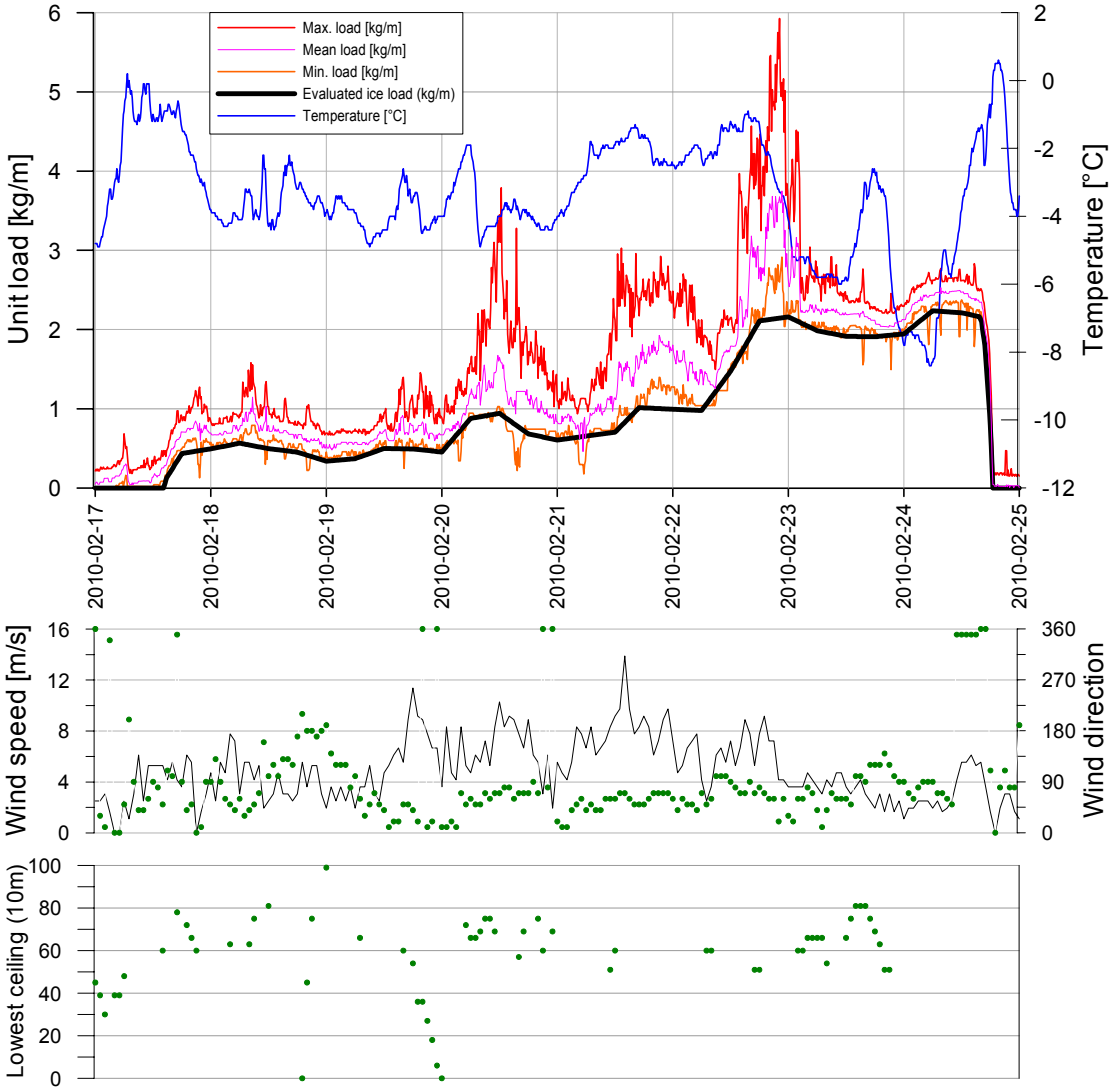

Figure 14. *Icing event 6 in test span 2009-1 and wind and ceiling height measurements at Daniel's Harbour.*

This icing event results in only small accretions, building up stepwise with time. The ice accumulation starts when the wind direction is from the E and is mainly in directions from NE to E. The temperature at the time of accumulation is in the range of -2 to -5°C.

Ice shedding takes place when temperature is around -1°C. Icing type is in-cloud icing.

2.4.2.7 Test span 2009-1, event #7 between 2010-03-13 – 2010-03-27

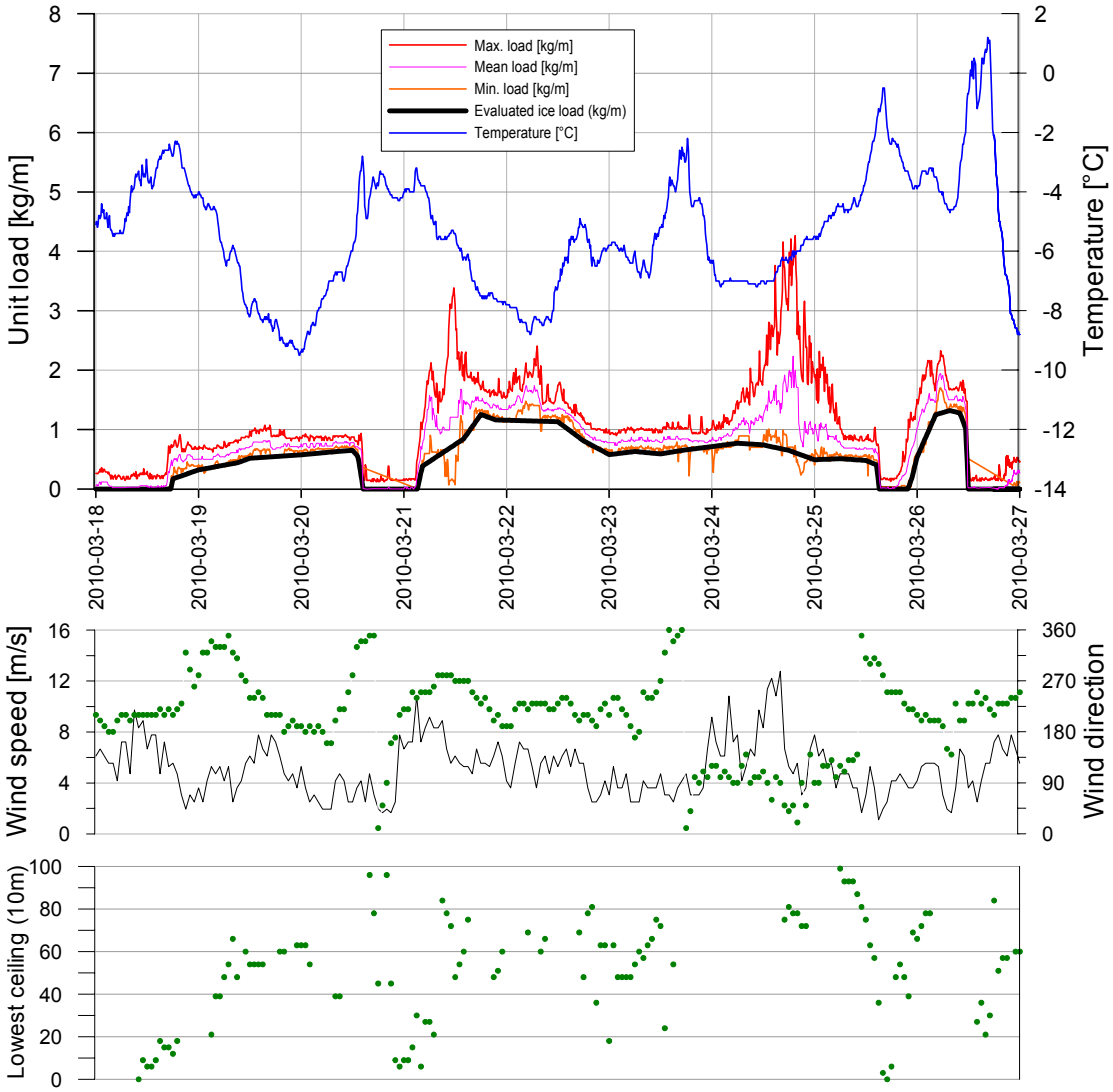

Figure 15. *Icing event 7 in test span 2009-1 and wind and ceiling height measurements at Daniel's Harbour.*

This icing event is rather small. The ice accumulation occurred when the wind direction was from W to SW and the temperature was between -4 to -6°C. Ice shedding takes place when the temperature is around -2°C. Icing type is in-cloud icing.

2.5 Measured icing in test span 2009-2

2.5.1 Icing events

During the measurement period (2009-11-24 to 2010-06-14) three icing events with an ice load greater than 1 kg/m were recorded in test span 2009-2. The maximum tension recorded during the period represents loading that was equal to 52.6 N/m, wind was a large part of that loading. The maximum ice load is evaluated as 1.5 kg/m.

For most part of the measurement period, the temperature was below zero (68.5% of the time). The temperature was between 0 to 2°C 13.9% of the time. Some galloping was measured and the largest event was measured on 2009-12-29. The base stringing (no ice or wind) 2 is estimated as 395 kg when the temperature is -3.4°C

The following figure shows unit loading and temperature for the whole measuring period.

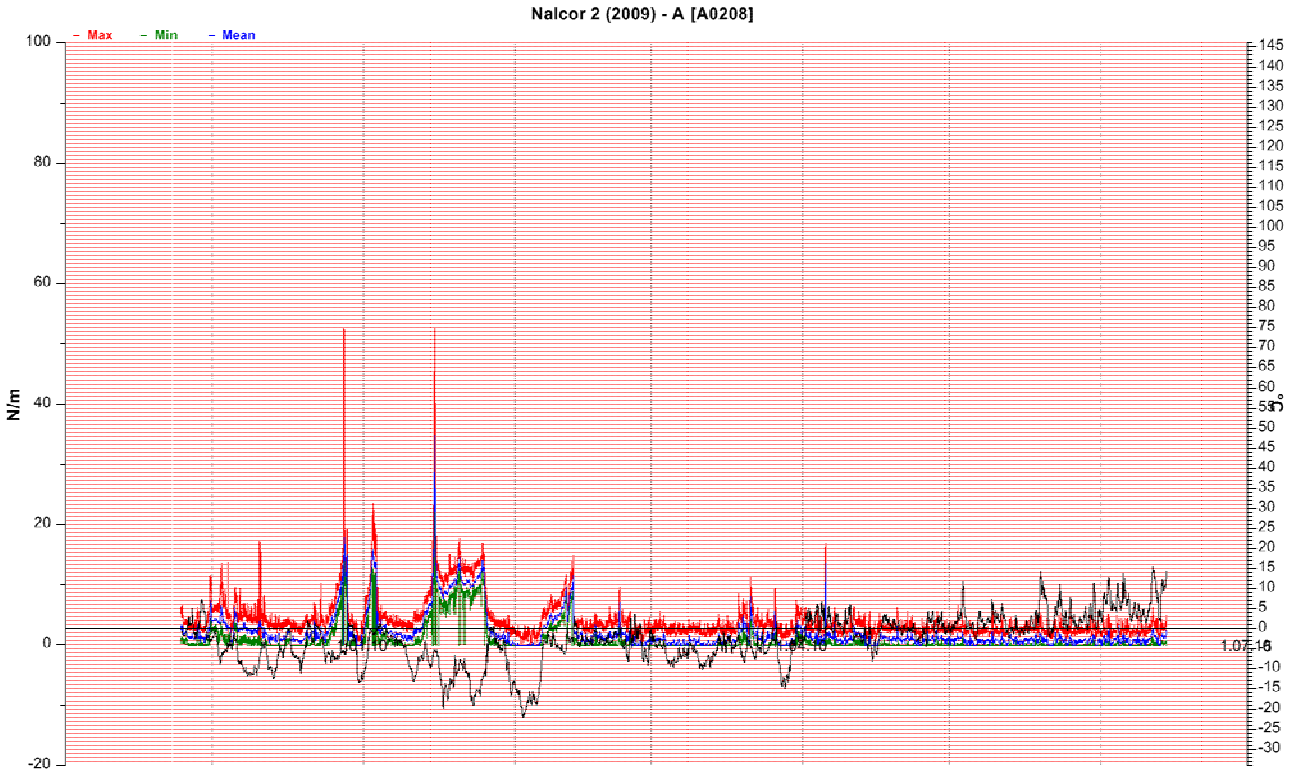

Figure 16. *Test span 2009-2, all measurements in the period of 2009-11-24 to 2010-06-14. The red curve is the maximum load; blue is the average load and green is the minimum load, all measured within a 10 minute period. The black curve is the temperature.*

Icing events that were identified as greater than 1.0 kg/m are given in following table, three events were identified.

Table 3. *Icing events in test span 2009-2 with ice loading greater than 1.0 kg/m.*

Icing event	From	To	Temperature range			Maximum value of measuring curves			Evaluation of max. ice load
			Max. value	Mean. value	Min. value	Max. curve	Mean. curve	Min. curve	
			[°C]	[°C]	[°C]	[Kg/m]	[Kg/m]	[Kg/m]	[Kg/m]
1	2009-12-25 04:00	2009-12-28 20:50	0.4	-6.2	-8.7	5.4	1.8	1.7	1.5
2	2010-01-01 12:30	2010-01-03 16:20	-0.1	-2.6	-9.9	2.4	1.6	1.3	1.2
3	2010-01-13 06:00	2010-01-26 08:10	-3.0	-11.5	-19.8	5.4	3.6	2.4	1.3

2.5.2 Icing events intest span 2009-2

All icing events with an ice load greater than 1.0 kg/m are presented in following figures. Observations on wind speed, wind direction and lowest ceiling height from the weather station at Daniel's Harbour are also presented. For the icing event all three observed curves are displayed i.e. maximum, mean and minimum values each measured within a 10 minute measuring interval. A curve representing what is believed to be the actual ice load is also given.

2.5.2.1 Test span 2009-2, event #1 between 2009-12-25 – 2009-12-29

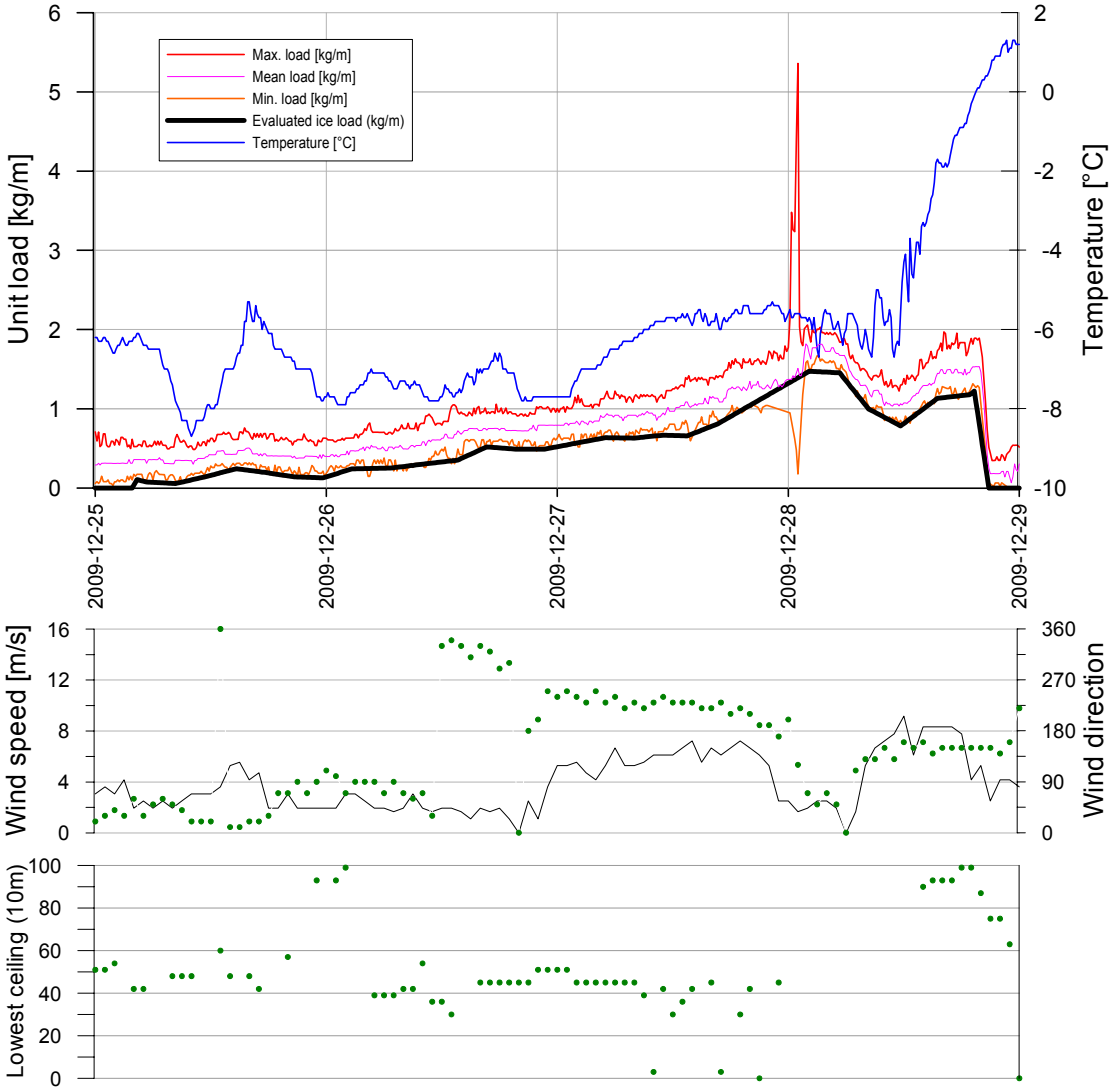

Figure 17. *Icing event 1 in test span 2009-2 and wind and ceiling height measurements at Daniel's Harbour.*

This ice accumulation happens at the same time as event 2 in test span 2009-1. The ice accumulation is gradually building up. The icing direction at the beginning is from NE but changes to the Westerly direction. The wind speed measured at Daniel's Harbour is low from the NE and it underestimates the wind at test span 2009-2 from that wind direction.

A galloping event is obvious on 2009-12-28 when the maximum loading curve gives a high peak while the minimum curve drops at the same time.

Ice shedding takes place when temperature passes 0°C. Icing type is in-cloud icing.

2.5.2.2 Test span 2009-2, event #2 between 2010-01-01 – 2010-01-05

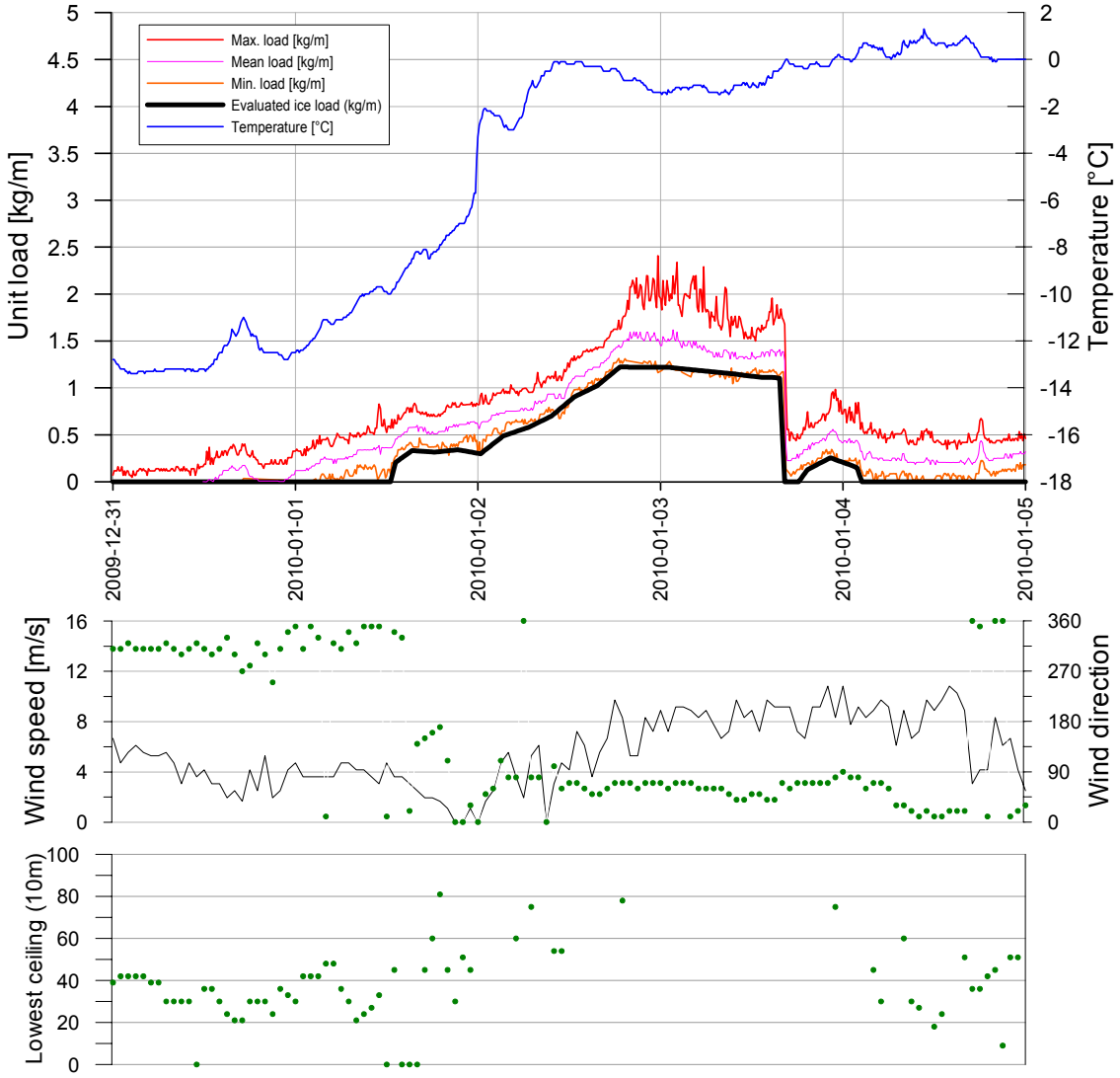

Figure 18. *Icing event 2 in test span 2009-2 and wind and ceiling height measurements at Daniel's Harbour.*

This ice accumulation happens at the same time as event 3 in test span 2009-1. The ice accumulation is mainly from the N to NE direction. Ice shedding takes place when temperature is between 0 and —1°C. Icing type is in-cloud icing.

2.5.2.3 Test span 2009-2, event #3 between 2010-01-13 – 2010-01-27

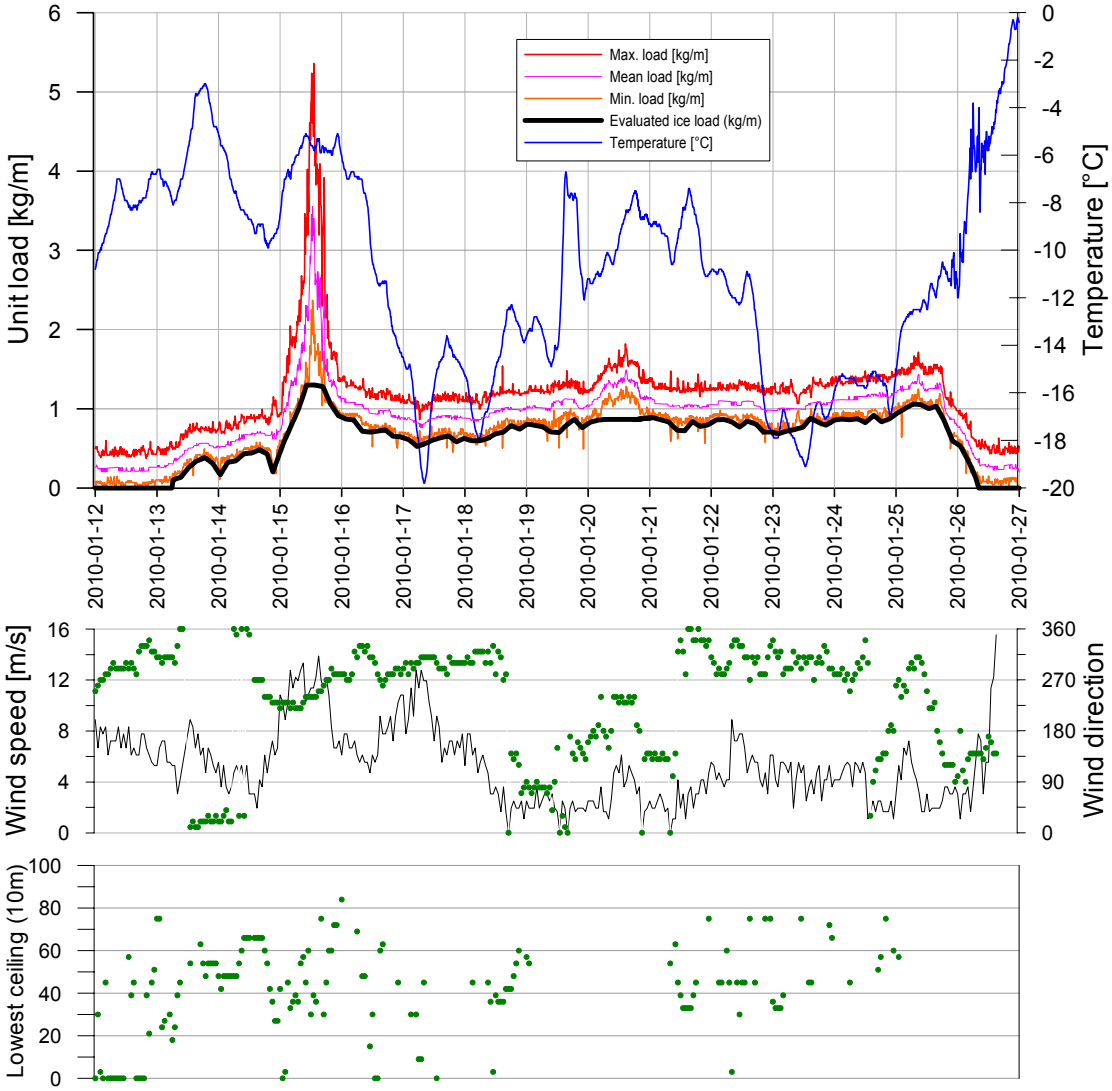

Figure 19. *Icing event 3 in test span 2009-2 and wind and ceiling height measurements at Daniel's Harbour.*

This icing event contains the largest icing measured in test span 2009-2 during the period. It occurred at the same time as event 4 in test span 2009-1, which was the largest icing event in test span 2009-1 for the measuring period.

The largest amount of ice accumulation comes the when wind direction is from the W and the wind speed is relatively high.

Ice shedding starts when the temperature is -11°C. The icing type is in-cloud icing.

3 Icing models used the in study

3.1 General overview on icing models

An overview on different Meteorological Icing Models is given in the Cigre report "Guidelines for Meteorological Icing Models, Statistical Methods and Topographical Effects" /Ref. 4/. Here we describe the icing models that are used in this study, it is based on the model in ISO 12494:2000 /Ref. 20/. The model is built on contribution of researchers as Makkonen, Stallabrass, Finstad and others. It describes how particles that can be either liquid (usually super cooled), solid, or a mixture of water, accumulate to objects. It can be used to model different icing types, such as: in-cloud icing, freezing rain and wet-snow icing. The following equation describes the model.

$$\frac{dM}{dt} = \alpha_1 \cdot \alpha_2 \cdot \alpha_3 \cdot w \cdot V \cdot D$$

Where

dM/dt	Ice accumulation on unit length of object with time [kg/m/s].
α_1	Collision coefficient, range of 0 to 1. It describes if a particle hits the object through a collision.
α_2	Sticking coefficient, range of 0 to 1. It describes if a particle that hit an object will stick to it or bounce back.
α_3	Accretion coefficient, in range of 0 to 1. It describes if a particle that sticks to an object will freeze or get blown off the object.
w	Mass concentration of particles [kg/m^3]. Particle can be liquid (usually super cooled), solid or a mixture of water.
V	Velocity of the particles, perpendicular to the object. The velocity of a particle is taken as the wind speed [m/s].
D	Object dimension with respect to the direction of the particle velocity vector, [m]

The equation for the icing model is general but the parameters depend on assumptions on icing shape and thus the rotational stiffness of the object. It is most common to assume that icing shape is vertical cylindrical, i.e. rotating object that collect icing from all directions, see Figure 20. Overhead transmission lines have conductors with a specific direction and the rotational stiffness depends on factors such as: span length, bundle configuration, conductor diameter etc. For single conductor of moderate size the assumption of rotating cylinder with horizontal direction is often reasonable, see Figure 21.

Figure 20. *Icing on a vertical rotating circular element.*

Figure 21. *Icing on a horizontal test span.*

3.2 Cylindrical icing model for in-cloud icing

The cylindrical icing model assumes that the object is a rotating cylinder and that the ice accumulation will therefore be cylindrical. Usually the cylindrical icing model is analyzed with a standard reference of a 30 mm object diameter, in accordance with icing classification in ISO 12494:2000.

The following assumptions can be made when the model is used for in-cloud icing.

- α_2 = 1.0, i.e. all particles will stick
- α_3 ≈ 1.0, i.e. most of droplets will freeze. α_3 can be determined from the heat balance on the icing surface as described in references /Ref. 20/ and /Ref. 18/.
- w Taken as liquid water content (LWC) of the cloud droplets

3.2.1 Collision coefficient, α_1

The collision coefficient accounts for particles deflected around the object by air flow. The airflow around an airfoil deflects some of the particles which would have struck the airfoil and results in the collision efficiency being less than 1. The collision coefficient is mainly dependent on wind speed, droplet diameter, and object diameter. Small droplets tend to follow streamlines around objects, while large droplets have a large inertia and tend to collide with objects.

The following empirical equations are used to describe the collision coefficient for slender cylindrical objects. The minimum value should be taken as α_1 = 0.01 and the maximum value as α_1 = 0.99.

$$\alpha_1 = A - 0.028 - C \cdot (B - 0.0454)$$

$$A = 1.066 \cdot K^{-0.00616} \cdot e^{-1.103 \cdot K^{-0.688}}$$

$$B = 3.641 \cdot K^{-0.498} \cdot e^{-1.497 \cdot K^{-0.694}}$$

$$C = 0.00637 \cdot (\emptyset - 100)^{0.381}$$

$$\emptyset = \frac{Re_d^2}{K} \qquad K = \frac{\rho_w \cdot MVD^2 \cdot V}{9 \cdot \mu \cdot D} \qquad Re_d = \frac{\rho_a \cdot MVD \cdot V}{\mu}$$

Where

- MVD Medium volume droplet diameter
- D Object diameter
- V Wind speed
- ρ_a Air density
- ρ_w Water density
- μ Absolute viscosity of air

The collision parameter is very important for estimating quantity of accumulation in the model and it can vary a lot depending on the values of V, MVD and D. The formulas for α_1 are based on slender cylindrical objects for moderate icing. For ice weights exceeding 15-30 kg/m (depending on V, MVD and D) the formulas are no longer valid and there is major uncertainty in the collision coefficient. The collision coefficient is often determined using the minimum value, α_1 = 0.01 in this case.

Figure 22 shows how α_1 changes with wind speed, object diameter and the number of droplets. The reference case has V = 10 m/s, object diameter D = 0.05 m, LWC = 0.3 g/m^3, number of droplets = 100 per cm^3 (gives MVD = 20 μm) and T = -5°C. These values give α_1 = 0.14, changes are shown when one of the parameters is modified.

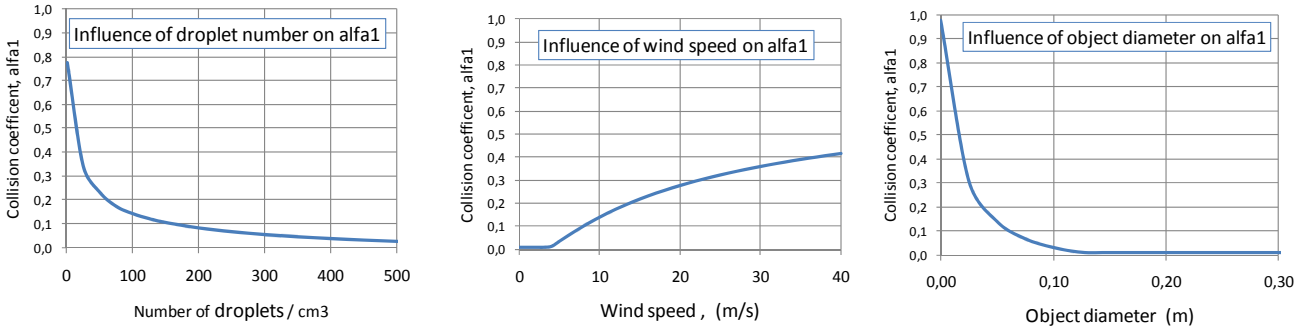

Figure 22. *Influence of medium volume droplet number, wind speed and object diameter on collision coefficient (α_1).*

3.2.2 Accretion coefficient, α_3

The accretion coefficient describes whether a particle that sticks to an object will freeze or be blown off the object. The accretion is said to be dry if all of the impinging water droplets freeze upon impact and then α_3= 1.0. The accretion is said to be wet if the accretion efficiency depends on the rate at which latent heat is transferred away from the surface of the object through the liquid water in the air. The water droplets that do not freeze when colliding with the surface, drop off the object as a result of gravity or wind drag. The accretion coefficient can be calculated by considering the heat balance of the icing surface. Formulas can be found in following references: /Ref. 20/ and /Ref. 18/.

When air temperature is very close to 0°C, that α_3 is reduced from 1.0. For most cases it can be taken as $\alpha_3 \approx$ 1.0 for in-cloud icing. The icing models used in this study use the heat balanced equation to determine α_3.

3.2.3 Medium volume droplet size (MVD)

Cloud droplet size is important because of its effect on α_1. The model uses medium volume diameter (MVD) as a representative droplet size and in this study it is determined from the assumption that cloud water follows a generalized gamma distribution. The MVD is determined as follows:

$$MVD = (3.672 + \mu)/\lambda$$

$$\mu = MIN(2 + \frac{100}{N_c}; 15) \quad \text{and} \quad \lambda = \left[\frac{\pi}{6} \cdot \rho_w \cdot \frac{\Gamma(4+\mu)}{\Gamma(1+\mu)} \cdot \left(\frac{N_c}{LWC}\right)\right]^{1/3}$$

Where

MVD	Medium volume droplet size
N_c	Number of droplets in cubic centimeter
LWC	Liquid water content of cloud
ρ_w	Water density
Γ	Gamma function

Determination of LWC is described in following chapters. The number of droplets is assumed to remain constant for different LWC, i.e. the droplet size increases with increased LWC. The model can not predict the number of droplets and it is an input parameter that needs to be determined from experience. Typical values of N_c are 75 – 100 droplets/cm^3 for maritime air masses and 250 – 450 droplets/cm^3 for continental air masses.

In this study it was determined to use N_c = 100 droplets/cm^3

3.2.4 Ice density

Ice density is given by the following equations:

$$\rho_{ice} = \begin{cases} 361 \cdot R^{0.38} & if\ R < 0.37 \\ 378 + 425 \cdot Log(R) - 82.3 \cdot Log(R)^2 & if\ 0.37 \le R < 128 \\ 917 & if\ R \ge 128 \end{cases}$$

$$v_0 = \begin{cases} 0.01 \cdot V & if\ k < 0.18 \\ (A - 0.04 - C \cdot (B - 0.029)) \cdot V & if\ k \geq 0.18\ and\ k < 1000 \\ 0.99 \cdot V & if\ k \geq 1000 \end{cases}$$

$$A = 1.03 \cdot K^{0.00168} \cdot e^{-0.796 \cdot K^{-0.78}}$$

$$B = 2.657 \cdot K^{-0.519} \cdot e^{-1.06 \cdot K^{-0.842}}$$

$$C = 0.00944 \cdot (\emptyset - 100)^{0.344}$$

$$R = \frac{-MVD \cdot v_0}{2 \cdot t_s}$$

Where

ρ_{ice}	Density of ice [kg/m^3]
MVD	Medium volume droplet diameter [μm]
K	Given in paragraph 3.2.1
t_s	Surface temperature of icing [°C]. In most cases it can be approximated by the air temperature.
v_o	Droplet impact speed [m/s].
ϕ	Given in paragraph 3.2.1, it shall not be less than 100

3.3 Brief description of the WRF modeling system (for getting V, T and LWC)

The Weather Research and Forecast (WRF) model is a state-of-the-art meso-scale numerical weather prediction system, used both in operational forecasting and in atmospheric research. The model source code is freely available for the public, and can easily be downloaded together with all necessary documentation from: http://www.wrfmodel.org/ and http://www.wrfuserspage.com. The WRF-model is developed jointly by several institutions in the US, the number of users is growing rapidly and the users have spread worldwide. WRF solves coupled equations for all important physical processes (such as winds, temperatures, stability, clouds, radiation etc.) in the atmosphere based on initial fields and lateral boundary values derived from global analysis data.

The model version used in this project is WRF-ARW V3.2, which is the most up to date version available. The model runs are initiated using state of the art three dimensional analysis of the atmosphere obtained from the ECMWF (European Centre for Medium-range Weather Forecasting) data archive. For simulations before 1989 the model is forced by data from the reanalysis project ERA40, while for more recent simulations data from the ERA-interim project is used.

Because atmospheric icing often occurs as a very local phenomenon, and icing intensity is varying greatly in space, especially in complex terrain, it is necessary to run the model at high horizontal resolution to produce useful icing maps. In order to obtain a good representation of the local terrain in the model, we have replaced the standard terrain data in WRF (USGS 30 arc sec) with a much higher resolution terrain data set at 3 arc sec resolution: SRTM. The model is set up with nested domains, applying a grid resolution in the range of 0.4 – 0.8 km in the finest resolution domain, which is considered as extremely high resolution for meso-scale models.

A second important factor for the simulation of atmospheric icing is how the model computes or parameterizes the cloud microphysics. There is a variety of different microphysics parameterization schemes of different complexity implemented in WRF and ready for the user to apply. In this project the model is set up with the Thompson microphysics. This scheme has a rather sophisticated way of treating the microphysical processes and was originally developed to improve aviation icing forecasts in the US. Sensitivity simulations carried out within COST 727 (http://www.cost.esf.org/index.php?id=205&action_number=727) have revealed that this scheme is also well suited for icing simulations at ground level.

It is important to keep in mind the limitations of numerical weather prediction models when analyzing and evaluating the model results. Even with sophisticated microphysics and high spatial resolution, explicit prediction of atmospheric icing will be far from perfect, especially when looking at single icing events. This is

related to the chaotic nature of the atmosphere and limitations in the predictability of small scale processes. Uncertainties are also introduced from errors in the initial fields (Interpolated from global models like ECMWF or GFS). Even though the predicted accumulated ice load does not match observations perfectly in single cases, the predictions have great value in terms of studying the horizontal distribution of icing severity. The main intention of simulating several icing events with WRF is to study the relative difference in icing exposure/severity between different locations, rather than predict or estimate extreme values of accumulated ice loads.

The icing simulations are carried out in a two step manner:

1. Meteorological data is produced at high spatial and temporal resolution using the WRF model. In addition to standard variables like wind speed, temperature and humidity, the WRF model also outputs data like mass concentration of supercooled cloud water (LWC), and also an estimate of the median volume droplet size.

2. The data from WRF is processed through an accretion model for rime icing calculated using the standard ISO specification (ISO 12494, 2001) (Makkonen model), as described in Chapter 3.2.

Accumulated ice load is calculated in all grid cells in the model domain serving the basis for an icing map, as an overlay in Google-Earth. The Google-Earth files also contain information about predicted precipitation, wet snow and maximum wind speed.

3.4 Weather observation model (WObs-model) for getting V, T and LWC

Observation from high quality routine weather stations with hourly observation can be used to estimate the main input parameters for icing models; i.e. wind speed, temperature and LWC. The methodology is based on a physical model and cloud physics and was first used by Knut Harstveit /Ref. 18/ and /Ref. 19/. Others have made similar approach but with slight modification, M.Drage /Ref. 9, Ref. 10/ and K.Jones /Ref. 47/. According to Harstveit, the model seems to give reasonably good results for sites of 10, 50 and 80 km distance from the meteorological data source. The model has shown good strength by modeling correct ice amounts of 10-20 kg/m at sites exposed for moist maritime air mass, forming fresh clouds on the windward side of the mountain, in altitude up to 700-800 m at the tops of Norwegian coastal mountains.

The model is based on representative weather observations that are available upwind from the icing site. The observations need to be frequent and preferably every hour. The observations should at least contain: ambient temperature, wind speed and ceiling height. Other parameters, such as wind direction, pressure, cloud opacity etc. can also be used to improve the model.

In this study the model is based on Harstveit ideology but with some modification. The model is called WObs as an abbreviation of Weather Observational model. The following is a brief description is made of the model.

3.4.1 Determination of air temperature

Air temperature at the height of icing location (z) is determined from information of temperature and ceiling height (cloud height) at a nearby weather station.

$$T(z) = T_0 - \gamma_d \cdot (z - z_0) \qquad if\ z \leq H_c$$

$$T(z) = T_0 - \gamma_d \cdot (H_c - z_0) - \gamma_w \cdot (z - H_c) \qquad if\ z > H_c$$

Where

T_0	Temperature at lower level observation station
γ_d	Lapse rate (temperature gradient) below cloud base (unsaturated conditions).
γ_w	Lapse rate (temperature gradient) above cloud base (saturated conditions).
H_c	Height of cloud base

Values of γ_d and γ_w are estimated by correlation if some temperature observation exists on the icing site. If no observations are available at the icing site, then the lapse rate can be assumed to be near adiabatic and taken as:

γ_d = 0.0098 °C/m
γ_w = 0.0065 °C/m

3.4.2 Determination of wind speed

Observations of wind speed are available at weather stations. Wind speed at the icing site is estimated to be related as:

$$V_z = a + b \cdot V_0 \ + c \cdot V_0^2$$

Where

V_z	Wind speed at icing location
V_0	Wind speed at lower level observation station
a, b, c	Constants, may be dependent on wind direction

The parameters a, b and c need to be determined. They can be estimated with regression if some wind observations exist at the icing location or they can be estimated otherwise, for example with WRF simulation. In some cases it may be needed to let the parameters depend on wind direction, for example when the observation station is sheltered to a specific direction.

3.4.3 Determination of liquid water content

The model assumes that the water vapor pressure is saturated at the cloud base and the liquid water content is proportional to the condensation water from the adiabatic saturation curve, as may often be assumed at exposed sites in maritime regions.

The liquid water content (LWC) is calculated based on the assumption that the total mixing ratio (liquid and vapor) of the air is constant with height. Liquid water within clouds (z) is calculated as

$$LWC(z) = \alpha \cdot w \cdot p_w(T(z)) \ \cdot f(cloud)$$

With

$$w = \varepsilon \cdot \rho_{air}(T(H_c), P(H_c)) \cdot \left[\frac{e_s(T(H_c))}{P(H_c)} - \frac{e_s(z)}{P(z)}\right]$$

$$e_s(T) = 6.112 \cdot e^{17.67 \cdot T/(T+243.5)}$$

$$\rho_{air}(T, P) = \frac{0.348 \cdot 10^{-3} \cdot P}{T+273.15}$$

Where

w	Water content [kg/m^3]. It is assumed to be proportional to the adiabatic cloud water gradient and the height above the cloud base. The approach from M.Drage /Ref. 9 / is used here to evaluate w.
α	Expresses the deviation from the adiabatic cloud water gradient ($\alpha \leq 1$). For exposed location it may be taken as α = 1 but may be lowered from 1.0 due to loss of cloud water in old clouds or by partly or slowly lifting of the air allowing droplet loss due to mixing, freezing or precipitation washout to occur. In a wooded hill area in Central Finland it was found as α=0.5 to 0.6 (Harstveit). Alpha can be taken as a constant value for the site but it can also be defined to restrict maximum LWC.
ε	Ratio of molecular weights of water vapor and dry air, ε =0.622.
ρ_{air}	Density of dry air [kg/m^3] , calculated from temperature and pressure.
$e_s(T)$	Saturation vapor pressure over water
P	Atmospheric pressure at given height
H_c	Height of cloud base [m]
T	Temperature at given height, [°C]

Z Height of icing location [m]

$P_w(T(z))$ Fraction of liquid water of the water content. P_w is used to ensure that clouds containing mainly ice crystals will not be included as a source of icing. The following ad hoc formula is used in this study: P_w =1 if T(z)>-10°C, P_w =1-(10+T(z))/10 when T(z) is between -10°C and -20°C. P_w = 0 when T(z)<-20°C.

f(cloud) Reduction function to take into consideration when cloud amount and/or cloud opaque are not fully covered.

3.4.4 Ice melting and ice shedding

Ice shedding is an important factor when modeling extreme in-cloud icing in an area with frequent icing and low temperature. Main factors for ice shedding are: (i) melting, (ii) sublimation and (iii) mechanical ice break. Some attempts have been made to model ice shedding but no widely accepted model exists that has been validated with sufficient field data. It is commonly known, that ice loss processes frequently go faster than the ice melt model suggests due to ice fall. Sublimation is a slow process that takes place when the temperature is less than -1°C. The ice mass reduction rate by sublimation is low but the phenomenon can be observed during several consecutive days and the total ice mass reduction can be important. Sublimation rate increases with increased wind speed and temperature and reduced relative humidity.

Ice melting and ice shedding at any given hour is modeled as:

$$dM_{Shedding} = MAX\{k_{ice\ break} \cdot M_{icing} \mid k_{sublimation} \cdot \pi \cdot D_{ice}\}$$

$$k = \begin{cases} \frac{1}{3} \cdot (1 + 0.075 \cdot V) & T(z) > 0°C \\ \frac{1}{3} & if\ T(z) + 0.05 \cdot V > 0\ \ and\ \ T(z) \leq 0°C \\ 0 & otherwise \end{cases}$$

Where

$dM_{Shedding}$ Weight of ice reduction in given hour

M_{icing} Mass of accumulated icing when shedding may take place

$k_{ice\ break}$ Shedding factor for ice break and melating

V Wind speed [m/s]

T(z) Temperature at height of icing location [°C]

$k_{sublimation}$ Shedding factor related to sublimation, taken as 0.00125 [gr/m^2*hour]

D_{ice} Diameter of icing

This formulation of ice shedding has not been validated with field data, but takes notice of: (i) Sundin & Makkonen /Ref. 45 / where it was assumed that ice shedding took place when the air temperature was > 0 °C for 3 hours. (ii) Mechanical ice fall is often relevant and it is influenced by wind speed. (iii) Sublimation factor is estimated but has not been validated with field data.

4 Icing in LRM estimated by WObs icing model

4.1 General

The intention of modeling icing by weather observational icing model (WObs) in the Long Range Mountains is to make an attempt to quantify the icing in the most severe in-cloud icing area along the line route passing the Long Range Mountains. It is evaluated that the most extreme location is where the 2009-1 test span is located. The model is thus primarily used to predict icing in that location and in the direction of the test span.

This chapter describes the available weather data to use as an input to the model and how model parameters are selected. Comparison is made between the icing predicted by the model to icing measured in the test spans 2009-1 and 2009-2 in the winter 2009-2010 and to previously collected icing data in the area. The model is then used to predict the 50 years ice loading based on long term weather observations.

4.2 Description of available data from weather stations

This study uses CWEEDS files from Environment Canada where they are available. The data files were downloaded from the site http://www.climate.weatheroffice.gc.ca. The data files contained data until 2005-12-05, although some stations have shorter series. The CWEEDS files are computer data sets of hourly weather conditions occurring at 145 Canadian locations for up to 48 years of record, starting as early as 1953, and ending for most locations in 2001. The primary purpose of these files is to provide long term weather records for use in urban planning, siting and design of wind and solar renewable energy systems, and the design of energy efficient buildings. The following figure shows the location of weather stations that are available with data in the CWEEDS file system.

STATION	WBAN	RAD.CSN	WX.CSN	LAT	LONG
ARGENTIA A	CAN85	8400100	8400100	47.30	54.00
BATTLE HARBOUR	CAN06	8500398	8500398	52.25	55.60
BONAVISTA	14522	8400600	8400600	48.70	53.08
BUCHANS A	CAN87	8400700	8400700	48.85	56.83
BURGEO	CAN88	8400798	8400798	47.62	57.62
CAPE HARRISON	CAN95	8500900	8500900	54.77	58.45
CARTWRIGHT	15503	8501100	8501100	53.70	57.03
CHURCHILL FALLS A	CAN83	8501132	8501132	53.55	64.10
COMFORT COVE	CAN89	8400798	8400798	49.27	54.88
DANIELS HARBOUR	15504	8401400	8401400	50.23	57.58
DEER LAKE A	14523	8401501	8401501	49.22	57.40
GANDER INT'L. A	14509	8401700	8401700	48.95	54.57
GOOSE UA	15601	8501910	8501900	53.32	60.37
HOPEDALE	15642	8502400	8502400	55.45	60.23
PORT AUX BASQUES	CAN90	8402975	8402975	47.57	59.15
ST. ANDREWS	CAN91	8403300	8403300	47.77	59.33
ST. ANTHONY	CAN92	8403400	8403400	51.37	55.58
ST. JOHN'S A	14506	8403506	8403506	47.62	52.75
ST. JOHN'S WEST CDA	14521	8403600	8403506	47.52	52.78
STEPHENVILLE A	14503	8403800	8403800	48.53	58.55
TWILLINGATE	CAN94	8404000	8404000	49.67	54.82
WABUSH LAKE A	15628	8504175	8504175	52.93	66.87

Figure 23. *Location of weather stations in Newfoundland with CWEC data.*

Environment Canada was contacted and asked if further data was available that was recorded on hourly basis and contained good information on ceiling height. Bob Morris from Environment Canada sent additional up to date information from Daniel's Harbour. The observation from Daniel's Harbour is of most importance for evaluating in-cloud icing at the Long Ridge Mountains. They should give a good description of the source of icing when the icing direction is from the west. They should however, be treated with care when the icing

direction is from the east. The distance from Daniel´s Harbour to test span at 2009-1 is 18.2 km and the distance to test span 2009-2 is 22.6 km.

The weather station at Twillingate may be a representative for evaluating in-cloud icing from easterly directions. The weather observations are however limited since useful observations are only available in the period 1954-1966.

In addition to Daniel's Harbour the following weather stations were used: Twillingate, Deer Lake and St. Anthony.

4.2.1 Observation from Daniel's Harbour

Observation exist from Daniel's Harbour weather station from from 1953 to 1966 at 3 to 6 hour intervals. Since then observations are available every hour, with few exceptions.
Below is data on the location, type and code of the station:

DANIEL'S HARBOUR, NFLD	**Climate ID: 8401400**	**Lat: 50.24**	**Long: -57.58**
Elevation: 19.0 m	**TC ID: WDH**	**Station Type: AU5**	**WMO ID: 71185**

The following information and data has been provided by Bob Morris of Environment Canada:

The climate station ID stayed the same in our data management system for this station for this entire period so there are periods with where the observations were taken by humans up to about 1996, times when the human and autostation observations were mixed together (human obs during the daylight periods) up to 1997, and it looks like just autostation observations from 1997 to the present.

This is a general report format that contains the hourly observational elements that you need. Note that the units for ceiling are stated as 30's of m but are really just 100's of feet and are unchanged as observed for aviation weather purposes.

Note too that after the 1980's there is a way to distinguish between the human and autostation observations. A human observation has both the total cloud amount and total cloud opacity for an hour. The aviation autostation only has a total opacity observation. And the ceiling and visibility, although reported in the same format and units actually represent quite different physical measurements.

- *Ceiling in a human observation represents the height above ground where the summation opacity exceeds 5/10 at the time of observation.*
- *Ceiling from the autostation represents the height above ground directly above the station where the summation opacity exceeds more than 5/10 of the hour (I believe for lower ceilings the duration is the most recent 20 minutes of the hour). Also clouds and ceilings higher than 10,000 feet are not detected.*
- *Visibility from human observations is prevailing visibility based on the observer being able to see various range markers.*
- *Visibility from aviation autostation observations is determined from optical measurements in a volume about the size of a bread box. So they can be much different than human visibility observations.*

Further, the human observations report both forms of precipitation (including more than one at a time) and obstructions to visibility as present weather. Aviation autostations only report forms of precipitation - only one at a time and no obstructions to visibility such as fog or blowing snow.

4.2.2 Variation of temperature at Daniel's Harbour

Temperature plots for Daily Maximum, Minimum, Mean and Extreme Minimum are presented in Figure 24 for Daniel's Harbour.

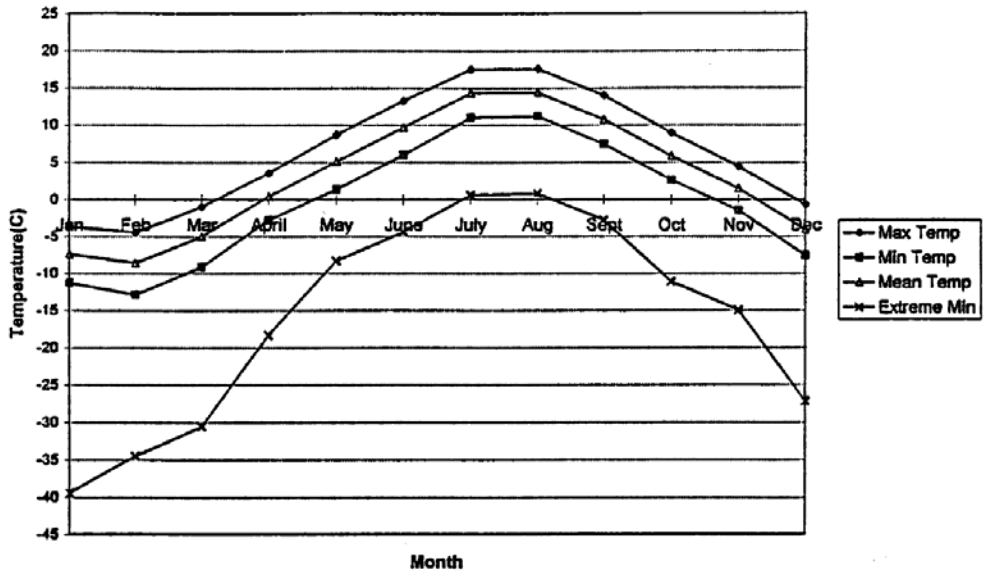

Figure 24. *Daily temperature statistics for Daniel's Harbour, from /*Ref. 40*/.*

4.3 Wind speed and ceiling height

Following figures shows distribution of wind and ceiling height for the weather stations that are used in the study. Average wind speed and maximum wind speed are given for each direction. The ceiling height is also given as a as percentage of time for each wind direction.

The wind speed observation is an estimate of the one-minute mean wind speed per each hour for the years before 1985 and a two-minute mean wind speed thereafter. The average wind speed and maximum wind speed for each station is given in Table 4.

Table 4 Wind speed at weather stations.

Weather station	Average wind speed [m/s]	Maximum wind speed in observation [m/s]
Daniel's Harbour	6.2	36.7
Dear Lake	4.0	25.8
Twillingate	7.2	32.2
St. Anthony	5.5	26.9

Further information on wind statistics on the west and east coasts of Newfoundland is shown in Appendix D.

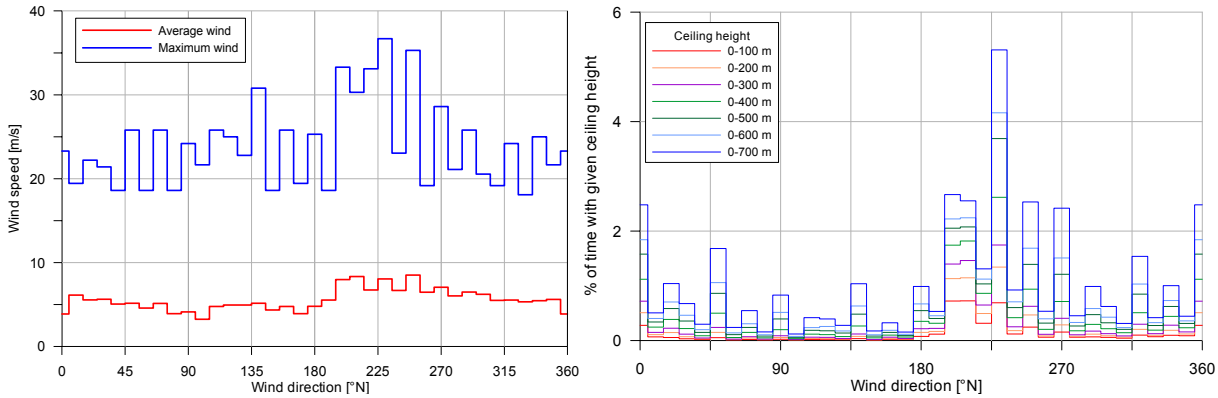

Figure 25. *Daniel's Harbour, wind speed and ceiling height (0-700m) depending on wind direction.*

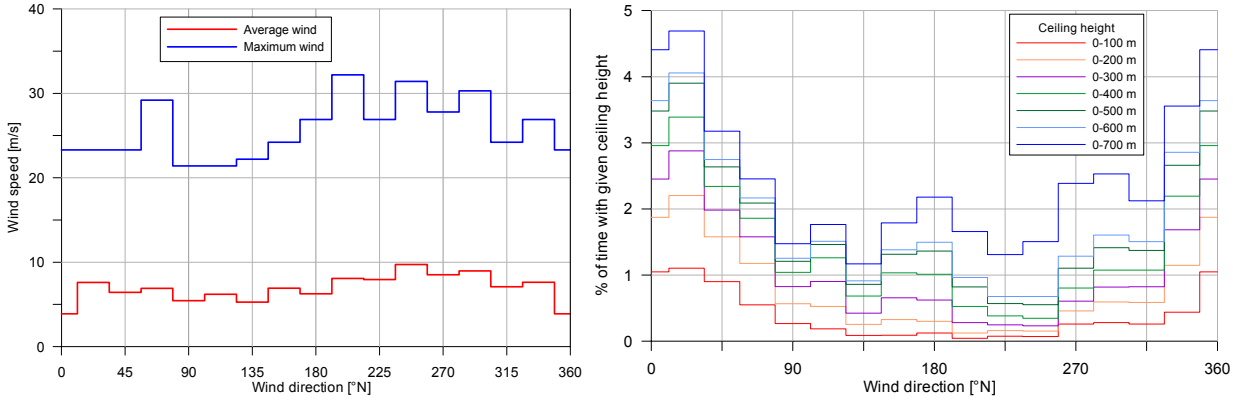

Figure 26. *Twillingate, wind speed and ceiling height (0-700m) depending on wind direction.*

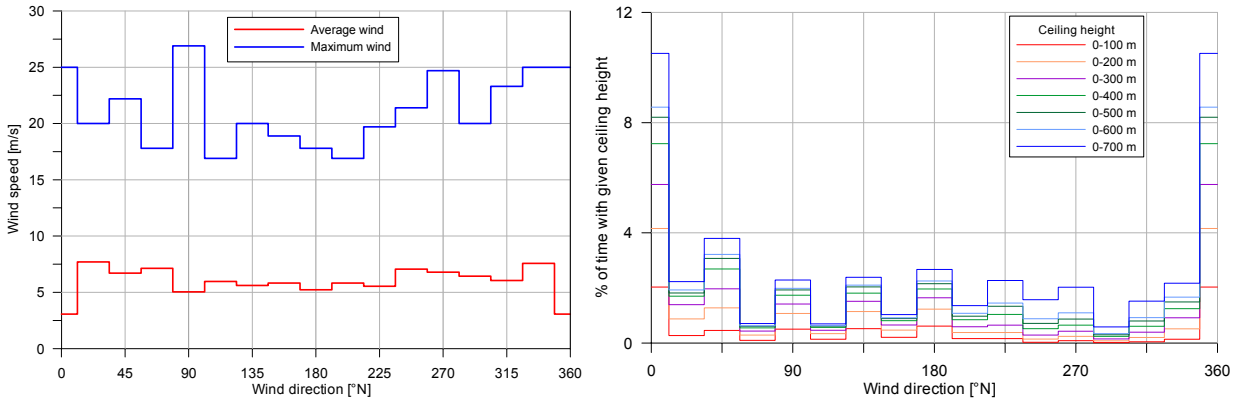

Figure 27. *St.Anthony, wind speed and ceiling height (0-700m) depending on wind direction.*

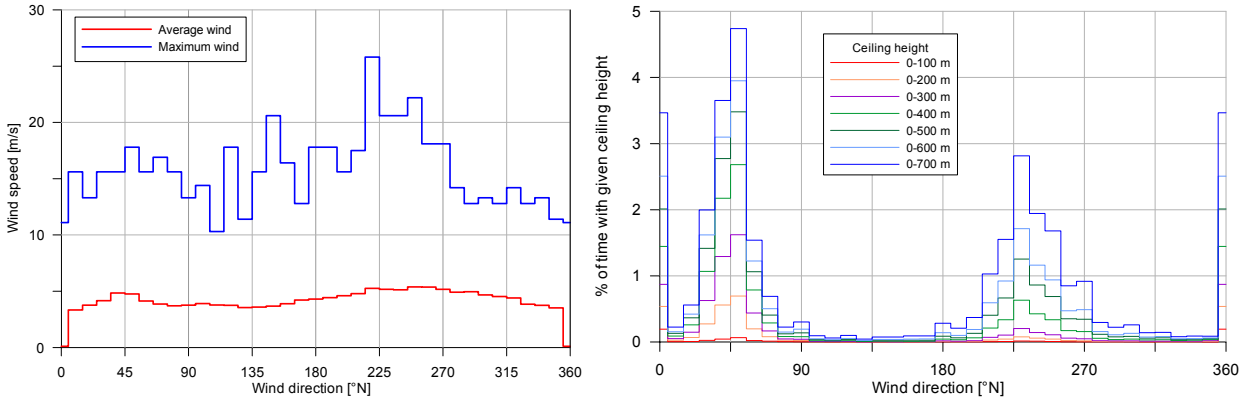

Figure 28. *Dear Lake, wind speed and ceiling height (0-700m) depending on wind direction.*

4.4 Description of parameters used to model test sites 2009-1 and 2009-2

4.4.1 Determination of air temperature

Values of γ_d and γ_w were estimated by comparing observation of temperature and ceiling height at Daniel's Harbour in icing conditions to measurement of temperature at test sites of 2009-1 and 2009-2. The following values were found to be appropriate:

γ_d = 0.0090 °C/m.
γ_w = 0.0065 °C/m.

4.4.2 Determination of wind speed and wind direction

Parameters "a", "b" and "c" used in the analysis are given in Table 5. It is expected that the wind observation at Daniel's Harbour will underestimate wind from the east if only one set of parameters is used for all directions. Therefore, different parameters were used for wind from east when using observations from Daniel's Harbour. The values are gradually converging into the general values when the wind is from north or south, using a cosine function.

Table 5. *Parameters for wind.*

Wind parameter	Test span 2009-1		Test span 2009-2	
	General	Easterly wind at Daniel's Harbour	General	Easterly wind at Daniel's Harbour
a	2	4	1.9	3.9
b	1.2	2	1.19	1.86
c	-0.002	-0.015	-0.0029	-0.0131

Wind direction is taken as observed at the Daniel's Harbour measuring station. When the cylindrical icing model is calculated with horizontal icing direction, i.e. depending on how icing is with respect to span, then a tolerance is used for the wind direction to take into account the uncertainty in actual direction. I.e. wind direction is treated with a tolerance of 20° in each direction.

4.4.3 Determination of liquid water content, ceiling height and droplet number

The following values were used to restrict LWC and droplet size in the model:

- Number of droplets = 100 droplets/cm^3
- Minimum cloud height = 150 m
- Cloud height from east is decreased by 150 m
- Adiabatic reduction factor, alpha = 1.0 for test span 2009-1 and alpha = 0.5 for test span 2009-2. Maximum LWC is restricted to LWC ≤ 0.5 g/m^3
- Reduction of LWC due to cloud amount and cloud opaque is taken as ratio of observed cloud opaque (0 to 1)

Minimum cloud height is used to avoid extreme LWC when clouds are low, i.e. cloud height is increased to the minimum value. Quite many observations from N to W have low ceilings and they are often believed to represent fog or thin water layer.

Reduction of cloud height from east is made since the observation at Daniel's Harbour overpredicts cloud height from that direction. The reduction is gradually decreased to zero in north and south using a cosine function of the angle.

The values of adiabatic reduction factors and maximum LWC were determined after the experiment with the parameters. They were selected to give results close to the observed icing, but so that the model would give a somewhat higher prediction.

These parameters for LWC, ceiling height and droplet number have much influence on the quantity of icing but they have limited influence on the start and end of each icing event.

4.5 Comparison of WObs icing model to measurements in test site 2009-1

The WObs icing model was used with weather observation data from Daniel's Harbour to evaluate the capacity of the model to capture the measured icing in test span 2009-1. The following figure shows comparison between observed icing and the predicted icing by the WObs model.

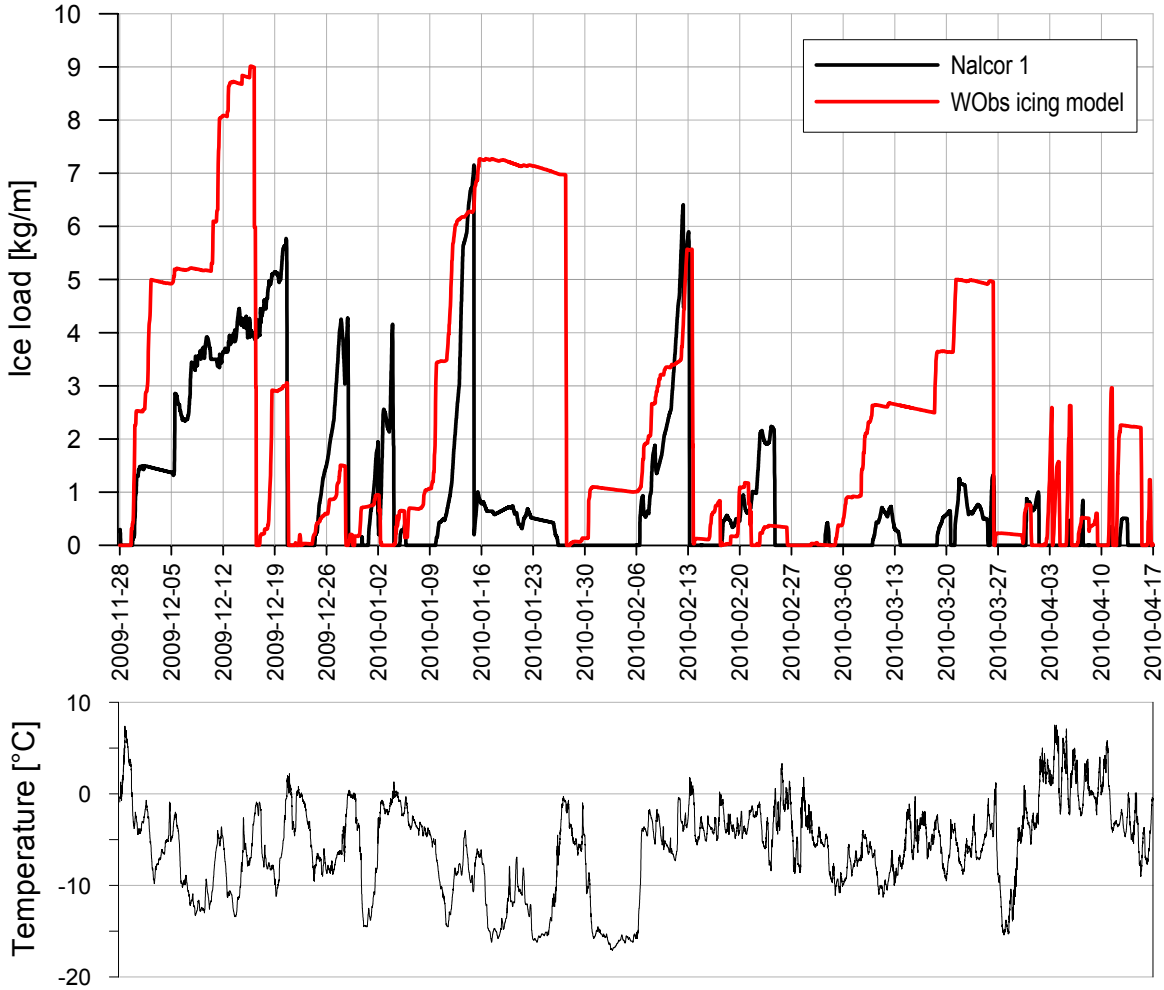

Figure 29. *Comparison between observed icing in* test span *(black) and predicted by WObs model (red).*

The following figures show the three biggest icing events, but all icing events with icing higher than 1 kg/m are given in appendix B.

The measured icing is given by a black line and the icing predicted by WObs model is given by a red line. Measured temperature in test span 2009-1 is given by a blue line, and the wind direction measured at Daniel's Harbour is shown as green dots.

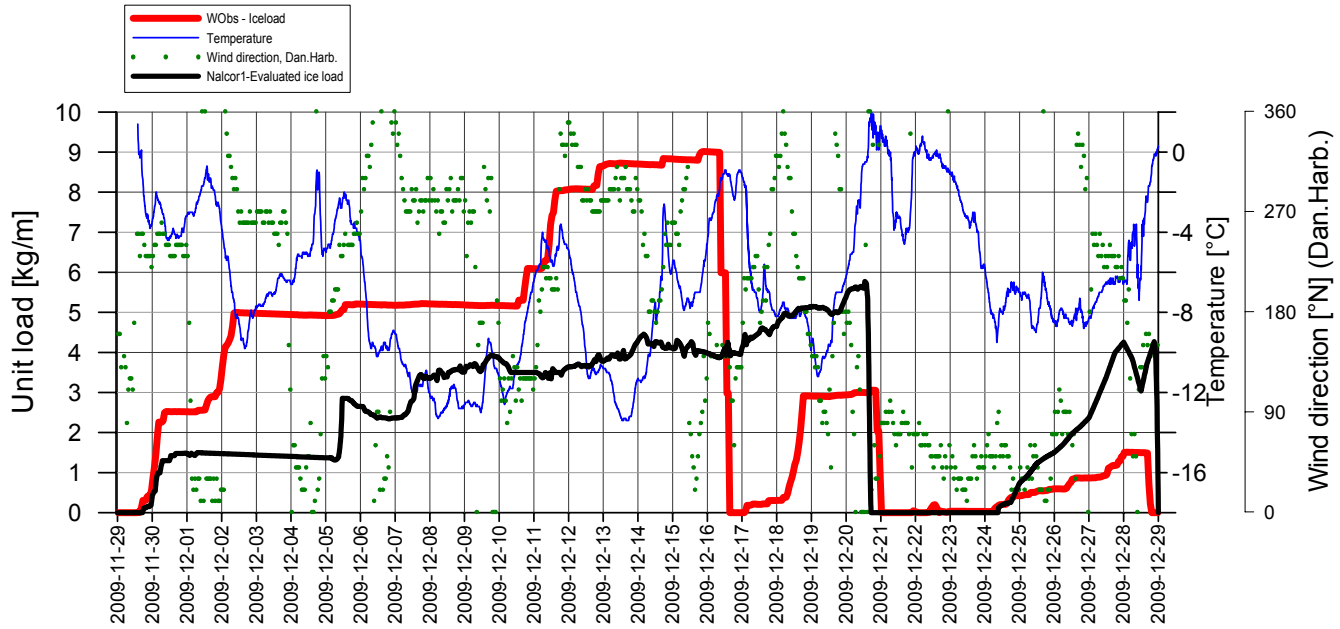

Figure 30. *Icing event 1 (2009-1), comparison between measured icing (black) and predicted by WObs model (red).*

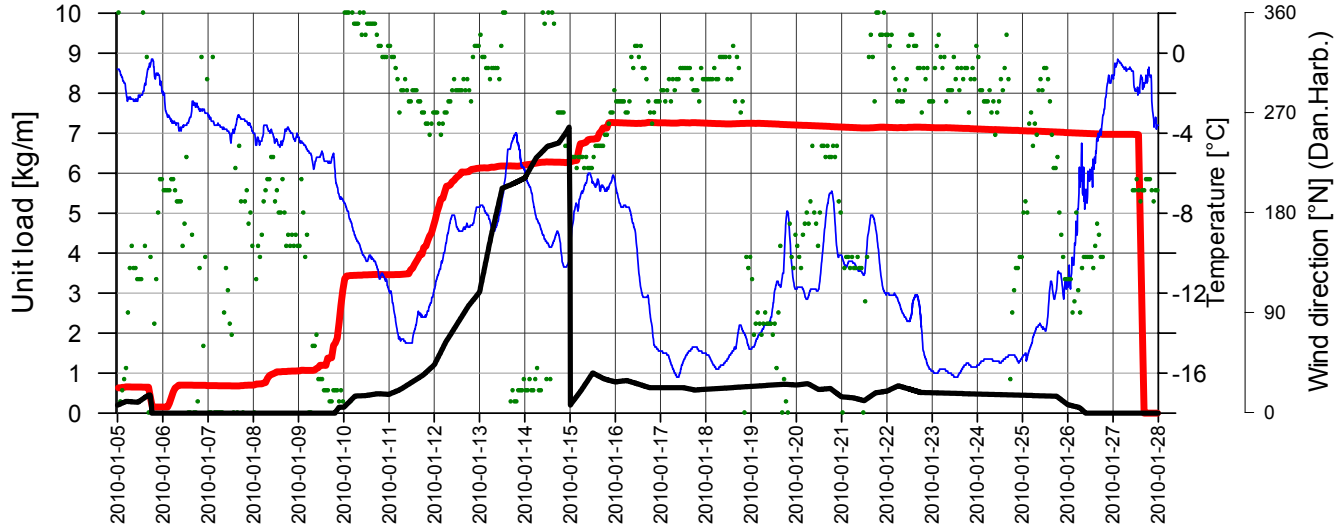

Figure 31. Icing event 4 *(2009-1),* comparison between measured icing (black) and predicted by WObs model (red).

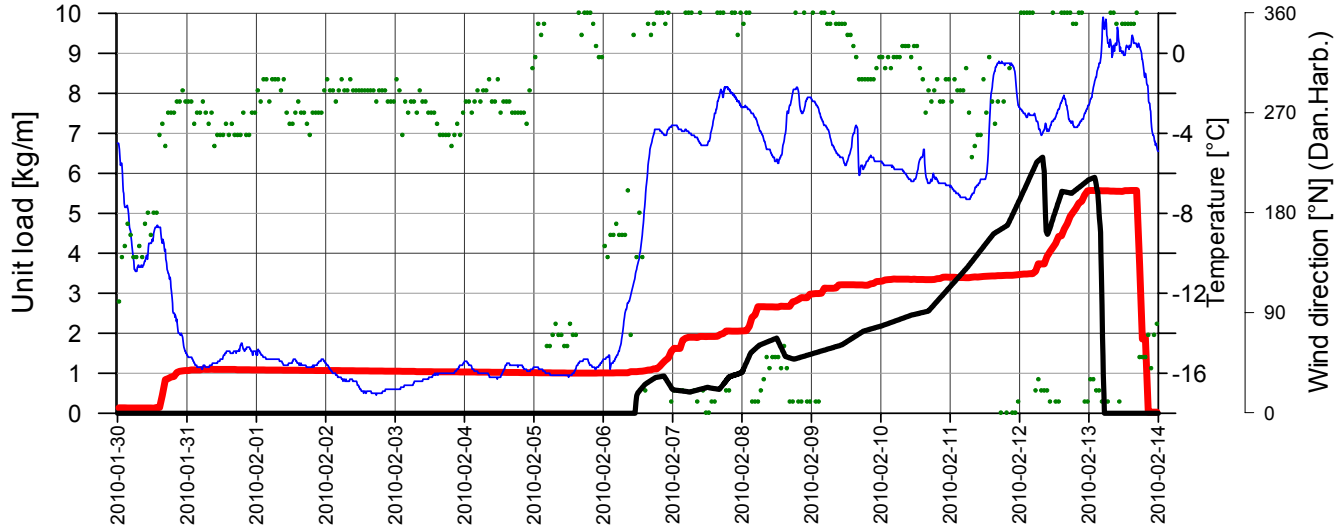

Figure 32. Icing event 5 *(2009-1),*, comparison between measured icing (black) and predicted by WObs model (red).

More complete information regarding comparison and further weather information can be found in Appendix A and Appendix B.

The following remarks can be made from the comparison:

- The WObs model identifies almost all accumulation periods. The main deviation is 2010-01-02 to 2010-01-04 where icing was from the easterly direction.
- The icing rate is generally somewhat higher than measured. In a few cases it seems though to be lower in easterly directions.
- The WObs model predicts some icing events in the range of 1-2 kg/m that are not measured.
- There is some difference when ice shedding takes place. Generally the measurement shows ice shedding before it takes place in WObs model. The main deviation is 2009-12-16 to 2009-12-21 where the WObs model predicts it 5 days before it occurred.
- This comparison is made for ice loading in the range of 0 to 10 kg/m and the length of the icing event within 21 days. It remains to verify how the model compares to measurements when the quantity of icing and duration of icing is well above that.

Generally it can be concluded that the WObs model with observation at Daniel's Harbour captures the icing in test span 2009-1 reasonably well and should be capable to predict historical icing events in the period 1966-2010 using data from Daniel's Harbour. To improve the performance of the model it would be necessary to get better observational data from easterly directions.

4.6 Comparison of WObs icing model to measurements in test span 2009-2

The WObs icing model was used with weather observation data from Daniel's Harbour to evaluate the capacity of the model to capture the measured icing in test span 2009-2. It should be noted that the adiabatic reduction factor is taken as α= 0.5. Figure 33 shows how the WObs model prediction is in relation to the measurements for the whole measuring period. Appendix C shows a closer look at the biggest icing event.

The comparison of the WObs icing model to the measurements in test span 2009-2 reveal similar results as the comparison made in test span 2009-1. The model does capture the accumulation periods and overpredicts icing except in some easterly directions.

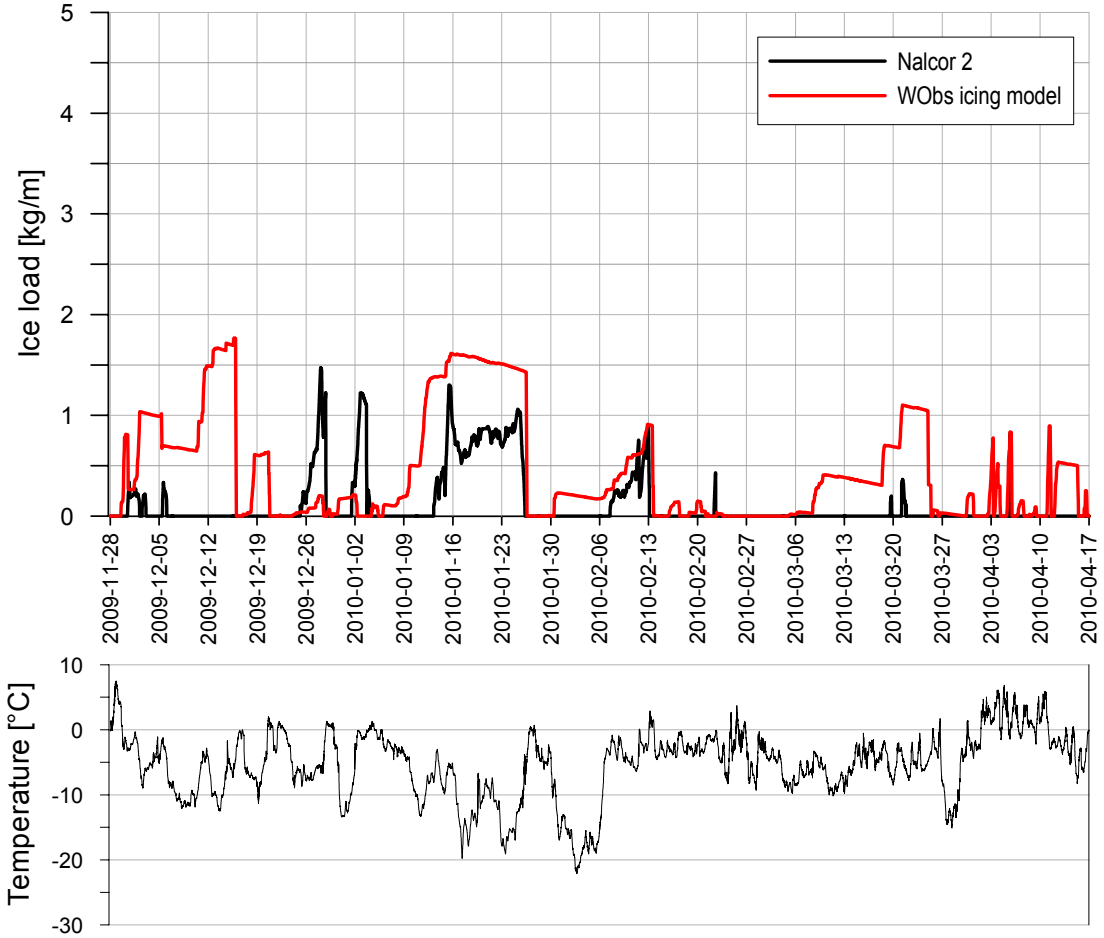

Figure 33. *Comparison between observed icing at test span 2009-2 (black) and predicted by WObs model (red).*

4.7 Comparison between WObs results in test span 2009-1 and icing observations made between 1974-1987

The icing data collection program that was operated from 1974-1987 gives information on ice accumulation at selected locations in the Long Range Mountains. For a short time there were test spans in operation, but observations were mainly of icing on guyed triangular lattice test towers, with section 0.4m·0.4m·0.4m. The towers were not instrumented but were visited regularly, often on a monthly basis. Any ice accretion was measured (thickness) and photographed, and the type of ice and direction from which the ice accreted, was recorded. The initial data registration sheets are not available but main conclusion from each visit is available.

One test span (Inner Pond x=467312E y=5551240N) and two of the tower sites (#2 and #2b) were located in a neighboring area of the test span 2009-1. Tower #2b (x=469620 y=5549616) was around 300 m from test span 2009-1 and tower #2 (x=461712 y=5547734) was located around 6-8 km from test site. Location of tower #2, tower #2b, test span 2009-1 and test span 2009-2 is given in Figure 34.

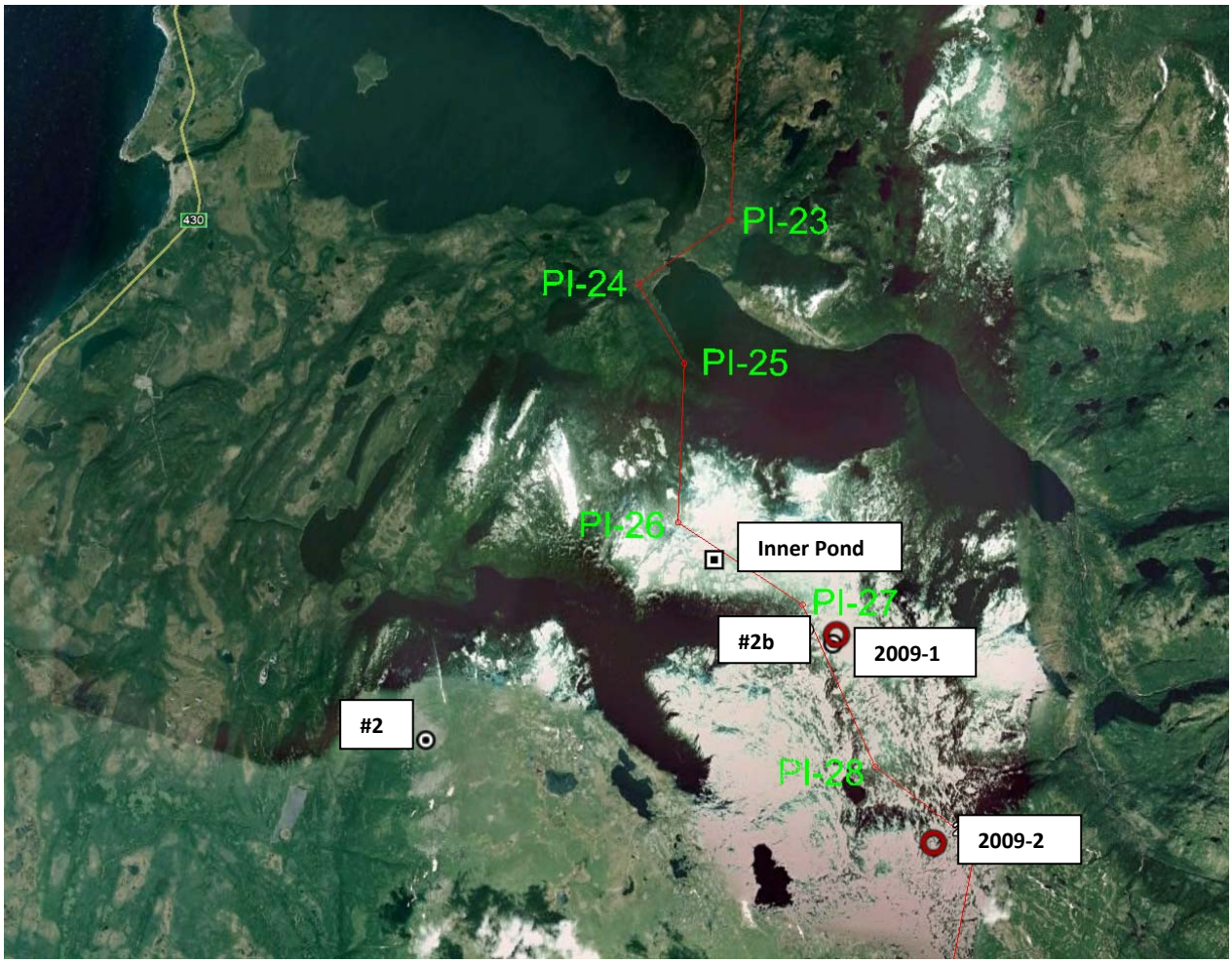

Figure 34. *Location of Inner Pond and test towers #2 and #2b in relation to test span 2009-1 and test span2009-2.*

The following is a comparison made between observed icing at the Inner Pond test span and the location of tower #2 and #2b and icing predicted by WObs at test span 2009-1.

4.7.1 Icing at Inner Pond test span in January 1975

Test line was operated at Inner Pond (test span at site #2 in Ref. 42) from October 1974 to June 1975. It consisted of two 30-foot towers erected approximately 54 feet apart, spanned by a cable 1.338 inches in diameter. An ice rate meter (IRM) that measures increased tension due to ice loading was connected to the cable. At top of each tower there was a Mechanical Weather Station that recorded wind direction, wind run, temperature, and relative humidity.

The IRM'c began service in mid-October, 1974, and the MWS's in mid November, 1974. Measurements were deactivated in June, 1975. Following description is from /Ref. 42/.

> *At site #2 there were 12 periods ranging in duration from 1 to 166 hours when ice accumulations exceeded six pounds per foot of cable (9 kg/m). Maximum amounts occurred at the end of the longest icing period, between January 13-20 (1975), when 14.5 pounds per foot was recorded (21.9 kg/m). On the average, about 540 pounds of ice remained on the cable during the entire period.*

Figure 35 shows the icing calculated by WObs in the period 1974-12-07 to 1975-03-14. It can be seen that the WObs model predict considerable icing in the period, although loading between 13-20 January is lower in the WObs model, 10.3 kg/m compared to measurement 21.9 kg/m. The model has only partial ice shedding on the 1975-01-20 and peak loading is later, 13.7 kg/m. It may be understood that complete ice shedding occurred in test span.

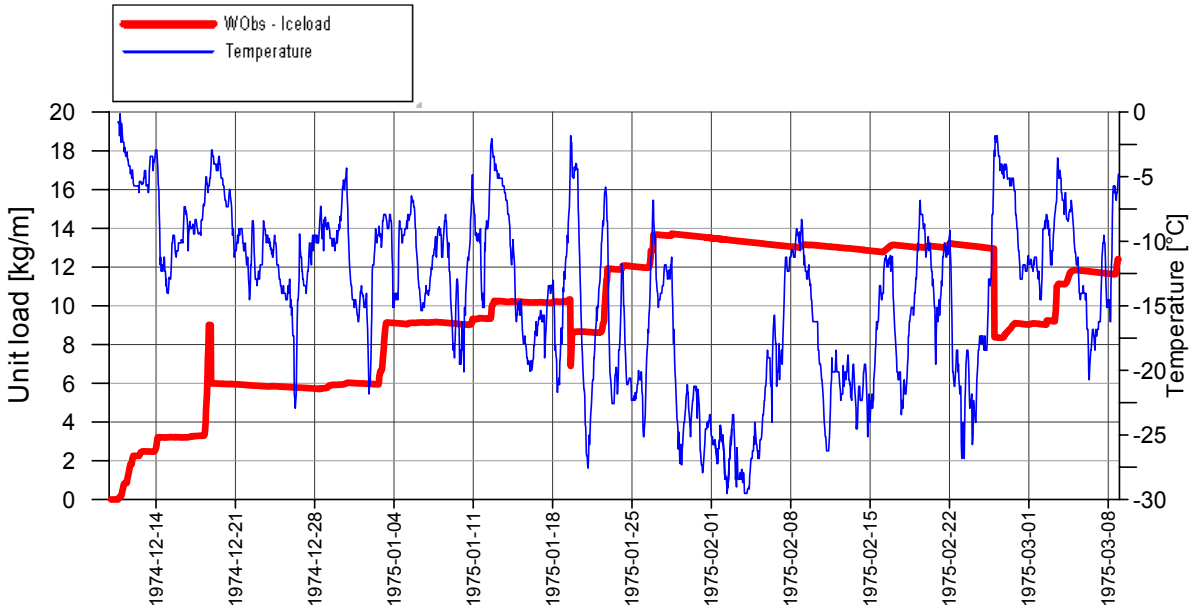

Figure 35. *Icing in test span 2009-1 according to WObs when the Inner Pond test span obtained peak icing loading of 21.9 kg/m in the period 13-20 January 1975.*

4.7.2 Icing on site #2 in December 1976

Figure 36. *Site #2. December 1976. Exact date is unavailable. Maximum icing according to WObs in December was 16.9 kg/m*

The following description was given in /Ref. 26/ of accumulation:

> *Massive accumulation of mixed glaze and rime on tower and guys. 18" tower completely encased and measured 3' wide at 5' above ground and increased to 4' at 10" above ground. ¼" guy wire surrounded by 14" of same mixture. Direction of accumulation: Northwest.*

Figure 37 shows a prediction of icing and temperature in test span 2009-1 in December 1976 along measured wind direction at Daniel's Harbour.

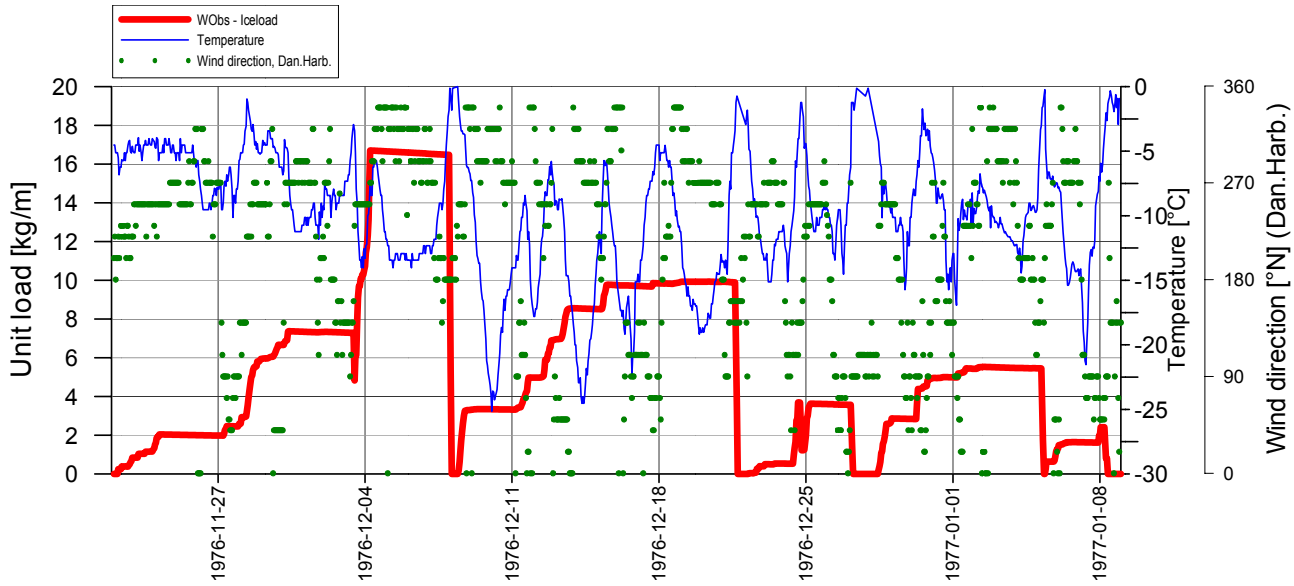

Figure 37. *Icing in test site 2009-1 according to WObs in December 1976 when site #2 experienced big icing.*

The WObs model predicts considerable icing in December 1976. It is unknown when in December the photo was taken. If it was taken in the period December 04-08, then the ice load according to WObs is 16.7 kg/m and the icing direction is from the west or northwest.

4.7.3 Icing on site #2 and #2b in 1980-02-11

Huge icing was observed on towers #2 and #2b during a site visit in February 11, 1980, see the following figures.

The following description was given in /Ref. 28/ of accumulation on the tower at site #2:

> *Hugh deposits of soft rime. Tower completely encased and deposit measuring 3' across at eye level and 4.5 ' at tower top. 1.5-2' wing shaped formation on rods. Direction of accumulation 270°.*

The following description was given in /Ref. 28/ of accumulation on tower at site #2b:

> *Massive deposits of soft rime. Tower completely encased in a deposit of soft rime. 1.5' across at 5' level of tower and 2'-2.5' across at top. Direction of accumulation 270°.*

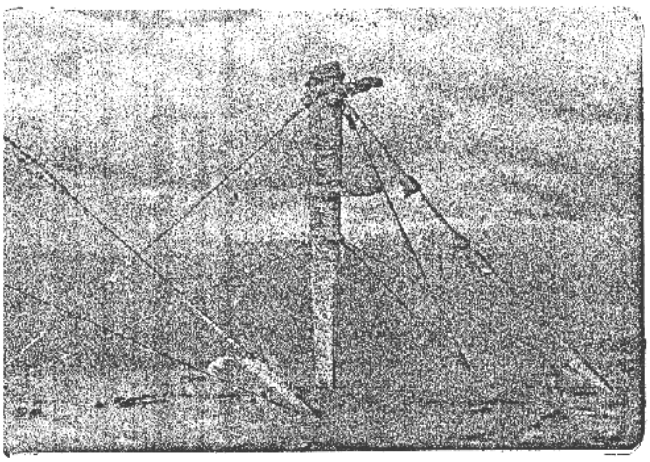

Figure 38. *Site #2. 1980-02-11.*

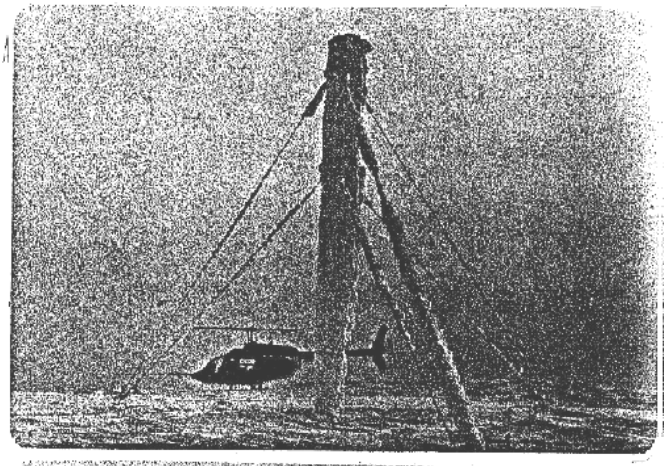

Figure 39. *Site #2b. 1980-02-11. WObs predicts 16.6 kg/m*

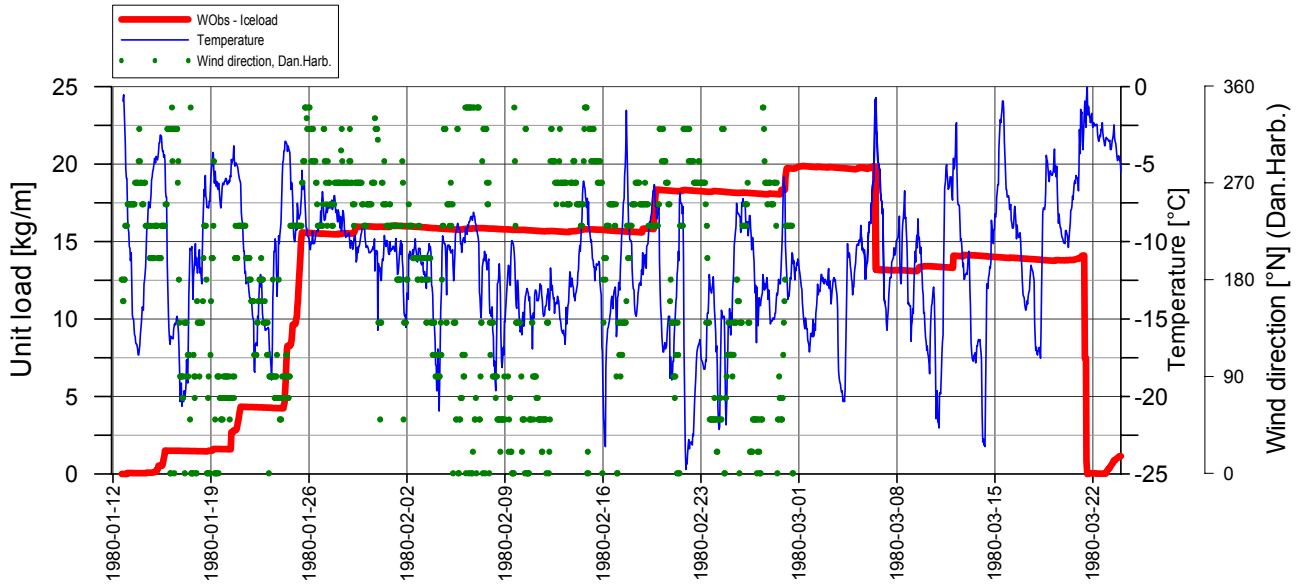

Figure 40. *Icing according to WObs between January-March 1980.*

The WObs model predicts considerable icing (16.6 kg/m) at the time the photos were taken 1980-02-11. The ice accumulation was in January, it may have been accumulating from the east in the beginning but the last 8 kg/m are from the west as given in description.

4.7.4 Icing on site #2 and #2b. Comparison on all available observations

Table 6 gives the icing information available for towers #2 and #2b, i.e. the date of observation, temperature and icing description. Ice weight according to the WObs model is given for comparison. The exact time of inspection within the day is unavailable and the values from the WObs model are taken at 14:00.

The lines in the table are marked with a dark green color when icing is high in observation and/or WObs model. Lines are marked with light green color where there is medium ice and no color is applied to lines with low icing. It is difficult to correlate descriptions of icing on tower to loading in kg/m, which applies especially the later years when shorter description is given than before.

Generally it can be said that there is a good correlation between observations and icing in the WObs model. It especially applies to the extreme icing cases. It should be noted that the WObs model predicts 15.4 kg/m on the 1985-02-12 and 1985-02-13 when no ice was found on the towers. However, it is noted on 1985-02-13 that turnbuckle had failed, thus it is a strong indication of much ice shortly before.

Table 6. *Comparison between predicted icing using WObs icing model and icing observation at towers #2 and #2b from the program that was operated between 1974-1987.*

Date	WObs icing model		Site #2			Site #2b		
	Temp °C	Icing kg/m	Temp. °C	Accumulation noted	Direct. of acc.	Temp. °C	Accumulation noted	Direct. of acc.
1978-11-09	1.1	0	0	Bare		0	Bare	
1978-12-14	-15.1	2.1	-10	Three massive accumulations of rime. Hard rime from NE; medium density rime from SW; soft rime from W. Tower completely enchased.	NE, SW and W	-10	,5" rime from NE covered by soft rime from SW at 5' level of tower leg. 1/4" hard rime on guys covered by 1/4" soft rime	NE, SW
1979-01-18	-18.1	2.1	-22	3" pennant of soft rime formed on guys and tower at 5' level. Accumulation increased	E	-22	Remainents of glase formed by east wind; approximimately 1/4" pennant.	E
1979-02-12	-27.1	4.1	-25	Tower completely encased at top in 12" to 14" of rime; 12" on rods; rime 5" wide and 2" thick	NW, N			
1979-02-21	-13.1	3.1				-14	Tower encased in snow ower rime over glaze approximately 10" thick at tower top; 6" to 7" of rime pennant on guys	N, NE
1979-03-26	7.1	0	7	Bare		6	Bare	
1979-05-09	-1.1	0	4	Bare		4	Bare	
1979-12-20	-15.1	0.1	-15	Large deposits of hard rime on tower and guys. 6"-8" pennants on tower top, 8"-10" pennants on rods, 6" pennants on lower end of guys	W	-15	Some pennants of hard rime on guys measuring 1" at lower end and approx. 3" at top.	W
1980-01-16	-14.8	1.5	-15	Large deposits of hard rime on tower and guys. 9" pennants on lower tower leg, 15" pennants on rods, 6" pennants on guys	SW	-16	5"-6" of hard rime on bottom of tower and 10" at top all covered by soft rime. 6"-8" pennants on guys.	SW
1980-02-11	-12.8	15.7	-12	Hugh deposits of soft rime. Tower completely encased and deposit measuring 3' across at eye level and 4,4' at tower top.	W	-13	Tower encased in a hugh deposit of soft rime. 1,5' across at 5' level of tower and 2'-2,5' across at top.	W
1980-03-29	-4.3	2.7	-4	Trace of glaxe on lower tower leg.	NE	-3	Large deposit of rime ice in 10" to 12" pennants at	NE
1980-04-16	-0.5	0.0	8	Bare		5	Bare	
1980-12-01	-4.6	2.4	-5	,5" rime at 5' level of tower leg, 1" rime over same location	E, W	-6	1,5" to 2" pennants of hard rime at 5' level of tower leg	WNW
1981-01-10	-11.0	2.3	-10	1" pennant of hard rime at 5' level of leg and increasing to 6"-8" at tower top	WSW	-10	Hard rime at 5' level of leg 9" thick and 7" wide	NW, SW
1981-04-13	-5.7	3.4	-5	3" hard rime on tower leg	SW, N	-5	1" hard rime on guy	N, SW
1981-11-25	-4.1	1.0	-4	2"x7" soft rime pennants at 5' level of leg	195°	-4	1" hard rime at 5' level of leg. 1,5" soft rime over hard rime	15, 195
1982-01-07	-8.2	1.0	-8	8"x10" hard rime completely encasing tower at 5' level	225	-8	4"x5" hard rime at 5' level of leg. 6"x8" soft rime at 5' level of leg.	135, 225
1982-02-06	-15.6	29.4		Tower filled with 36" of hard rime at 5' level of	240			
1982-02-18	-24.5	29.5				-24	Tower filled with 28" of hard rime at 5' level of leg	240
1982-03-19	-14.5	3.3	-15	6" hard rime at 5' level of tower leg	240	-15	6" hard rime at 5' level of leg. 2"-3" hoar frost over rime	240
1982-05-04	2.0	0	8	Bare		8	Bare	
1982-12-14	-15.1	2.7	-18	3" soft rime at 5' level tower leg. 4" soft rime guys.	210	-21	2,5" soft rime at 5' level of tower leg. Guys 2"-4" soft rime.	210
1983-01-27	-18.4	3.7				-18	6" rime on tower leg. 3" rime on guys.	210
1983-01-28	-17.5	3.7	-18	1,5" rime on guys	210			
1983-03-02	-3.1	1.9	-4	1/4" glaxe 5' level of tower leg.	210	-10	Bare	
1983-04-05	-1.6	0	-2	3" hard rime	120	-4	6" hard rime	120
1983-05-04	0.9	0		1" pennant glaxe on 5' level of tower leg	120			
1983-05-06	1.6	0				10	Bare	
1983-12-18	-14.8	1.6	0	12" soft rime on 5' level of tower	240	0	2" pennant soft rime at 5' level of tower	240
1984-01-16	-14.1	2.5				-13	2,5" soft rime pennant at 5' tower level	300
1984-01-17	-8.7	2.5	-2	2,5" soft pennant rime at 5' tower level.	300			
1984-02-09	-18.1	4.8	-2	2" pennant rime, glaxe underneath	90	-2	2" rime pennants glaxe underneath	90
1984-03-08	-12.7	3.1	-6	Bare		-2	12" rime	200
1984-04-16	-2.9	0	5	Bare		5	Bare	
1984-05-14	4.9	0	10	Bare				
1984-12-14	-15.1	2.1	-12	12" pendant glaze	225	-12	12" pendant glaze	225
1985-02-12	-10.1	15.4				-9	2" rime on tower	
1985-02-13	-11.2	15.5		Tower is down, failed turn buckle				
1985-03-15	-7.2	1.6				-4	1" rime on tower	
1985-12-12	-9.8	6.0				-10	6" pendant glaze	280
1986-01-17	-14.7	4.8	-10	1" rime	280	-10	1/2" rime	
1985-03-15	-7.3	1.6				-1	3" pendant rime	300
1986-04-27	4.1	0	-1	Trace of rime	7	-1	Trace of rime	
1986-12-12	-11.0	17.0	-12	15" rime on tower		-12	18" rime on tower	
1987-01-22	-15.9	12.9	-25	12" rime on tower		-25	18" rime on tower	
1987-03-12	-15.1	31.1	-11	20" rime on tower		-11	14" rime on tower	
1987-04-16	-3.1	2.1	-3	Bare		-3	Bare	

4.8 Evaluation of historical icing (1966-2010) at test span 2009-1 with WObs icing model

The WObs icing model was used with weather observation data from Daniel's Harbour to predict the historical icing at site of test span 2009-1 in the period of 01 January 1966 to 10 July 2010.

The maximum icing predicted was 50.8 kg/m and it resulted from a very long cold period with continuous icing for 83 days. The maximum accumulation that occurred within a week time was 24 kg/m. Figure 41 shows the size of all icing events above 1 kg/m. Figure 42 shows a distribution of maximum icing and Figure 43 shows the relation between maximum icing and the number of days with continuous icing.

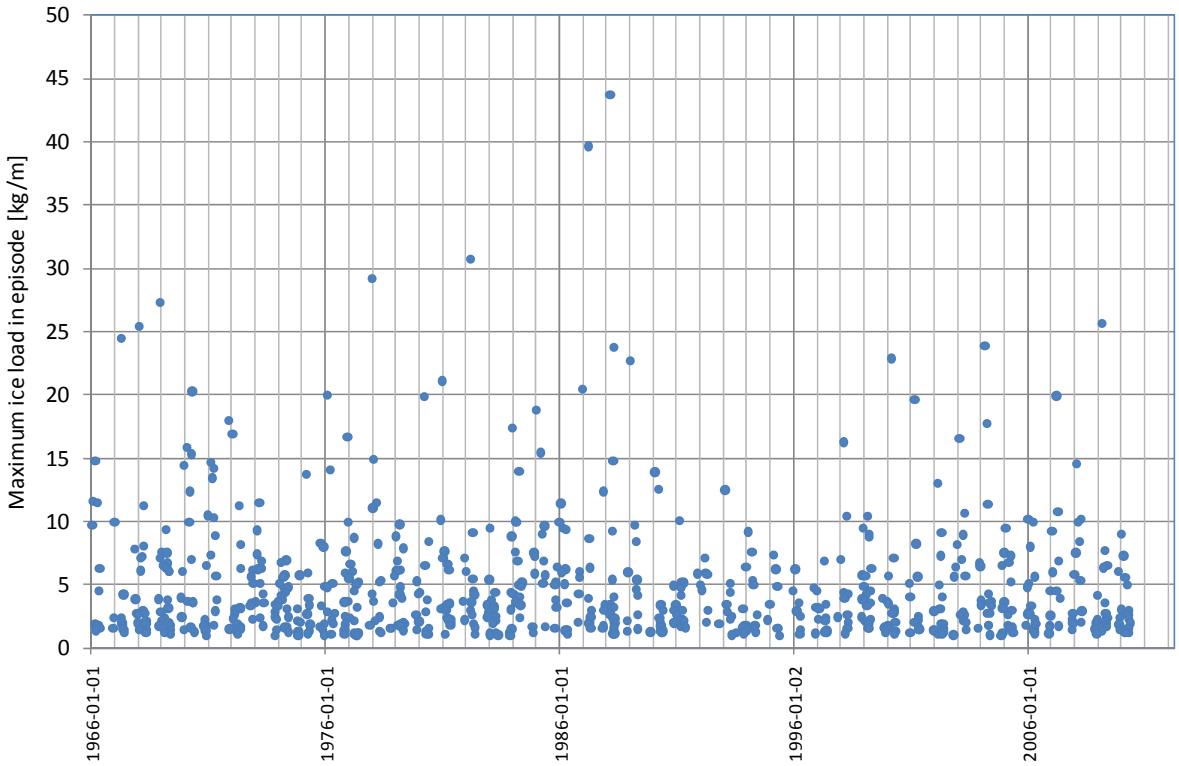

Figure 41. *Icing events at test site 2009-1 between 1966 - July 2010, predicted by WObs model.*

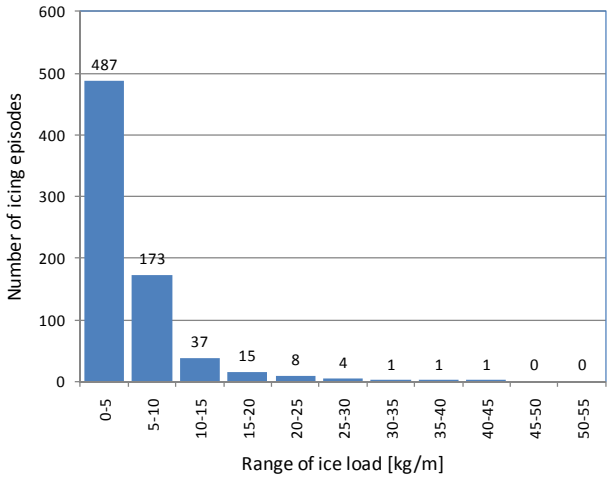

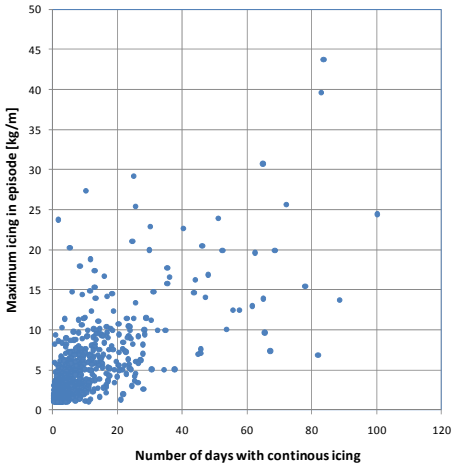

Figure 42. *Distribution of maximum icing in events.* Figure 43. *Max. icing in relation to days with icing.*

Table 7 shows all icing events with icing above 15 kg/m. It is important to note that many of the icing events are within the period when the icing data collection program operated test towers, in 1977-1988. Comments are made in the table when towers #2 and #2b were visited and there is a brief description of the observed

icing. The visits of towers #2 and #2b confirm that heavy icing was ongoing in all cases although it is difficult to compare description of icing on a tower to a unit ice weight on a 30 mm conductor.

Table 7. *Maximum icing events between 1966-July 2010 and site information from tower #2 and #2b.*

Number of event	Max icing [kg/m]	Number of days with icing [days]	Start of icing	End of icing	Visit of tower #2 and/or #2b	Acccumulation noted
1	43.7	83.6	1987-12-02	1988-02-23	1987-01-22 and 1987-03-12	1987-01-22 was 12" icing on #2 and 18" on #2b, 1987-03-12 was 20" on #2 and 14" on #2b
2	39.6	82.9	1986-12-26	1987-03-19		
3	30.7	64.9	1982-01-06	1982-03-12	1982-02-06 and 1982-02-18	1982-02-06 Tower #2 filled with 36", 1982-02-18 tower #2b filled with 28".
4	29.2	24.9	1977-11-27	1977-12-22		
5	27	10	1968-12-06	1968-12-16		
6	25.7	72.1	2008-12-17	2009-02-27		
7	25	26	1967-12-30	1968-01-24		
8	24.4	100.1	1966-12-31	1967-04-10		
9	23.9	51.1	2003-12-31	2004-02-20		
10	24	2	1988-04-19	1988-04-21		
11	22.9	30.1	2000-01-27	2000-02-28		
12	23	40	1988-11-29	1989-01-08		
13	21.1	24.6	1980-12-06	1980-12-31		
14	20.5	46.2	1986-11-10	1986-12-26	1980-01-16 and 1980-02-11	1980-01-16 Large deposit 9-15" on #2. 5-6" on #2b. 1980-02-11 Hugh on #2 range of 3'-4.4'. Large on #2b, 1.5'-2.5'.
15	20.3	5.3	1970-04-19	1970-04-24		
16	20.0	29.8	1975-12-23	1976-01-22		
17	19.9	52.4	2007-01-21	2007-03-14	1986-12-12	15" on #2 and 18" on #2b.
18	19.9	68.5	1980-01-13	1980-03-21		
19	19.6	62.4	2000-12-21	2001-02-21		
20	18.8	11.7	1984-12-13	1984-12-25	1984-12-14	12" on #2 and #2b. Tower #2 were next visited 1985-02-13 when turnbuckle had failed, ice?
21	18	8	1971-11-12	1971-11-20		
22	17.7	35.4	2004-02-20	2004-03-27		
23	17.4	12.9	1983-12-16	1983-12-29		
24	16.9	47.9	1971-11-27	1972-01-14	1983-12-18	12" on tower #2 and 2" on tower #2b
25	16.7	15.9	1976-11-22	1976-12-08		

Figure 44 shows how the WObs model predicts ice accumulation rate (kg/m/hour) depending on wind direction. The values are for the horizontal span model and therefore the influence of span direction (330°N) is strong. Peak accumulation rate is in directions perpendicular to the span, approx. 240°N and 60°N. High accumulation rate is both from the NE directions as well as the SW directions. The highest accumulation rate is around 2 kg/m/hour.

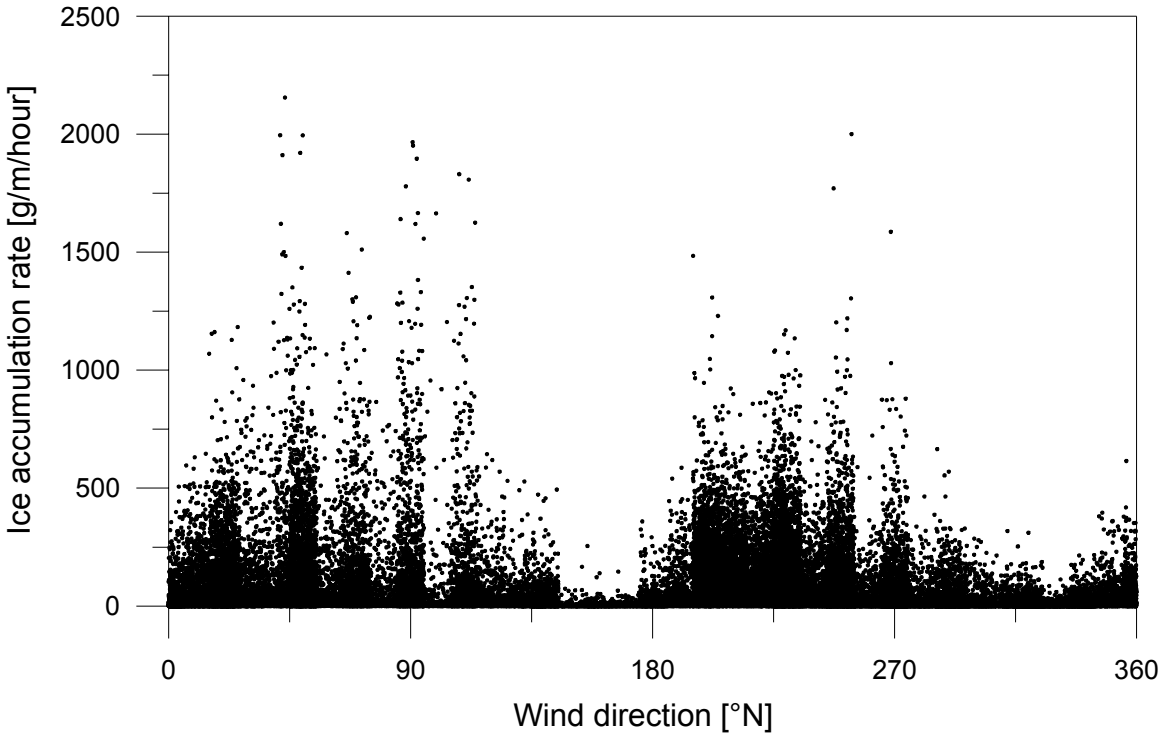

Figure 44. *Predicted accumulation rate [g/m/hour] at test site 2009-1 depending on wind direction.*

Some of the biggest icing cases are presented in the following figures, they show predicted ice accumulation (red line), temperature at site (blue line) and wind direction (green dots) measured at Daniel's Harbour.

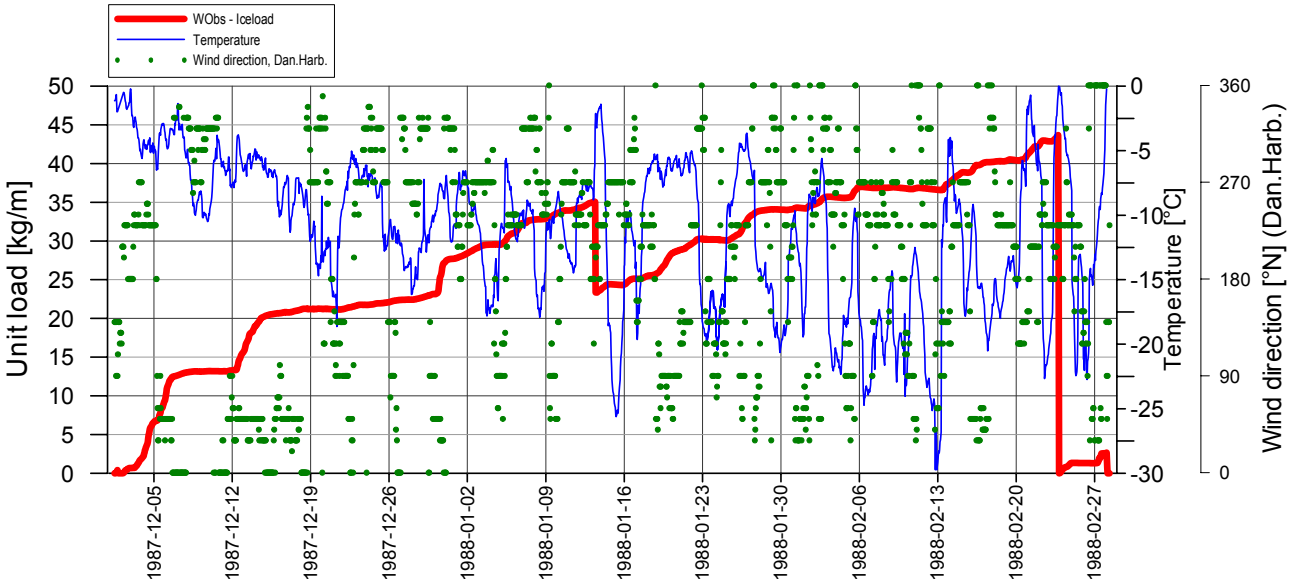

Figure 45. *Icing event according to WObs with the highest loading during the period 1966-July 2010. Test towers #2 and #2b were visited 1987-01-22 and 1987-03-12.*

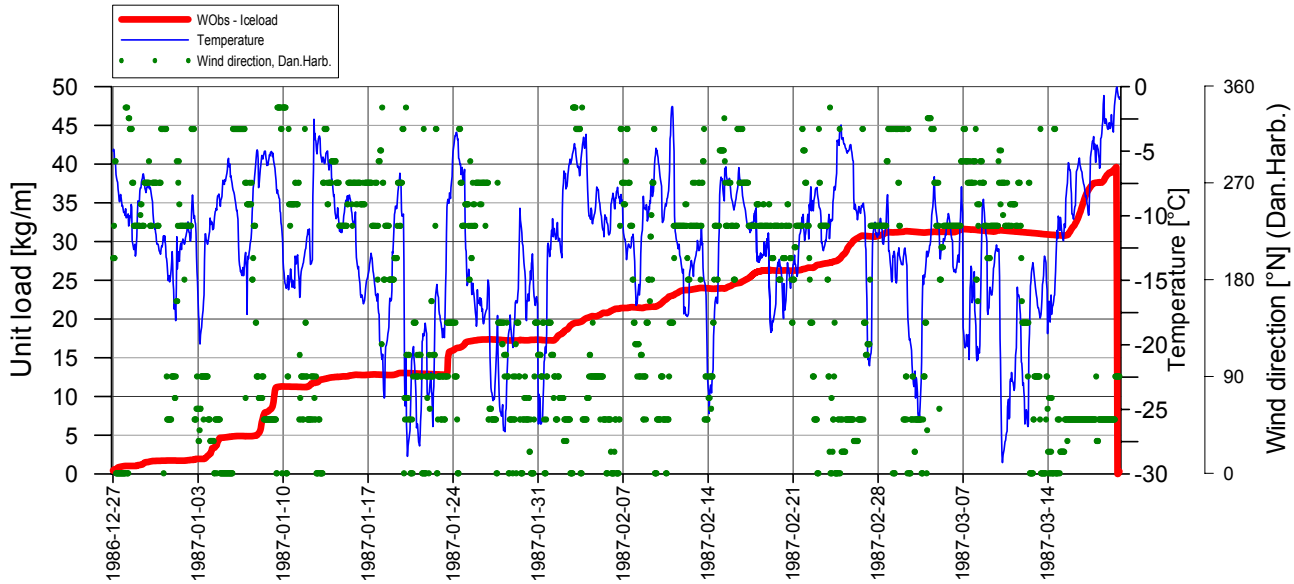

Figure 46. *Icing event according to WObs with the second highest loading during the period 1966-July 2010.*

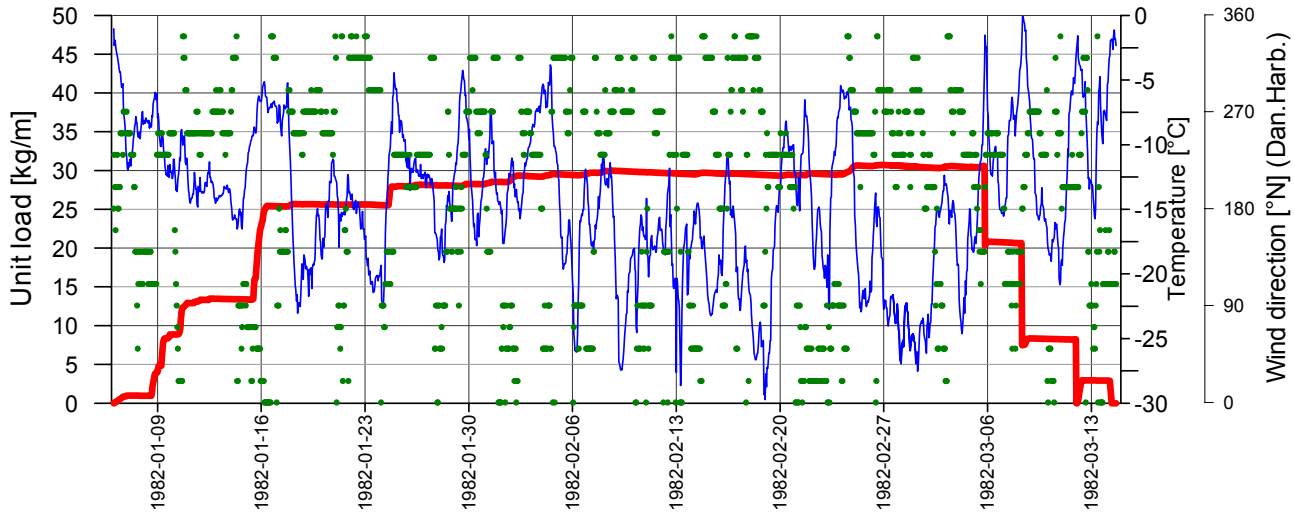

Figure 47. *Icing event according to WObs with the third highest loading during the period 1966-July 2010. Test towers #2 and #2b were visited 1982-02-06 and 1982-02-18.*

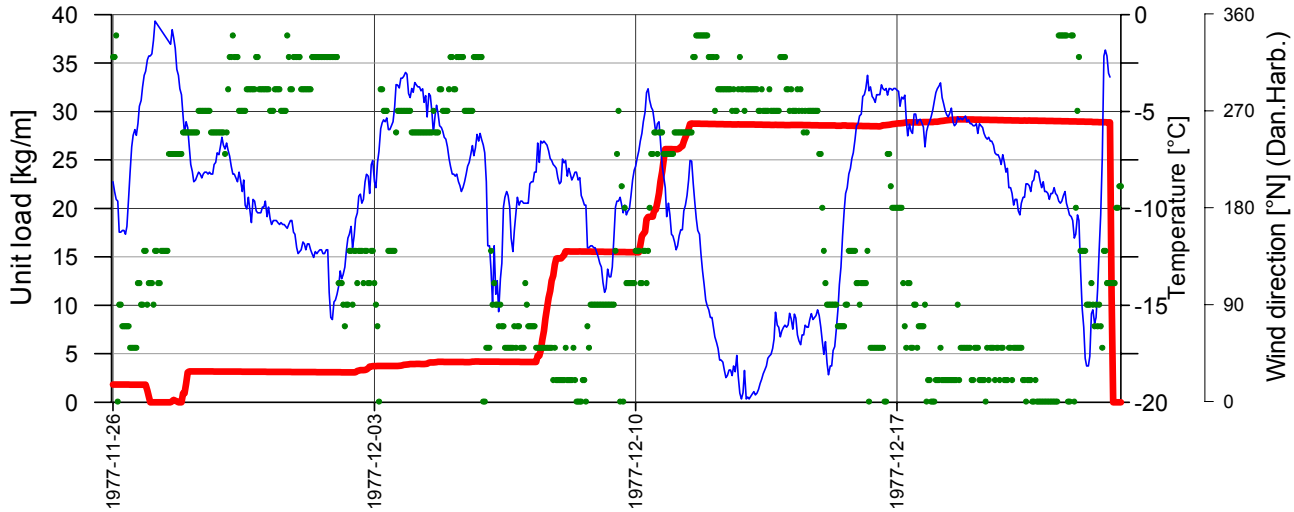

Figure 48. *Icing event according to WObs with the fourth highest loading during the period 1966-July 2010.*

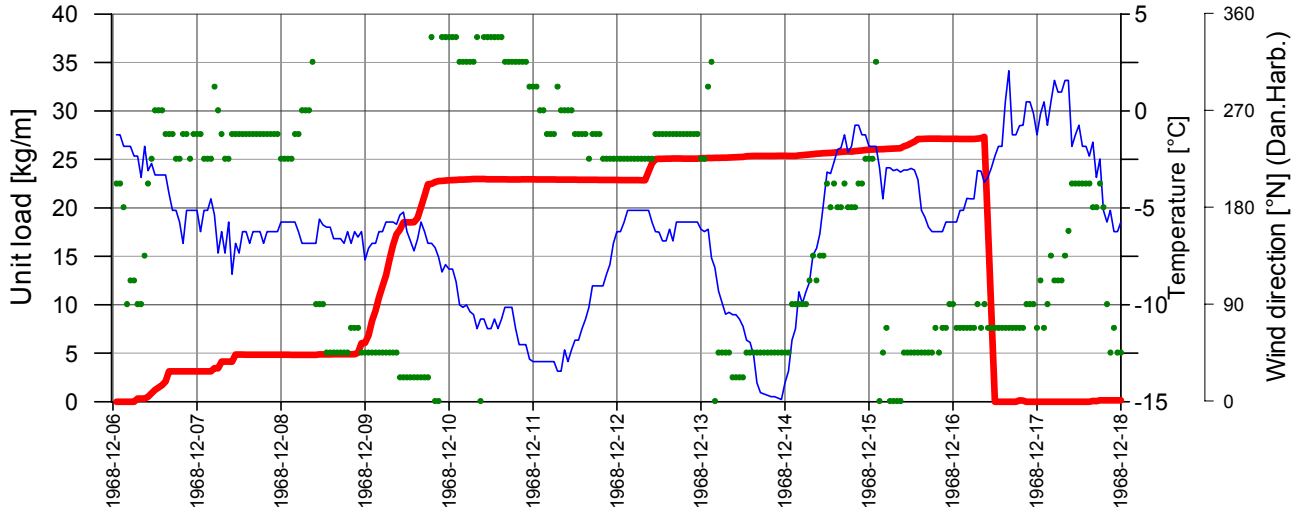

Figure 49. *Icing event according to WObs with a rapid accumulation, and the sixth highest loading during the period 1966-July 2010.*

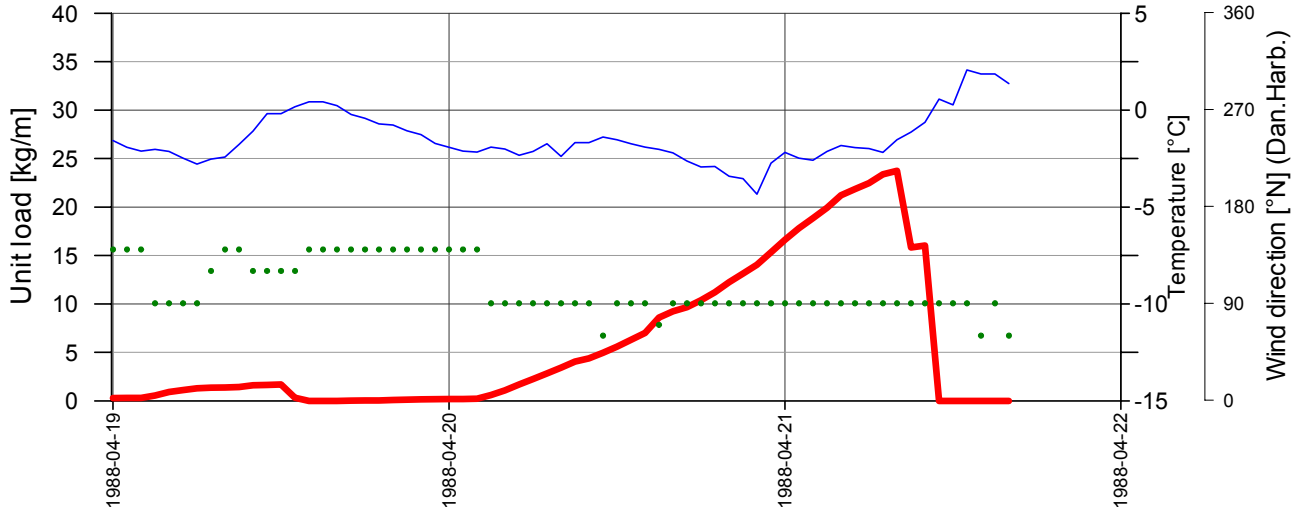

Figure 50. *Icing event according to WObs with rapid accumulation and a short duration, and the tenth highest event.*

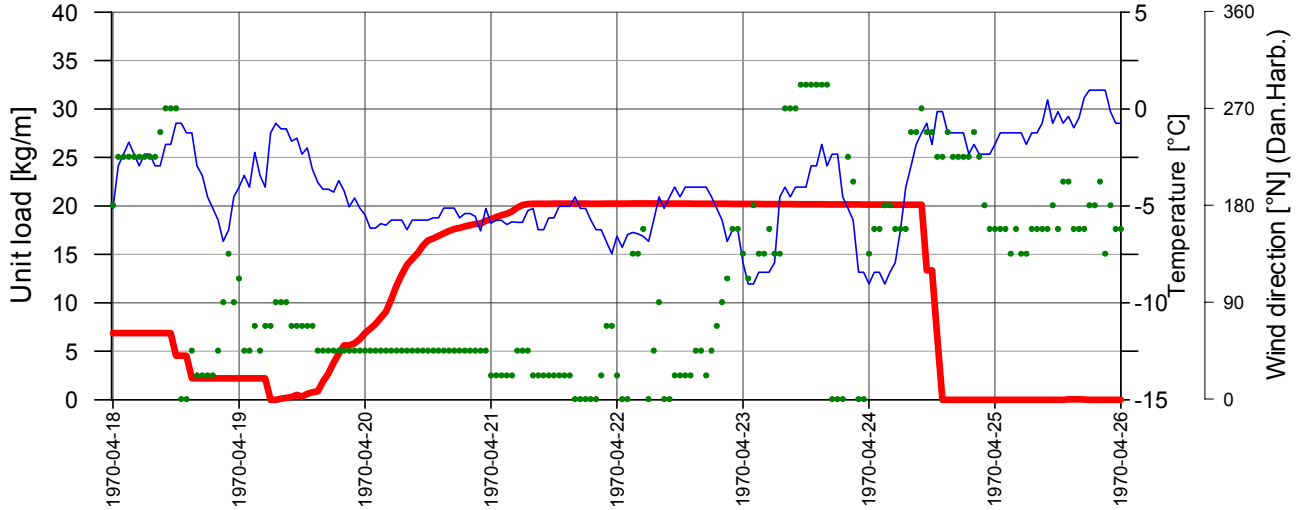

Figure 51. *Icing event according to WObs with a large accumulation from the NE, and the nineteenth highest event.*

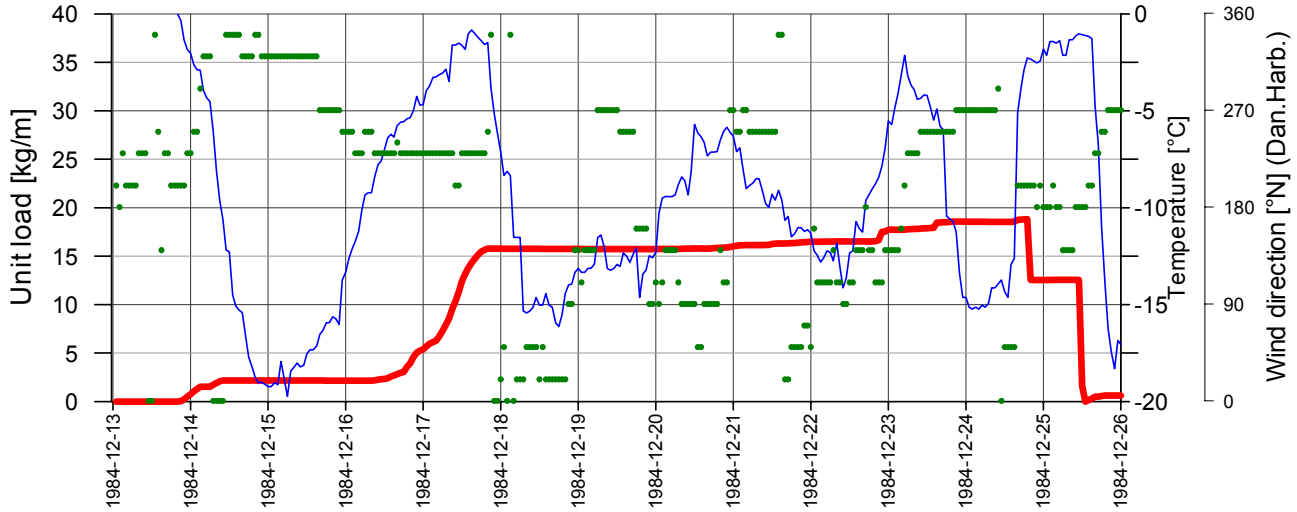

Figure 52. *Icing event according to WObs with the 20th highest loading during the period 1966-July 2010. Test towers #2 and #2b were visited 1984-12-14. Turnbuckle had failed in next visit at 2# 1985-02-13.*

The following remarks can be made from the evaluation of historical events:

- Observations of icing on test towers #2 and #2b during the period 1977-1987 confirm that many of the biggest events and correspond with the results.
- The winter of 2009-2010 when measurements took place in test span 2009-1 did not include large in-cloud icing events compared to the period of 1966-2010.
- Moisture from the east gives in many cases big accumulation, see for example 1970-04-20 when 20 kg/m accumulates in 1.5 day and 1988-04-20 and 1968-12-09. The accuracy of model should be much better in predicting icing from the west. The accuracy of the model to predict icing from the east should be further evaluated.
- The biggest events should be evaluated more closely, looking at weather observed at other weather stations.
- The maximum accumulation within 1 to 2 days is in range of 20-25 kg/m.
- The biggest icing events comes from long lasting cold weather with repeated accumulation. Ice shedding might be underestimated in the model in these cases.
- The cylindrical icing model is out of its range when icing is above 15-20 kg/m when the accretion coefficient α_1 is out of its range. There is a question about the accuracy above these values.
- If icing in the range of 12-20 kg/m will be measured in test span 2009-1 in ongoing measurements, it is important to verify it with the model.

4.9 Extreme value calculation of icing

4.9.1 Extreme icing in test span 2009-1 and test span 2009-2

The WObs model was used to calculate in-cloud ice load with 25, 50 and 150 year average return period in test span 2009-1 and test span 2009-2 using data from Daniel's Harbour, see Table 8. The model is as previously described based on horizontal rotating cylinder model with fixed orientation. It is assumed that the diameter of the conductor is 30 mm and the height of the object is 10 m above the ground.

The different return loading is evaluated based on the assumption that loading follows Gumbel distribution. The parameters of the distribution are evaluated using the Probably Weighted Moments approach.

Table 8. *In-cloud icing in test spans 2009-1 and 2009-2 with 25, 50 and 150 year average return period.*

Test span	Height above sea level [m]	Return loading [kg/m]		
		25 years	50 years	150 years
2009-1	600	35	40	47
2009-2	530	8	9	11

4.9.2 Icing at 400 m and 600 m above sea level, 50 year return period

The WObs model was used to calculate in-cloud ice load with a 50 year return period at 400 m altitude above sea level and 600 m above sea level, using four different weather stations, see Table 9. The weathers stations used were: Daniel's Harbour, Twillingdale, Dear Lake and St. Anthony.

The WObs model was analyzed using the vertical rotating cylinder model approach using the same input parameters for all stations, i.e. no special correction was made on wind speed or cloud height as was previously done for easterly directions when test spans 2009-1 and 2009-2 were analyzed based on observations at Daniel's Harbour. The following input parameters were used.

- Number of droplets = 100 droplets/cm^3
- Lapse rate for temperature; γ_d = 0.0090 °C/m and γ_w = 0.0065 °C/m.
- Parameters for wind speed at 400m above station; a=1.0, b=1.15, c=-0.001
- Parameters for wind speed at 600m above station; a=2.0, b=1.20, c=-0.003
- Minimum cloud height = 150 m above sea level
- Adiabatic reduction factor (alpha) = 1.0
- Maximum LWC is restricted to LWC ≤ 0.5 g/m^3
- Reduction of LWC due to cloud amount and cloud opaque is taken as the ratio of observed cloud opaque (0 to 1)
- Conductor diameter = 30 mm
- Height of conductor above ground = 10m
- Icing model: WObs with vertical rotating cylinder

Table 9. *Estimation of in-cloud ice loading on a 30 mm conductor with 50 year average return period.*

Source of data	Height of weather observation [m a.s.l.]	Length of data measurements [Years]	50 year return period [kg/m]	
			400 m a.s.l.	600 m a.s.l.
Daniel's Harbour	19	45	13	33
Twillingdale	92	13	17	54
Deer Lake	21	40	3	13
St. Anthony	30	12	19	114

The vertical cylindrical model gives higher loading than the horizontal model, since it collects icing from all directions. The return value at Daniel's Harbour is lower at 600 m altitude than predicted at 2009-1 since assumptions on wind speed and cloud height are different.

Loading at Twillingdale is considerably higher than at Daniel's Harbour, this is due to a high frequency of low clouds from N to NE and a higher wind speed at Twillingdale, around 16% higher.

Observation from St. Anthony gives the highest estimated 50 year loading. This seems logical, considering the location of this station on the NE tip of the Northern Peninsula. However, a factor of six from 400 to 600 m

may seem unrealistic. Further study is needed on the observations from St. Anthony before it can be concluded that the WObs model estimate is reliable for the area.

The evaluation of ice loading at the 400 m level needs to be used with caution since the model uses adiabatic reduction factor = 1.0 and assuming also that an exposed area where maritime air enters the area, forming fresh clouds on the windward side of the mountain. Probably no part of the line route passing the Long Range Mountain can be assumed to be in that type of area.

4.10 Evaluation of combination of wind and in-cloud icing in test span 2009-1

The combined wind and ice loadings related to wind on ice-covered conductors is of importance for the mechanical design of conductors and towers. Usually the statistics of wind speed during the ice presence on conductors are unknown and approximations are made for the combinations. IEC 60826 specifies the following load conditions for supports:

(i) Highest value of ice load to be combined with average of yearly maximum wind speed during ice persistence.

(ii) Highest value of wind speed during ice persistence to be combined with average of yearly maximum ice loads

In the WObs model an estimation of the wind speed and the ice load is known and can be used to generate the combined loadings of ice and wind corresponding to the selected reliability level. Figure 53 shows combination of wind and ice at test span 2009-1 for the period of 1966 to 2010. Values of wind and ice are scaled with the highest value in the period.

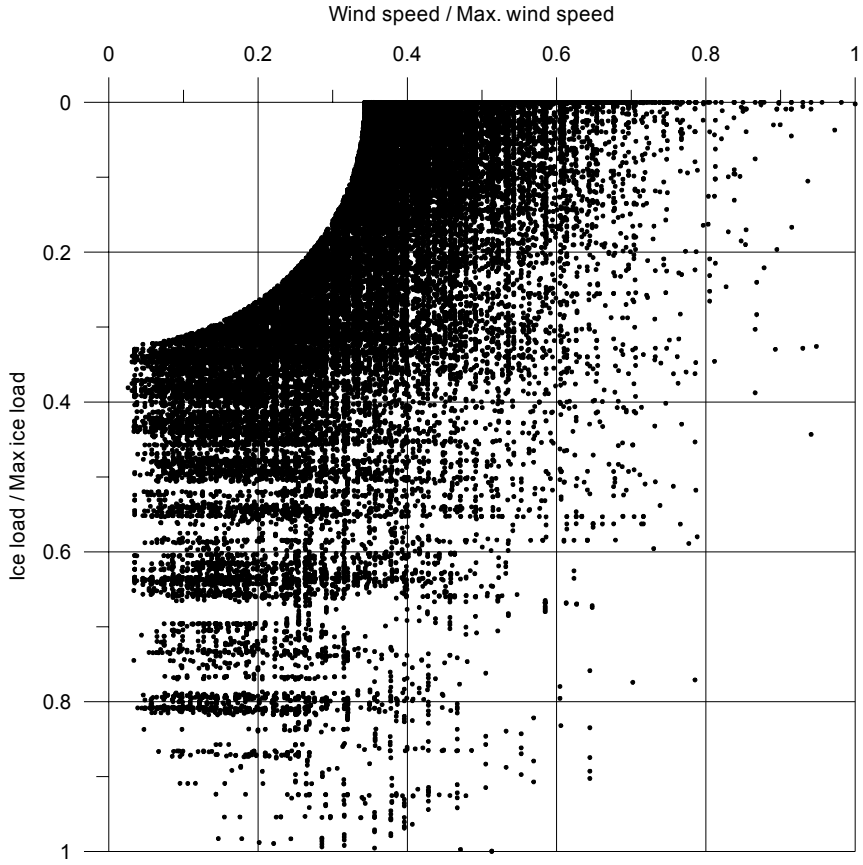

Figure 53. *Combined wind and ice loading in test span 2009-1.*

Figure 53 shows that it can be expected to have considerable wind combined with the maximum ice load, it may be around 50% of the maximum wind load with the same return period. The relative high combination of wind speed and ice is due to the long time ice stays on conductors each winter.

5 WRF icing simulation for the LRM

5.1 Selection of simulations

The WRF model is described in Chapter 3.3.

Based on the measurements from test span 2009-1 and test span 2009-2, together with review of current weather situations, three time periods were simulated with the WRF model:

1. Test span 2009-1, Icing event #3 2010.01.02 00:00 – 2010.01.04 12:00
2. Test span 2009-1, Icing event #4 2010.01.13 00:00 – 2010.01.16 00:00
3. Test span 2009-1, Icing event #5 2010.02.10 00:00 – 2010.02.13 12:00

For each of these three cases "top views" of the inner domain (Domain 4) in the Google Earth presentations are shown for 1) Maximum wet snow load and 2) Maximum rime ice load. Colour bars are in kg/m in both cases.

In addition screen dumps are shown looking from ENE towards WSW and the Gulf of St. Lawrence. The Gulf is shown on the top of each picture. All pictures are from the inner domain (Domain 4) of the WRF simulations.

5.2 Test span 2009-1, icing event 3: 2010.01.02 00:00 – 2010.01.04 12:00

In this case the prevailing wind direction at Daniel's Harbour was from the NE. The distribution of accumulated precipitation, wet snow load, rime ice load and maximum wind speed are shown in Figure 54. It is seen here that most of the precipitation (upper left picture) have occurred on the eastern side of LRM, and that a minimum appears over the higher part of the line route between PI 26 and PI 27. A new maximum appears over the high coastal mountains near the Gulf of St. Lawrence.

The potential wet snow load accumulated on a vertical cylinder (upper right picture) shows that the higher area towards the NE are prone to some wet snow in this case. Over the high areas along the line route the snow is too dry to give significant wet snow. However, south of PI 30 some wet snow load in the order of 3-4 kg/m is likely to occur.

In this case the risk of highest rime ice loads (lower left picture) is on the high mountains on the western side of the peninsula, as more than 10 kg/m may accumulate on the highest and most exposed tops. It also appears that the area around PI 27 can be at risk if the elevation of the conductors is close to the mountain ridge on the eastern side. As long as the line is placed down in the valley it should be here. It is also seen that a main valley further east is totally safe for rime icing in this case.

The last picture (lower right) shows the highest 10 minute average wind speed during this episode. It can be seen that on the highest tops on the western side the wind speed was higher than 30 m/s, while the highest wind speeds along the line route was close to 25 m/s around PI 27. Down in the major valleys the wind speed was less than 10 m/s.

After the simulation started the predicted ice load corresponds well with measurements during the first 18 hours. During the 3rd of February, the model overestimates the icing intensity in a period with winds from E and NE. Maximum predicted ice load (on a vertical cylinder) is 12 kg/m while the measured value on the test span stops at 4 kg/m. The timing of the start and end of the icing event are recognized quite well in the model.

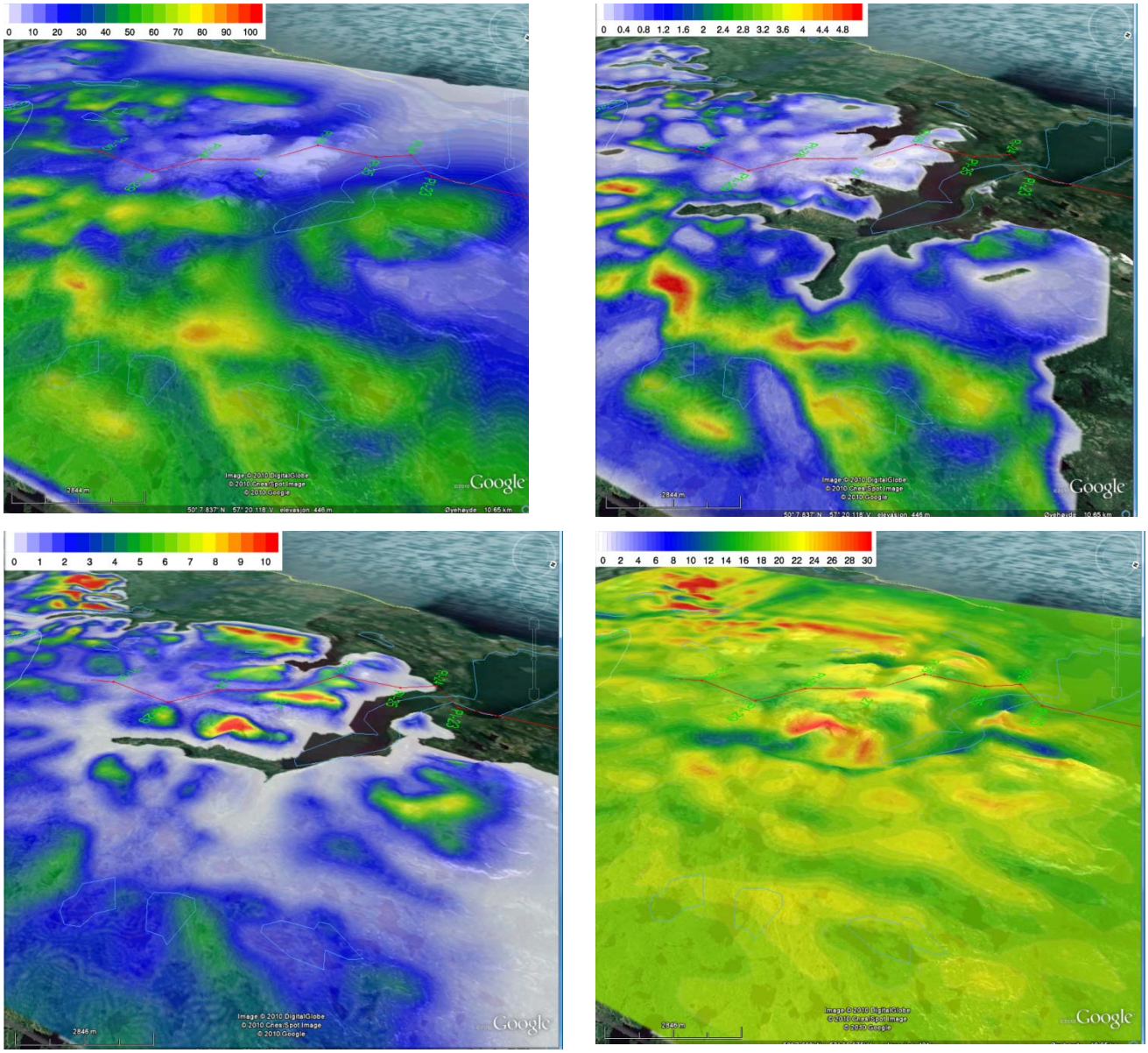

Figure 54. *2010.01.02. 00:00 – 2010.01.04 12:00. Upper left: Accumulated precipitation [mm]. Upper right: Wet snow load [kg/m]. Lower left: Rime ice load [kg]. Lower right: Maximum wind during this episode [m/s].*

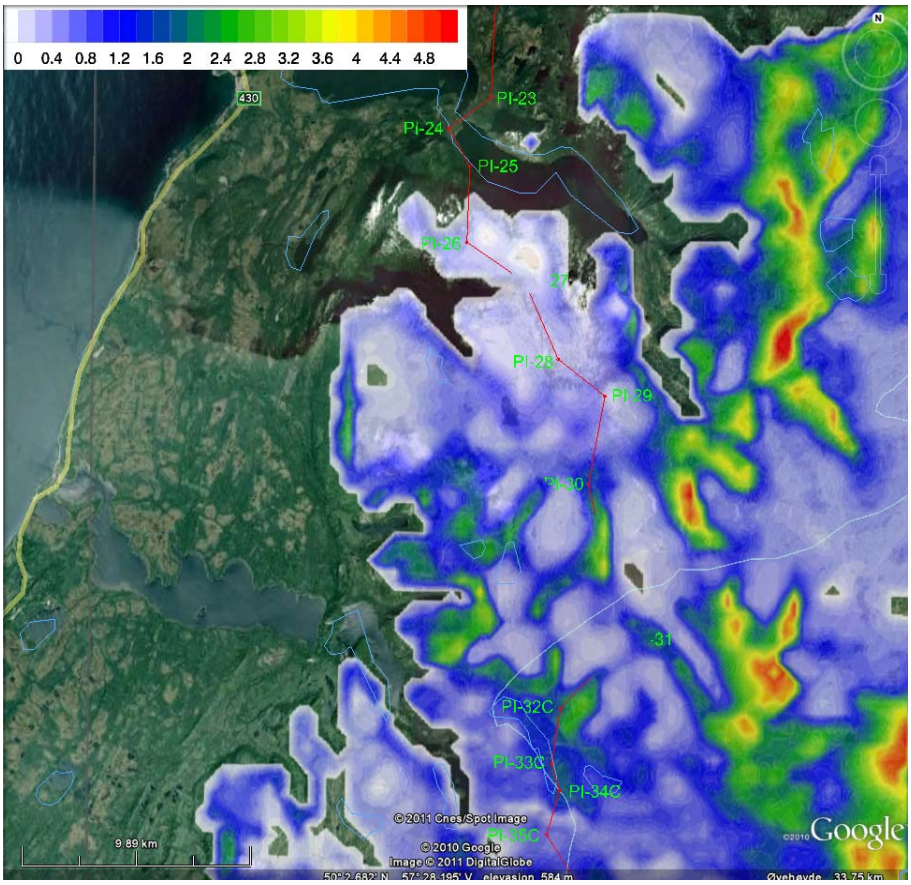

Figure 55. *Wet snow load (colour bar in kg/m) for 2010.01.02 00:00 – 2010.01.04 12:00*

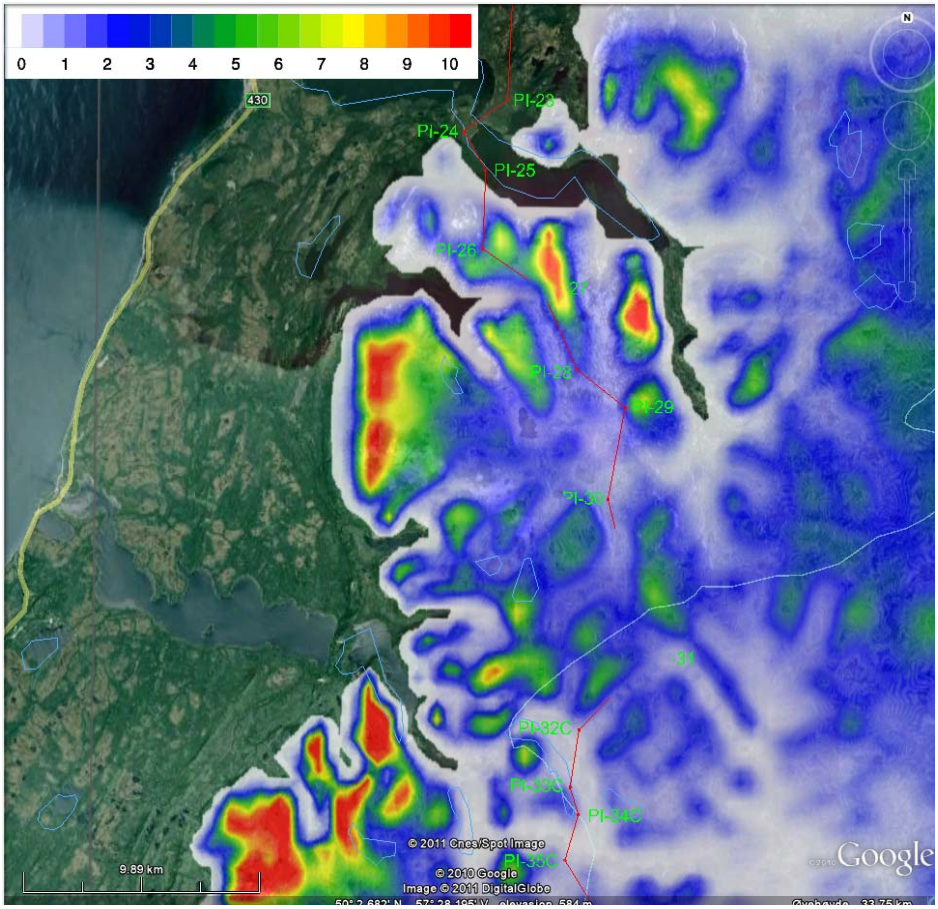

Figure 56. *Rime ice load (colour bar in kg/m) for 2010.01.02 00:00 – 2010.01.04 12:00*

5.3 Test span 2009-1, icing event 4: 2010.01.13 00:00 – 2010.01.16 00:00

In this event the main wind direction at Daniel's Harbour was around N, probably NW during the most intense icing rate. Figure 57 shows the same properties as above for this event. There is much less precipitation than in the previous case, but this time it is more on the western side than on the eastern (upper left picture). Since the temperature is significantly lower in this case there is only some small amounts of wet snow in the valleys, and no wet snow load anywhere in this domain. Also the amount of rime ice is less (lower left) than in the previous episode, however this time the maximum values are closer to PI 26. The maximum wind speeds (lower right) are also less than in the previous case.

At the start of the model test span 2009-1 has already 3.2 kg/m, so a direct comparison between the model and the measurement is not straight forward, due to different cylinder diameter and unknown density of the accreted ice. During the first 48 hours the ice load on Nalcor1 increases from 3.2 kg/m to 7 kg/m, while the predicted ice load increases from 0 to 0.25 kg/m, indicating an underestimation from WRF. After a very sudden ice shedding at 00UTC on the 16th of January there is a second icing event which is overestimated in WRF. WRF is predicting icing at Nalcor1 during the whole simulation. This is confirmed by the measurements.

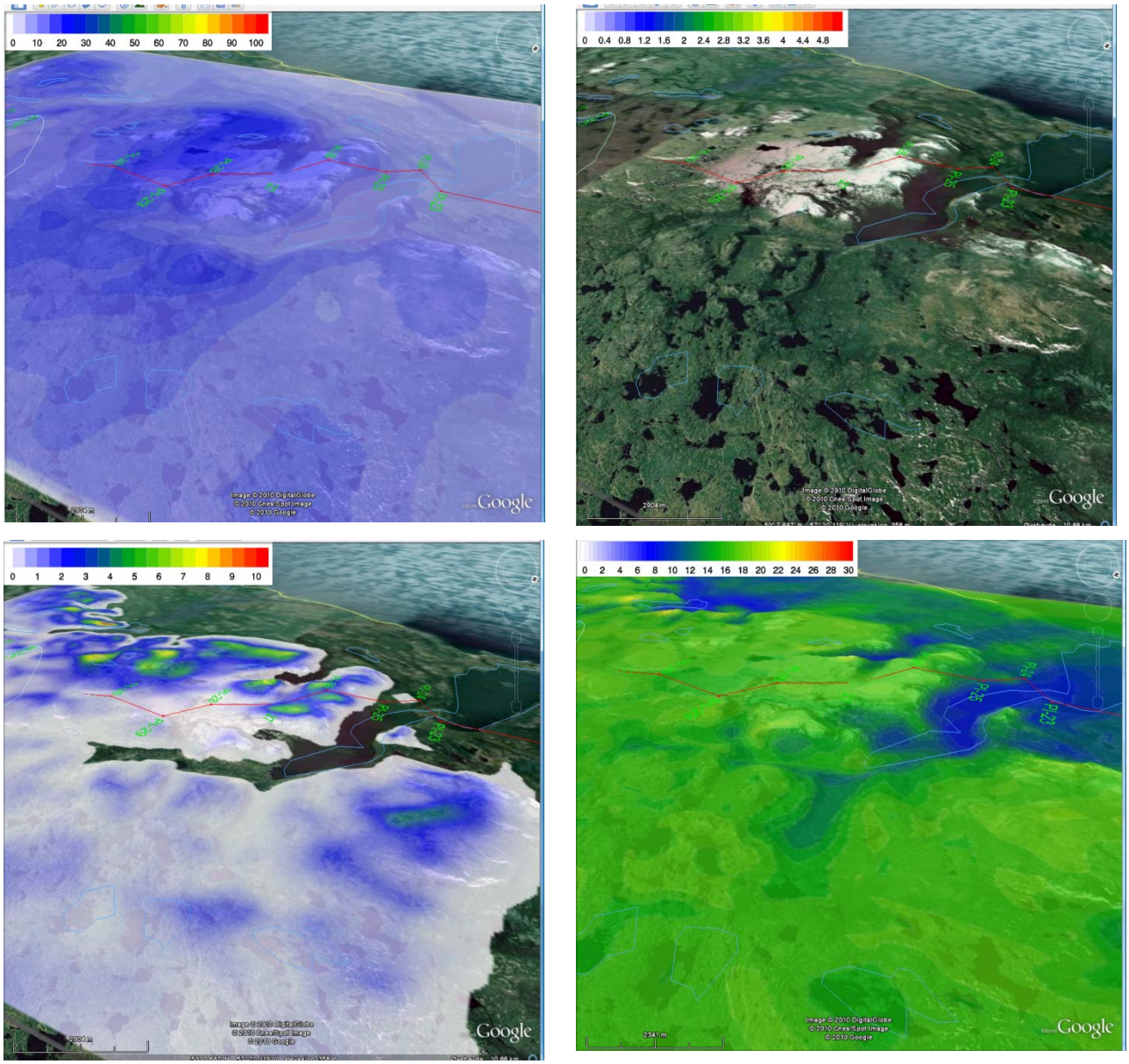

Figure 57. *2010.01.13. 00:00 – 2010.01.16 0:00. Upper left: Accumulated precipitation. Upper right: Wet snow load. Lower left: Rime ice load. Lower right: Maximum wind during this episode.*

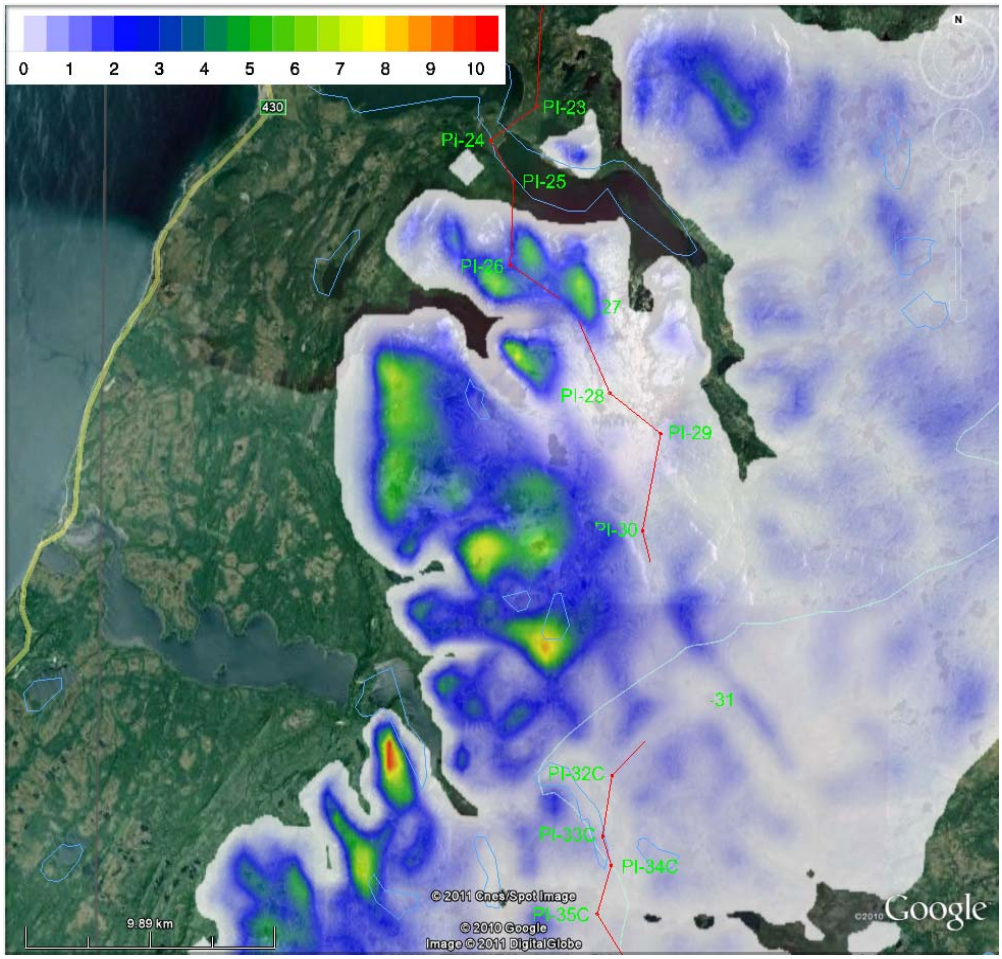

Figure 58. *Rime ice load (colour bar in kg/m) for 2010.01.13 00:00 – 2010.01.16 00:00*

5.4 Test span 2009-1, Icing event 5: 2010.02.10 00:00 – 2010.02.13 12:00

Also in this episode shown in Figure 59, the prevailing wind is between W and N at Daniel's Harbour. The total precipitation (upper left) is generally less than 40 mm, the maxima being over the higher hills. It is seen (lower left) that the wet snow load follows the major valleys from west to east, but the amounts are low. Also, in this case the temperature is too low to cause wet snow in the mountains. The accumulated rime ice loads (lower right) are less than in the previous cases. The maximum wind speeds (lower right) are also less, but it can be seen that the north-westerly winds are increasing somewhat in strength as it blows up the NW slopes.

Also, in this case the simulation starts after the icing has started in test span 2009-1, which already gained 2.2 kg/m at the start of the simulation. The timing of the icing event is well reproduced in the model, but the icing intensity seems to be underestimated.

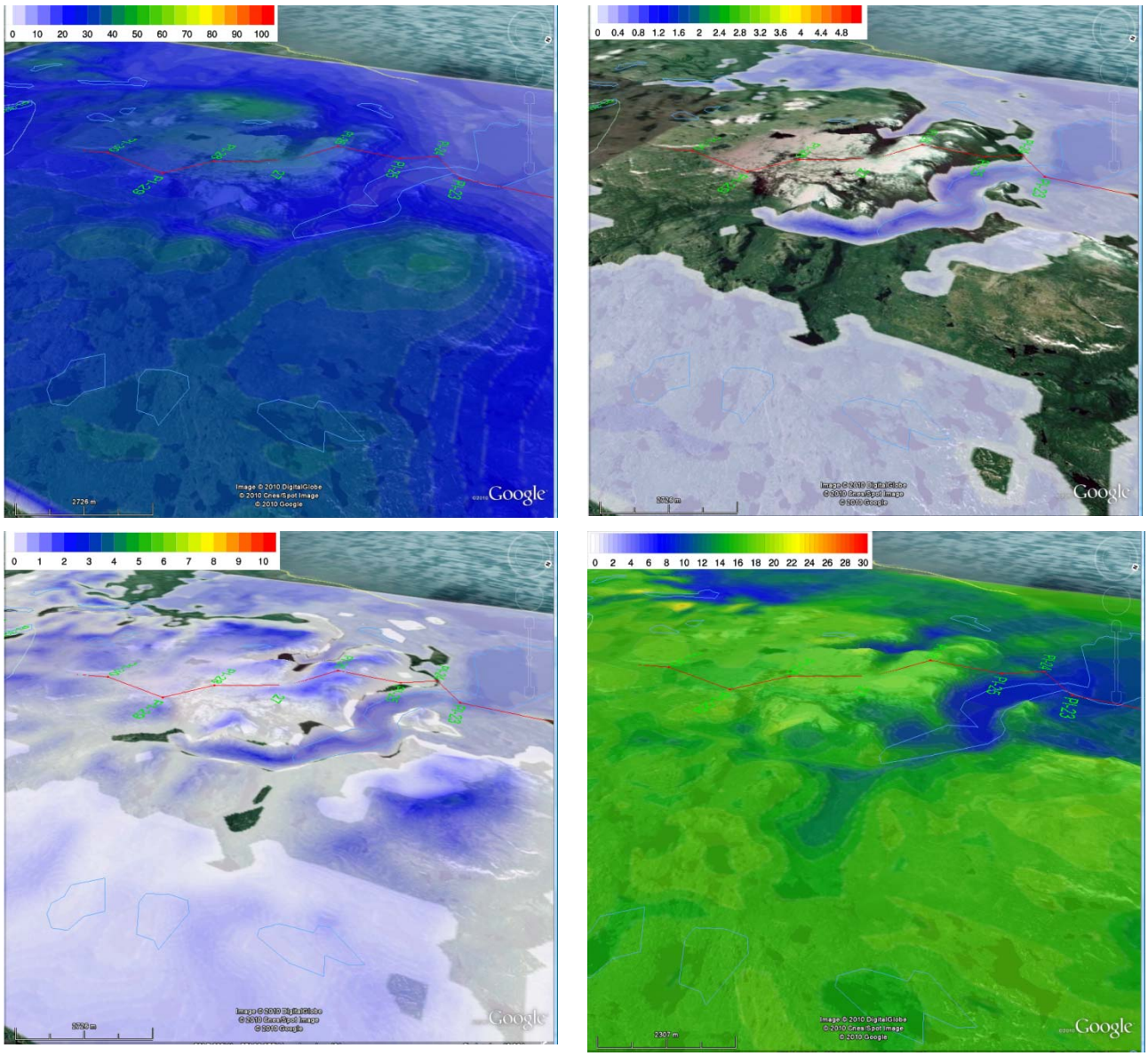

Figure 59. *2010.02.10. 00:00 – 2010.01.13 12:00. Upper left: Accumulated precipitation (color bar in mm). Upper right: Wet snow load (color bar in kg/m). Lower left: Rime ice load (color bar in kg/m. Lower right: Maximum mean wind speeds during this episode (color bar in m/s).*

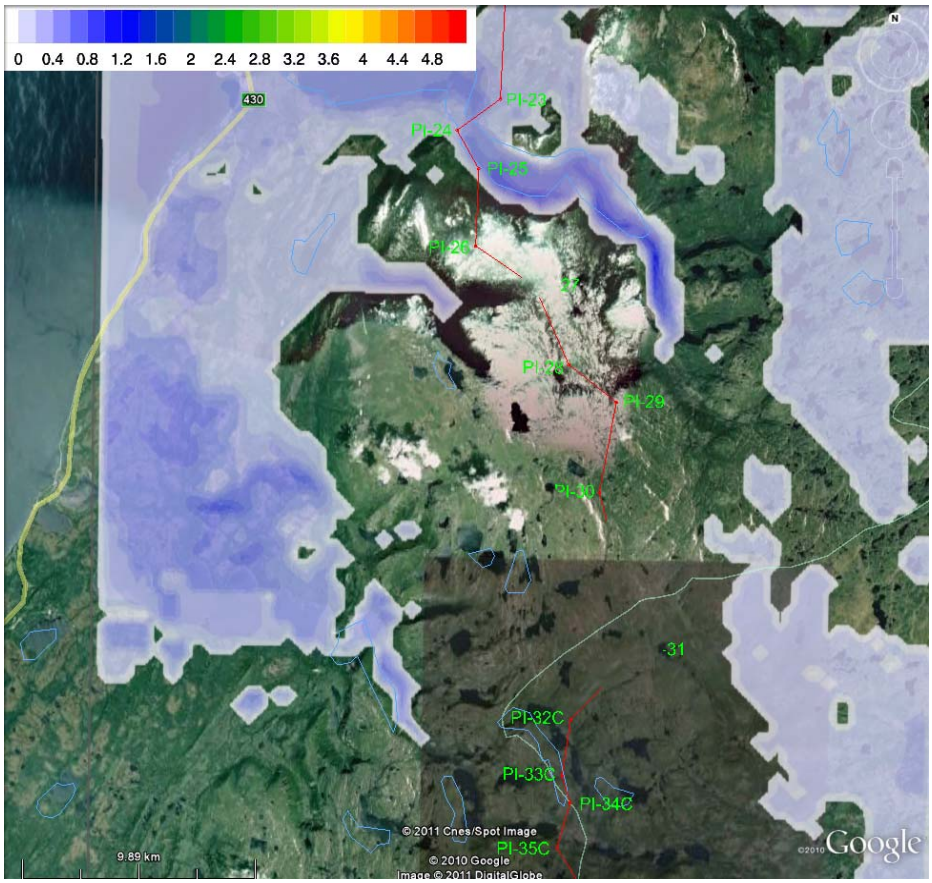

Figure 60. Wet snow load (colour bar in kg/m) for 2010.02.10 00:00 – 2010.02.13 12:00

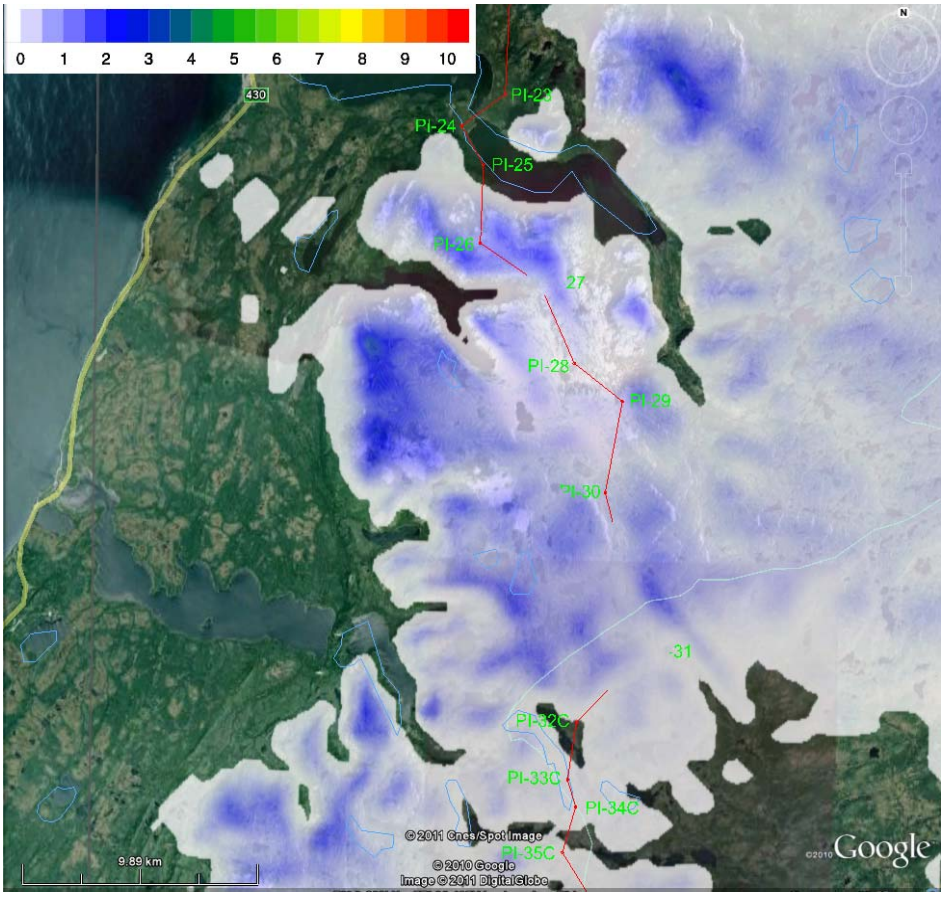

Figure 61. *Rime ice load (colour bar in kg/m) for 2010.02.10 00:00 – 2010.02.13 12:00*

5.5 Conclusions from this study

As described in Chapter 3.3 there are many possible reasons for the discrepancies between predicted and measured ice loads displayed in Appendix A. The accumulated ice load is a result of wind speed, lwc, droplet size and temperature, and there will always be small scale variability among these variables which is not predictable by the WRF model. There is also a shifting in timing of the most severe icing period in one of the simulations. This is most probably related to uncertainties in the global analysis data used as input to WRF. The quality of the global model analysis can vary in space and time, and are likely to be more accurate in areas with a dense network of weather stations. Based on the three cases simulated so far the discrepancy between predicted and measured ice loads seem somewhat greater than in similar studies in European countries (ref 25 and 26). More cases from the following winters need to be studied in order to draw conclusions about the quality of icing predictions for Newfoundland and surrounding areas.

In all these cases we have had winds from the northern sector (Daniel's Harbour). Significant rime ice is identified on the mountain tops and close to the highest parts of the HVDC line route. It is also shown that wet snow may occur at any level, but at least from these wind directions the amounts are low.

Further conclusions cannot be drawn until we have analysed some events with winds coming from the Gulf of St. Lawrence area (SW-W). This wind direction is however less frequent during the winter months December – February as shown in Appendix C. On the other hand, Table 7 shows that some of the most extreme icing events occur with winds from this direction. Furthermore, winds from SW are perpendicular to the line route and accordingly the transmission line will be more at risk from this direction. This should be a topic for future studies, especially when the test spans should record ice loads from this sector.

It is also a recommended option to apply the WRF model for the very severe icing cases during the winters 1986-87, 1987-88, 1977 and 1982, as shown in Table 8.

6 Icing simulation for Labrador

6.1 Observation of icing in Labrador

The icing data collection program that was operated from 1974-1987 gives information on ice accumulation on selected sites in Labrador. For some years icing was observed on guyed triangular lattice test towers, with section 0.4m · 0.4m · 0.4m. The towers were not instrumented but were visited on a monthly basis. Any ice accretion was measured (thickness) and photographed, and the type of ice and direction from which the ice accreted, was recorded. The initial data registration sheets are not available, but the main conclusion from each visit is available.

Huge icing was observed at tower #4 and Figure 62 shows icing from Feb. 1977, the exact date is unknown. Descriptions of ice accumulation noticed in the observation visits, before and after the photo is taken, is given in Table 10.

From the description of icing in Table 10 it can be anticipated that icing has been building up for a long time before the photo is taken

Figure 62. *Tower #4 in Feb. 1977.*

Table 10. *Observed icing at tower #4 in Labrador.*

Date of inspection	Accumulation noted by observer	Direction of accumulation
1976-11	Tower and guys were covered with a mixture of glaze covered by soft rime. Measurements on the tower were 6” deep by 2” wide pennant shaped to the east. Guys received similar accumulations.	East
1977-01	Towers and guys were completely encased in glaze covered by a little rime. At 20’ level guy was covered with 8” to 9” of solid ice. Tower body was covered by 3” to 4.5” of ice	East
1977-02	Tower and guys were completely encased in glaze covered by a little rime. Guys were covered by 8”-10” of solid ice. Lower portion of 18” tower was covered by ice measuring 28” across the face. The top measurements were estimated at 36” across the face	East
1977-03	Tower and guys completely encased by glaze covered with a light rime coat. Accumulation on guys measured 9” to 13” in diameter. 18” tower face measured 21” to 24” across at bottom.	Southwest to Northeast
1977-04	Old accumulation existed on tower body over laid by 2” to 3” of new glaze giving a total width of 37” across the east face of tower. 2” – 3” of glaze was measured on the lower portion of the guys.	East

6.2 Icing estimated by WObs model

The WObs icing model was used with weather observation data from Battle Harbour to evaluate the capability of the model to capture observed icing shown in Figure 62 and Table 10. The elevation of Battle Harbour is 10 m above sea level.

The following parameters were used:

- Number of droplets = 100 droplets/cm3
- Lapse rate for temperature; γ_d = 0.0090 °C/m and γ_w = 0.0065 °C/m
- Parameters for wind speed; a=1.75, b=1.175, c=-0.002
- Minimum cloud height = 150 m
- Adiabatic reduction factor (alfa) = 1.0
- Maximum LWC is restricted to LWC ≤ 0.5 g/m^3
- Reduction of LWC due to cloud amount and cloud opaque is taken as the ratio of observed cloud opaque (0 to 1)
- Conductor diameter = 30 mm
- Height of icing location above Battle Harbour = 500 m
- Height of conductor above ground = 10m
- Icing model: WObs with vertical rotating cylinder

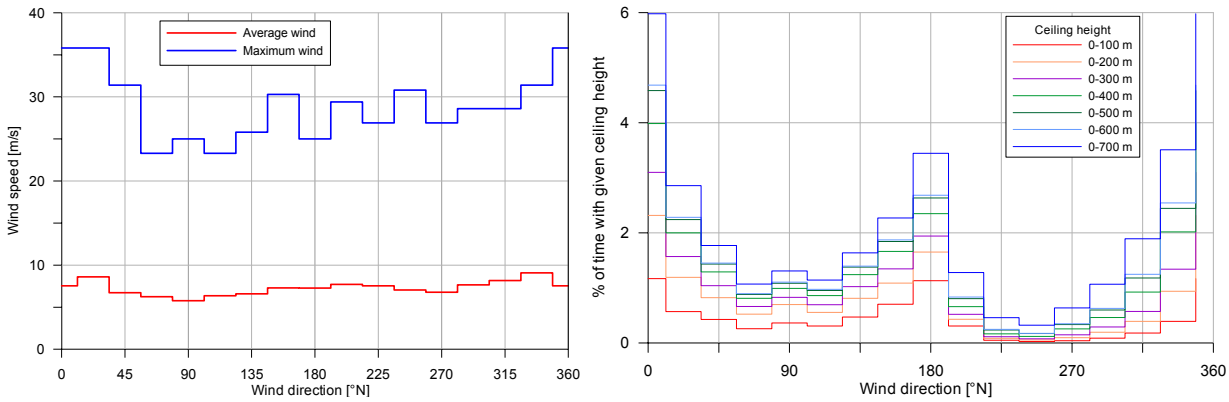

Figure 63. *Battle Harbour, wind speed and ceiling height (0-700m) depending on wind direction.*

The result from the WObs analysis is given in Figure 64. It shows that the icing is gradually building up. The temperature stays below zero from beginning of November to late April. The same uncertainty is if shedding is correctly predicted since the temperature does not pass the zero and shedding is predicted as a mechanical break from combination of strong wind and temperature close to zero. Maximum ice load would be considerably higher if shedding would not take place. Experience shows that ice shedding often takes place on conductors before ice disappears from towers, this may also explain some differences between the observation and the model.

The WObs model predicts this icing event (25.7 kg/m) to be the 17th largest in the period 1958.01.01-1983.10.17. The three largest events were in the range of 45-48 kg/m.

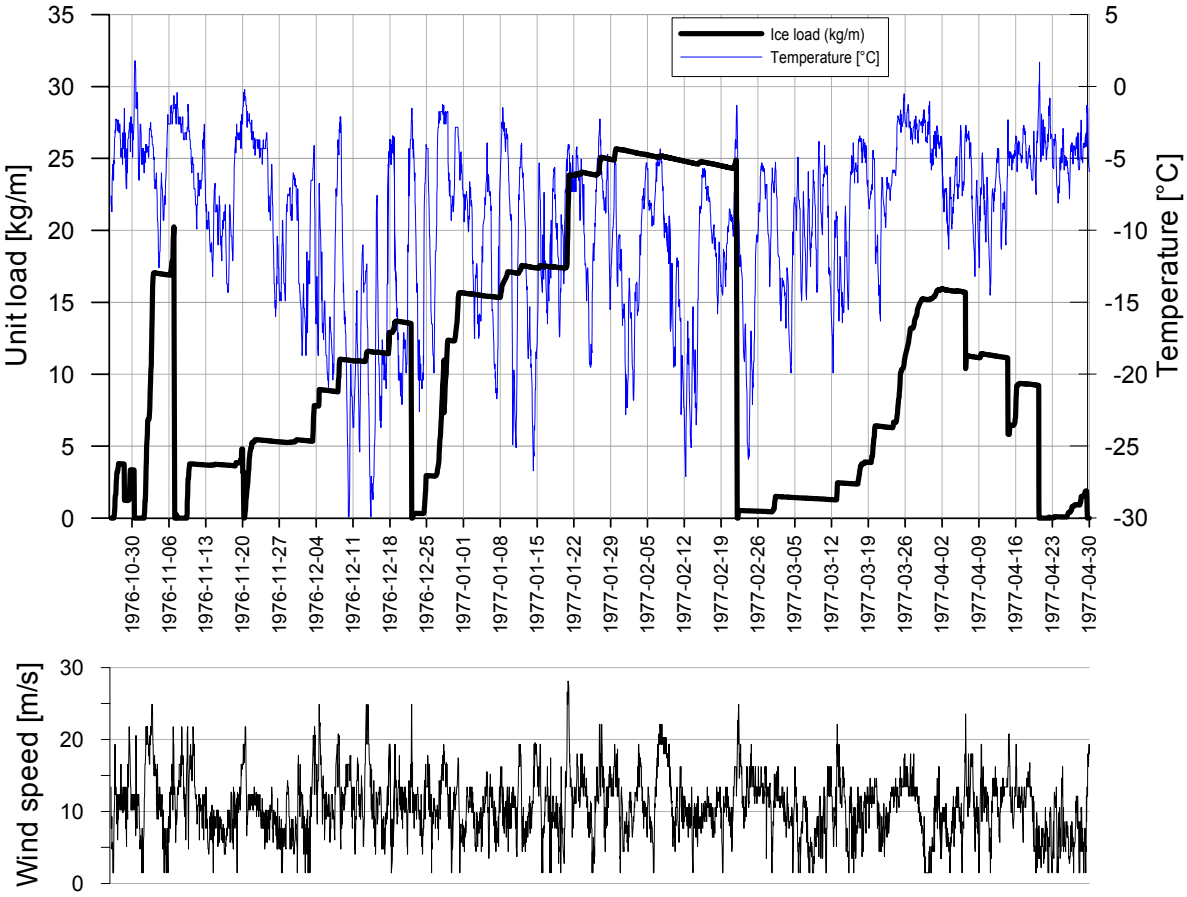

Figure 64. *Icing event at the site of tower #4 according to WObs model.*

6.3 WRF simulations for selected weather in Labrador

The WRF model Version 3.2 is configured with a triple nested domain with a grid spacing of 0.8 km in the finest mesh. The geographical coverage of the innermost domain is displayed in Figure 65, together with the line route (approximate).

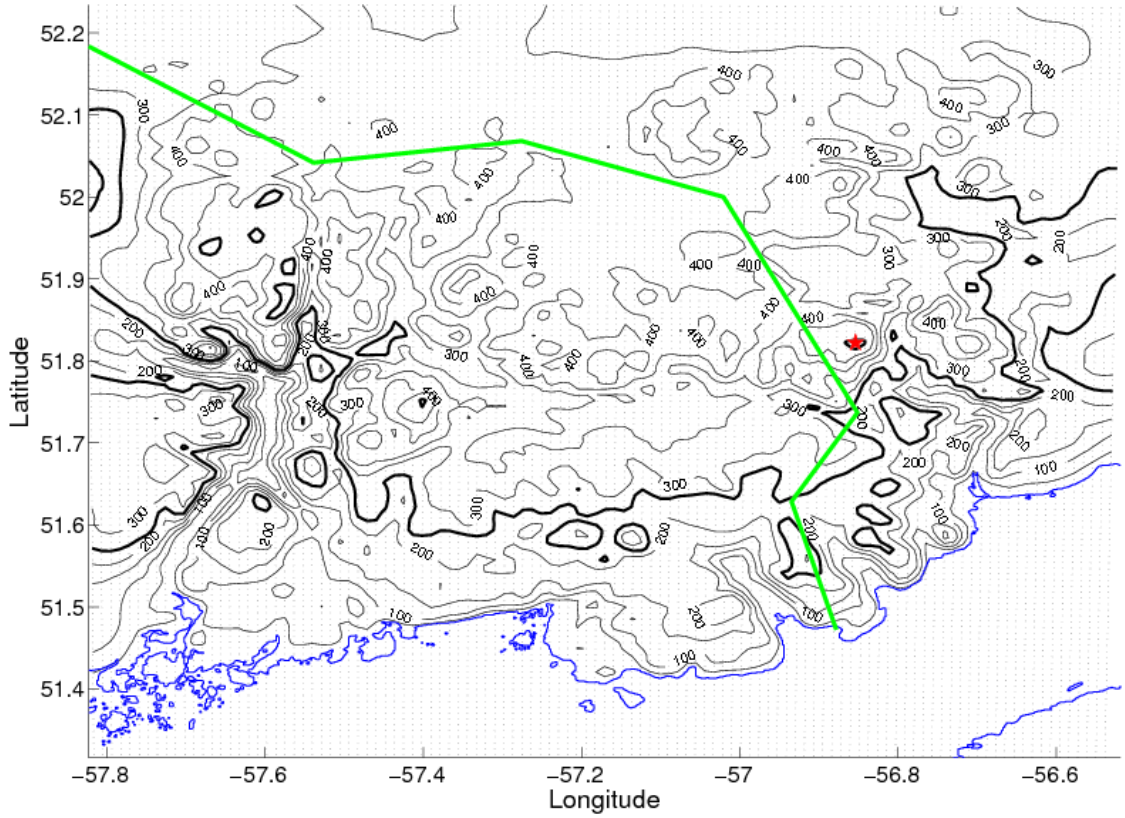

Figure 65. *Area covered by the high resolution domain in the WRF simulations. An approximate line route is indicated by the green line. A red star is put at the assumed location of tower #4.*

6.3.1 Location of tower #4

The exact location of tower #4 is unknown. However we know from old documents that it was located about 26 miles off the coast at an elevation of 1700 feet. The highest peek inside the high resolution domain in Figure 65, is about 512 meters (1680 feet), indicated with a red star. Taken into account that the model terrain is averaged inside each grid box of size 800 x 800 meters, this peak actually corresponds very well to the description of tower #4. For the further analysis of the WRF results, we assume that this is the location of tower #4.

6.3.2 Selection of time period

During the winter season in 1977 heavy ice accretion was reported from inspections at tower #4. The ice accretion was also documented with a photo taken at the test site in February 1977. There is no information available about when the actual icing occurred at the site of tower #4.

Results from the WObs model from Battle Harbor observation data suggest that the accumulation started already in December 1976 and that the icing reported in February 1977 was a result of many smaller events that allowed the ice to accumulate over a long time period. Based on this information the first time period for a WRF simulation was selected: During the days of the 20th and the 21th of January the WObs model gives an increase in accumulated ice load from 17.4 kg/m to 23.8 kg/m in less than 24 hours. The weather analysis in Figure 66 shows that this event was related to a deep low pressure system passing just south of the region, forcing strong winds from the east and north east.

The next time period selected for WRF simulation was the 26-28 th of January 1977 (shown in Figure 67) A low pressure system forces winds with relatively mild air from the south and south west, followed by the passage of a strong cold front. The WObs model indicates just a slight increase in ice load, however the weather situation was considered interesting because of the advection of mild and humid air, followed by a strong cold front.

A third time period was selected for further examination with WRF: the 6-8 th of February 1977. We find from the inspection notes that glaze ice was covered by a thin layer of soft rime, with the accumulation direction from the east. By searching through weather maps we find this particular time period interesting because it's presumably the last incident of strong winds from the east before the site visit when the photo was taken. Weather situation is displayed in Figure 68.

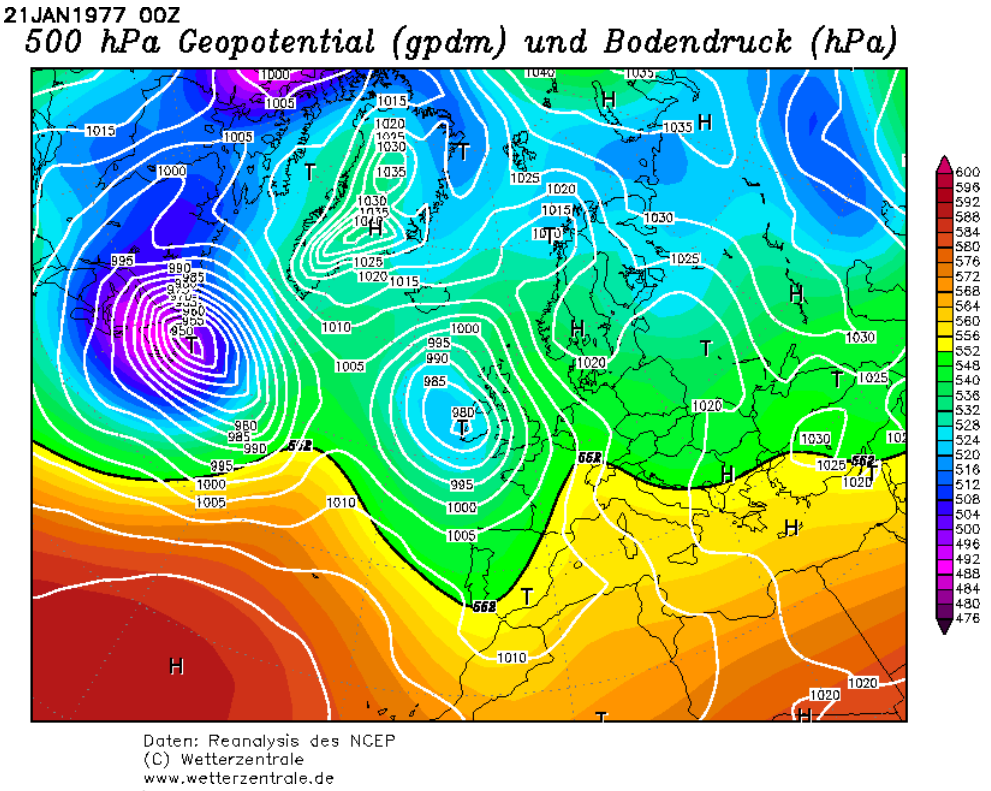

Figure 66 *Weather map from the GFS model giving the 500hPa geopotential height as color shading and sea level pressure as white contour lines. January 21st 1977 00UTC.*

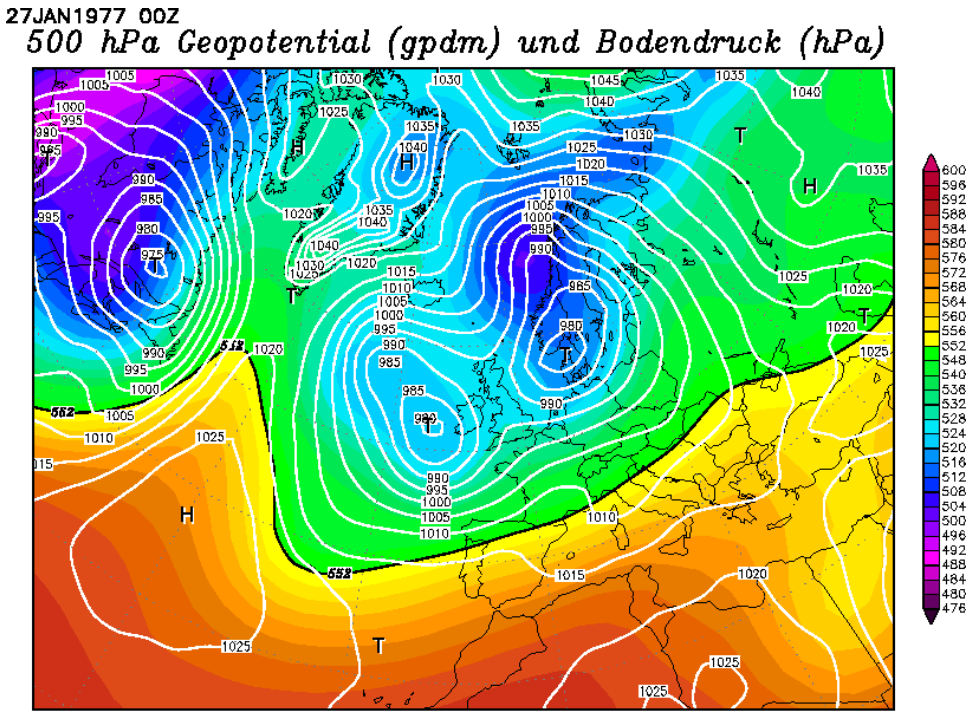

Figure 67 *Same as in* Figure 66*, but now for January 27th 1977 00 UTC*

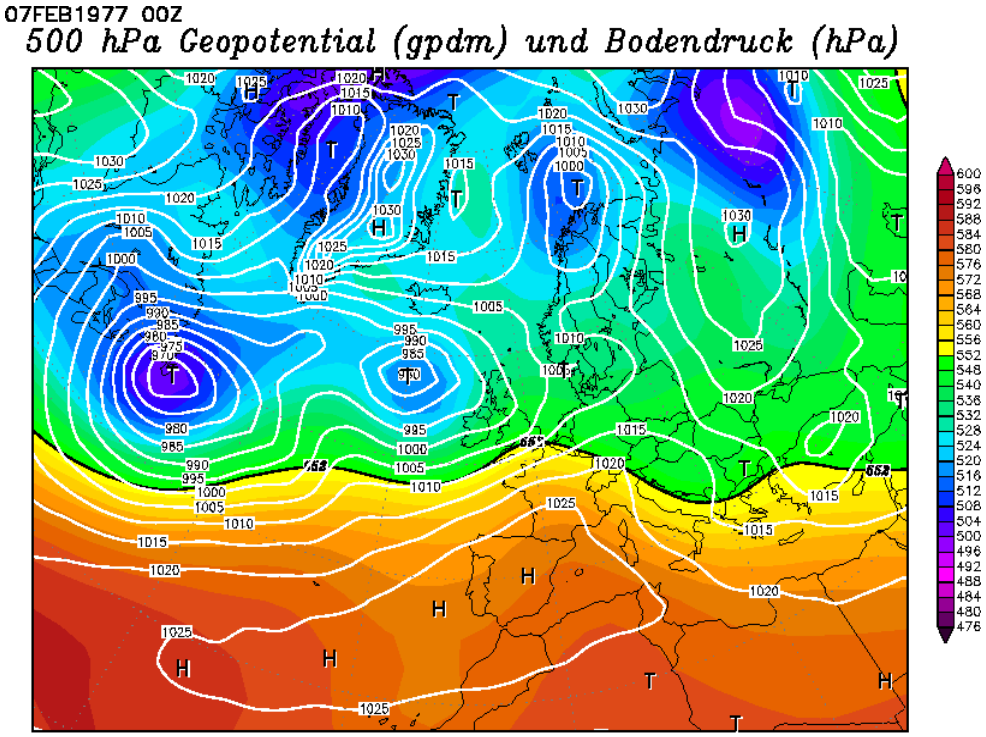

Figure 68 *Same as in* Figure 66*, but now for February 7th 1977 00UTC.*

6.4 Results of WRF simulations

The main results from the three high-resolution WRF simulations are compiled in a kmz-file for visualization in Google Earth. In general, the WRF simulations do not indicate severe icing in any of the cases considered. In order to understand the results and the model behavior in more detail, some additional figures are included in this chapter.

Results from the three high resolution simulations are shown in Figure 69, 70 and 71. The upper panels are so called time-height cross section plots, which give the time evolution of the different cloud variables (hydrometeors) for the column over tower #4. The lower panels are the time series of cloud hydrometeors at

ground level. In-cloud icing is predicted when cloud water (black line in lower panels) is present at ground level, in combination with temperatures below zero. Equivalently freezing rain/drizzle is predicted when rain water (red line) is present in combination with sub-zero temperature.

In the first simulation (Figure 69) the model predicts almost no icing at all. Instead heavy snowfall is predicted with accumulated precipitation reaching almost 80 mm at tower #4. The high concentration of falling snowflakes efficiently sweeps out any supercooled cloud droplets, and prevents in-cloud icing to occur.

We find very much the same characteristics in the second simulation (Figure 70), with precipitation amounts reaching more than 60 mm during the simulation time, and snowflakes that deplete most liquid cloud water. Around 00 UTC on the 27th January there is a substantial amount of freezing rain just a few hundred meters above ground level, but the temperature at the ground is above zero, hence warm rain is predicted at tower #4. This situation lasts about 6 hours before the cold front brings the temperature below 0°C. This temperature variation is confirmed by the data extrapolated from Battle Harbor.

The third simulation is displayed in Figure 71, with much less precipitation and in-cloud icing occurring at ground level, before precipitation starts to develop. The predicted icing event continues for approximately 18 hours. The wind speed is around 5 m/s from the east and north east (not shown here) during the icing. The low wind speed prevents the predicted ice load to reach more than a few hundred grams per meter.

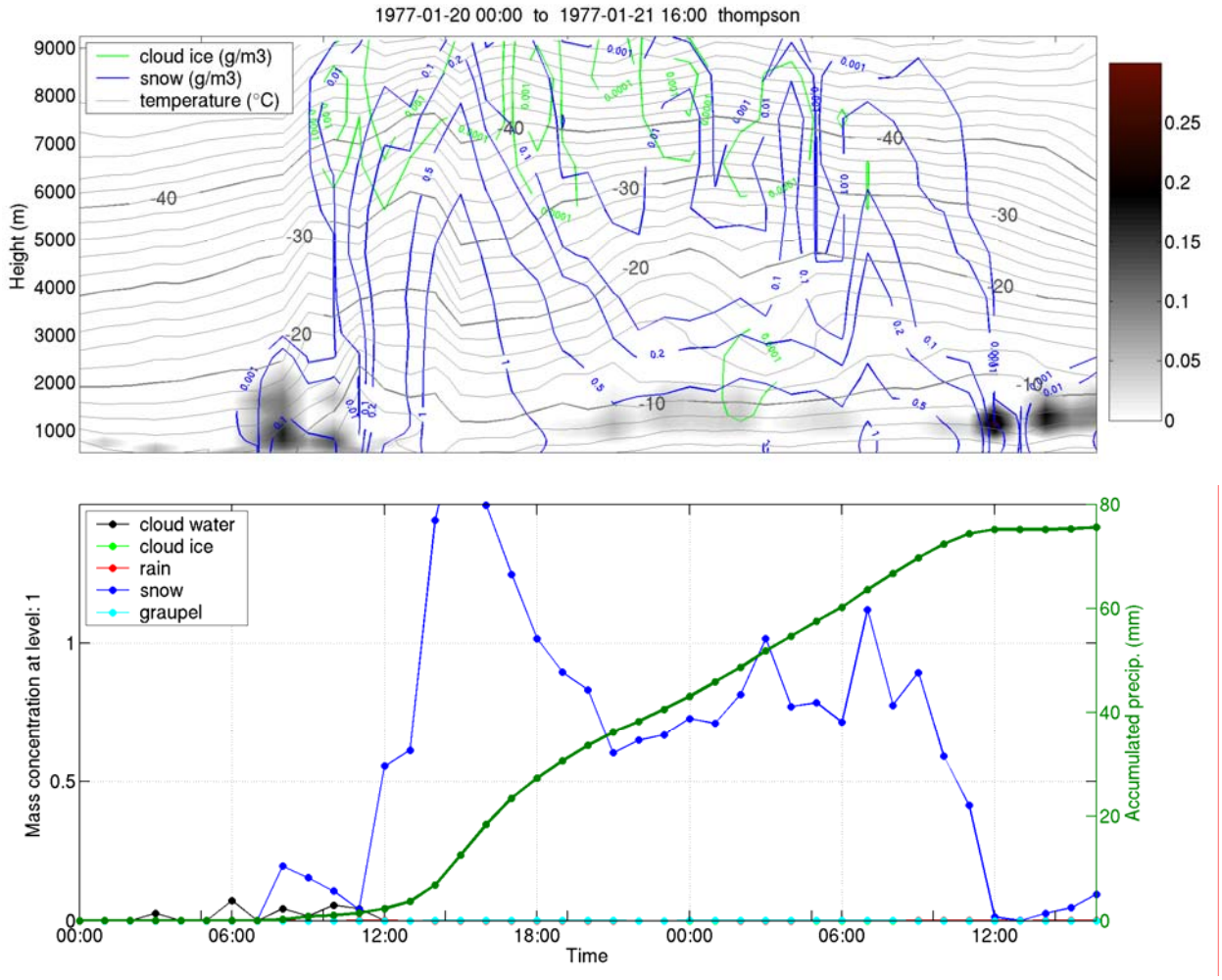

Figure 69. *Upper panel: Time-height cross section plot at the assumed location of tower #4. Colors: shading=cloud water, green contours=cloud ice, blue contours=snow, red contours=rain, cyan contours=graupel and grey contours=temperature. Lower panel: Time series of mass concentration of different hydrometeors at ground level. Colors as in upper panel. Dark green is accumulated precipitation with values given on the right hand side axis.*

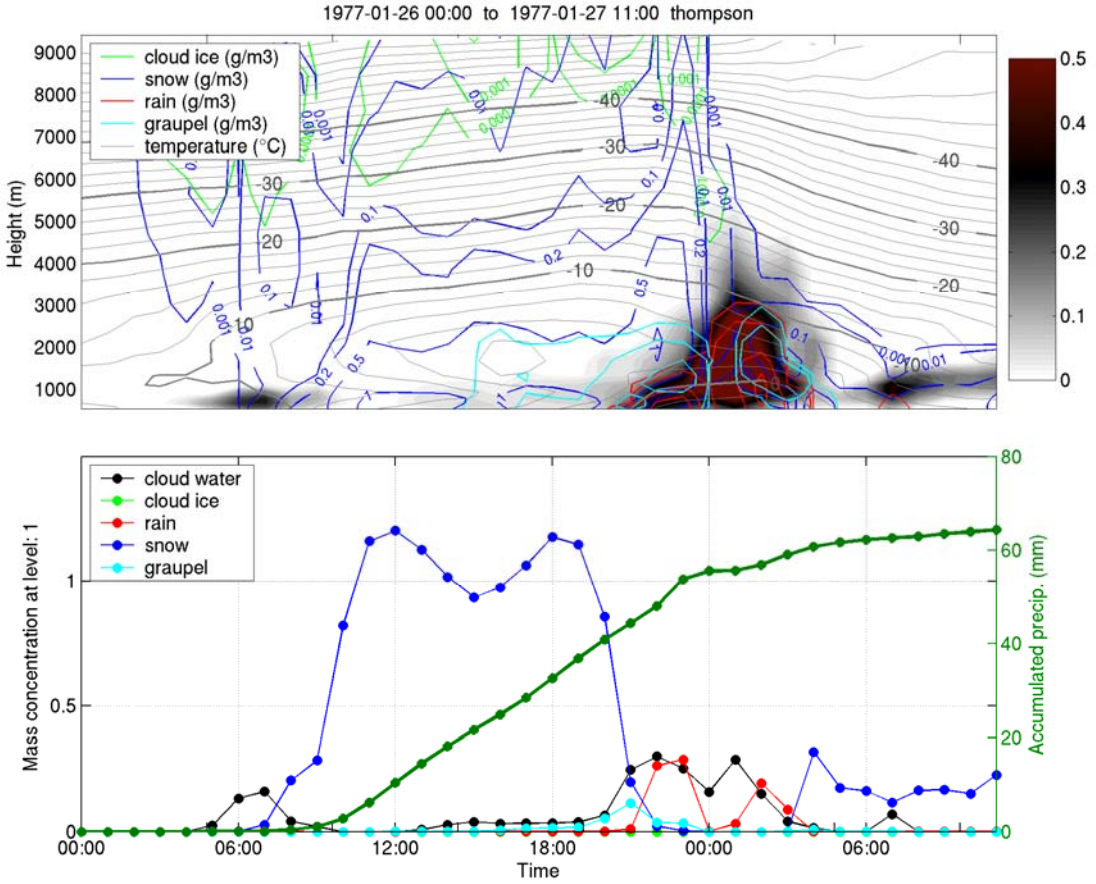

Figure 70. *Same as* Figure 69*, but now for the time period 26-27 Jan 1977*

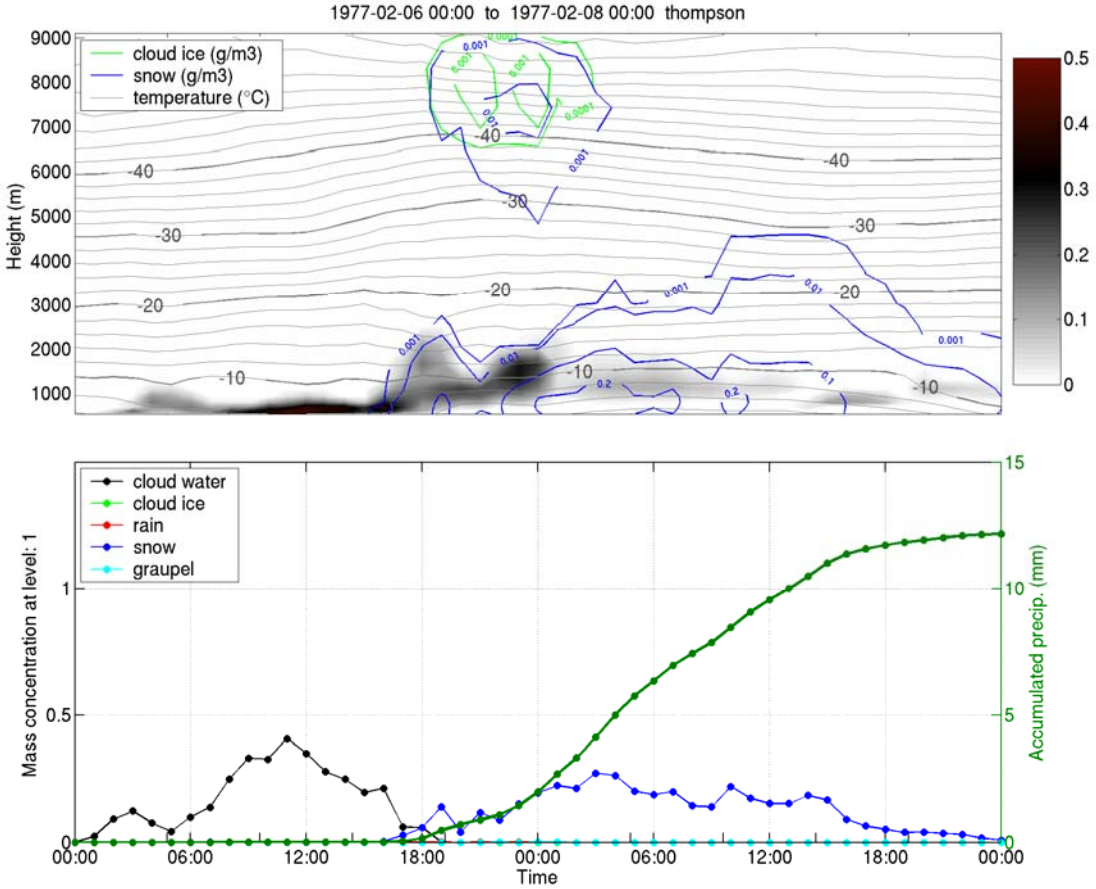

Figure 71. *Same as* Figure 70*, but now for the time period 6-8 Feb 1977*

6.5 Comparison with the WObs model results

There is a clear inconsistency between the results of the WRF model and the results of the WObs model from Battle Harbour, for the three cases studied here. In the first simulation the WObs model indicates strong icing, while the WRF model predicts snowfall, but no icing. In the last simulation there is no icing diagnosed from the WObs model, while the WRF model predicts light icing from the east. There might be several reasons for this inconsistency, and direct icing measurements are needed in order to identify model errors. Some key points are listed below:

- The most obvious source of discrepancy between the models is the LWC. The WObs model assumes that air is lifted adiabatically from the cloud base to the height of the site, and that cloud water is produced according to an adiabatic cloud water gradient. The WRF model parameterizes the precipitation processes and thus predicts much less cloud water (LWC) because it converts cloud water into precipitation, and allows snow, rain and graupel to deplete cloud water.
- The WRF model is forced by input data from the ECMWF global model, and the cloud physics in WRF is sensitive to the vertical profile of temperature and humidity. Because this case is more than 30 years old, the amount of remote sensing data (satellite, radar, etc) assimilated into the ECMWF model is very limited. This leads to uncertainty in the initial field and boundary conditions used in the WRF simulations. We can be more confident with the quality of the input data for more recent cases.
- The WRF model predicts the state of the atmosphere in all physical dimensions, while the WObs model is a two dimensional model (vertical and time). When the horizontal distance between the meteorological station and the site of interest is large, the WObs model will neglect the horizontal variations, and the results will differ from the WRF model.

6.6 General results of icing in Labrador based on WRF simulations

It is very difficult to draw conclusions from the results. None of the cases indicated significant icing, but we do not know if this is related to model errors or the selection of time periods when icing did not occur. It is recommended that the line route crossing Labrador is subject to a separate study.

7 Previously proposed design loading for in-cloud icing at LRM

7.1 General

The maximum loading specified along the at Long Range Mountain Ridge originates from a meteorological study made in 1973 /Ref. 43/. The following is a summary of the main findings and proposed design loading.

The in-cloud ice load was estimated using a climatology study using the empirical Leavengood ice accretion model with a limited data set obtained from the nearby airport and/or weather stations. In the study, the maximum rime ice which would have been formed in one icing period was determined for each year of record at appropriate heights above stations along the proposed routes. The heights were chosen to represent surrounding terrain. These maximum yearly values were used in extreme distribution.

Table 11 shows the weather stations used and the relation between ceiling height and wind speed. Table 12 shows the estimated return icing close to the weather stations.

Table 11. *Frequency of selected wind speeds with low ceilings and icing range temperature.*

Station	Period of Record (yr)	Average Hours per Year					
		Ceiling ≤300 ft Temperature 25-35°F Wind Speed (mph)			Ceiling ≤800 ft Temperature 27-37°F Wind Speed (mph)		
		≥200	≥15	≥10	≥20	≥15	≥10
St. John's Torbay	19	207	380	506	460	796	1029
Gander	19	78	153	266	275	505	763
Buchans	12	14	21	37	91	148	257
Deer Lake	6	3	4	5	11	70	117
Daniels Harbour	6	12	19	26	99	143	198
Battle Harbour	12	53	77	156	276	362	509
Argentia	17	28	51	78	115	226	359
Stephenville	19	6	10	17	16	36	77

It was mentioned in the study that the values 1000 ft above Daniel's Harbour do not necessarily represent expected conditions on the ridge of the Long Range Mountains. Storms coming in from the east would not have resulted in sufficient wind speeds or low enough ceilings at Daniel's Harbour to have been considered.

Table 12. *Return period values for rime icing, results from study presented in 1973.*

Location	Return Period Rime Amounts (radial inches)			
	10-yr	25-yr	50-yr	75-yr
300 ft above St. John's-Torbay	4.8	6.1	7.1	7.3
300 ft above Gander	3.4	4.3	5.0	5.5
300 ft above Buchans	0.6	0.8	1.0	1.1
800 ft above Buchans	2.7	3.4	3.9	4.2
1000 ft above Daniels Harbour	2.8	3.4	3.9	4.2
300 ft above Battle Harbour	2.2	2.9	3.4	3.6
1000 ft above Battle Harbour	7.5	8.8	9.9	10.4
1000 ft above Goose Bay	4.1	4.9	5.5	5.9

The same loading is specified for the Long Range Mountain Range from the top of the ridge on the north side of Main River (49°50'N) along the ridge to 51°N (1200 to 1800 ft). The following table shows the specified loading, it is based on the density of rime being 500 kg/m^3 according to In the MRI 73 FR-1131 report (/Ref. 43/).

It is pointed out that loading is defined as radial ice cover, it can be argued that it is better to specify loading based on kg/m in case of high in-cloud ice loading. It is not specified in the loading assumptions if the ice load is the same for all heights above ground. Usually the in-cloud icing is defined at 10 m above ground and shall increase with height.

Table 13. *Loading specified for Long Range Mountain Range, results from study presented in 1973.*

Specified ice load	Unit	Return period of loading (years)			
		10	25	50	75
Radial ice cover	[in]	7.3	8.5	9.5	10.0
	[cm]	18.5	21.6	24.1	25.4
Total ice diameter with 50.8 mm cond.	[in]	16.6	19.0	21.0	22.0
	[cm]	42.1	48.3	53.3	55.9
Unit loading on 50.8 mm cond.	[Lb/ft]	46.2	60.8	74.4	81.7
	[kg/m]	68.8	90.4	110.7	121.6
Unit loading on 58.0 mm cond.	[Lb/ft]	47.6	62.4	76.2	83.7
	[kg/m]	70.9	92.9	113.4	124.5

7.2 The Leavengood icing model

The Leavengood is an empirical model based on observed icing from California, Japan and Germany, it is described in references /Ref. 2/ and /Ref. 23/. The model is simple and considers only average wind speed during an icing condition and the duration of the icing condition in determination of ice diameter. Figure 72 shows how the diameter of rime ice is determined from duration of icing condition and wind speed. Ice density needs to be determined in order to get ice loading, the Leavengood model assumes that it is taken according to Figure 73.

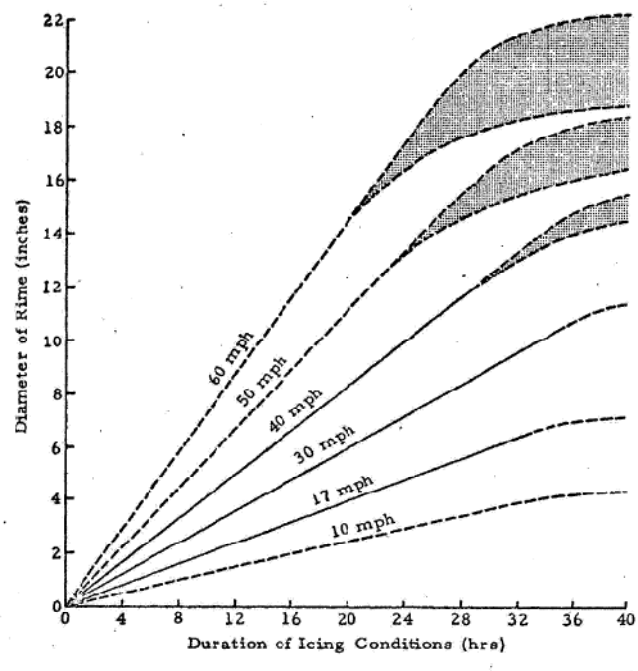

Figure 72. *Empirical relationships for estimating ice accretion diameter, from Leavengood 1972.*

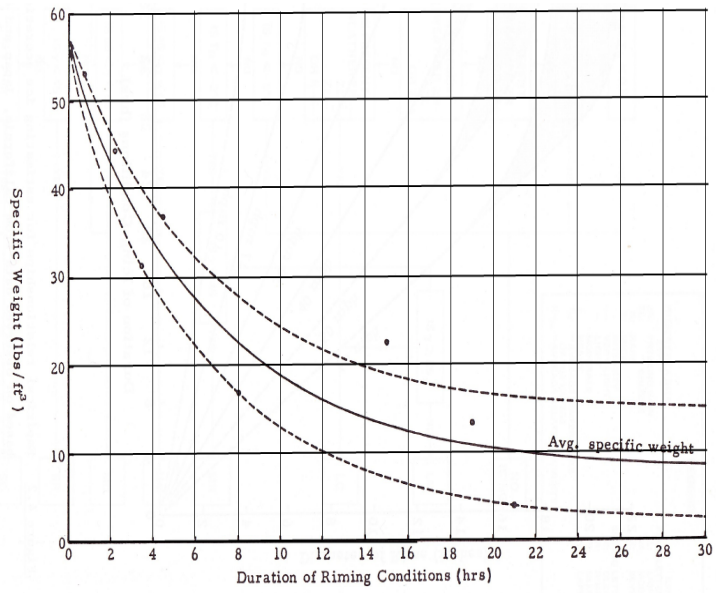

Leavengood	Density	
hours	lbs/ft3	kg/m3
0	57	913,1
4	35	560,7
8	23	368,4
12	17	272,3
16	12,5	200,2
20	11	176,2
24	9	144,2
28	8,5	136,2
32	8,5	136,2
36	8,5	136,2
40	8,5	136,2

Figure 73. *Density of in-cloud icing for the Leavengood model.*

It should be noted that the density of ice was taken as 500 kg/m^3 when determining the ice loading for the LRM which is considerably higher density than the Leavengood model assumes. The difference is at least factor in the range of 2-3.

In the MRI 73 FR-1131 report (/Ref. 43/) it is informed that the model was derived under the assumptions that the LWC in the cloud was 0.5 g/m^3 and the cloud drops were about 15 microns in diameter. These values are not mentioned in other references. Figure 74 shows a comparison between the Leavengood model and the icing model described in Chapter 3.2 (Makkonen model). The Leavengood model is given both with the density function, and the fixed density (500 kg/m^3). The Makkonen model is based on 30 mm conductor, LWC = 0.5 g/cm^3 and droplet $N_{droplet}$ = 100 droplets/ *cm^3* (it leads to MVD= 23.8 micron).

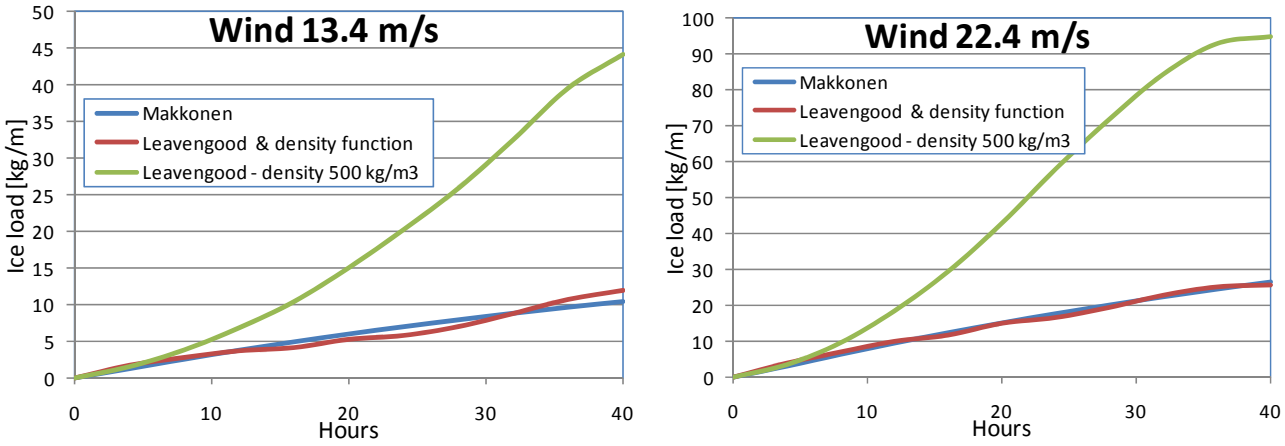

Figure 74. *Comparison between the Leavengood model and circular cylindrical model (Makkonen), using LWC = 0.5 g/cm^3 and droplet number = 100 droplets/cm^3 (that gives MVD= 23.8 micron). Two different wind speeds are used: 13.4 m/s and 22.4 m/s.*

The comparison between the models shows surprisingly good correlation between the Makkonen model and the Leavengood model with the density function, they give almost identical results. The Leavengood model with fixed density 500 kg/m^3 gives much higher loading.

7.3 Conclusion on the previously proposed in-cloud icing load

The previously proposed design in-cloud ice loading on the Long Range Mountain ridge is 110.7 kg/m for 50.8 mm conductor and 50 years return period. This proposal is very high and it is based on an icing model (Leavengood model) that is simple compared to models used today. The Leavengood model has not been used in practice for the last 25 years to the knowledge of the authors of this report.

The high design value largely related how the Leavengood model is used and what data is taken as a reference:

- It seems to use the most severe weather station (Battle Harbour) as a main reference for icing. It is located quite far from the area and not the best suited observation station.
- The ice density is taken as 500 kg/cm^3 which is not in accordance with the Leavengood model. It should be lowered by factor 2 to 3 to be consistent although value of 500 kg/m^3 is often reasonable density for in-cloud icing.

8 Evaluation of ice loadings in the LRM

8.1 Introduction

In this chapter we also give some comments of a more general nature concerning winter climate, icing processes and concepts for ice loadings. In conclusion we indicate a classification of ice loadings based on the given data and general experiences. These load assessments are to be taken as first draft estimates and will be revised in parallel with new field data and model results that will be provided in the future.

8.2 Winter climate

The winter climate of Newfoundland is characterized by its location on the eastern side of the North American continent, surrounded by the Atlantic Ocean and the Gulf of St. Lawrence. On the Northern side of Labrador and Newfoundland a cold ocean current comes southward from the western side of the Davis strait bringing cold waters, often with drifting ice and ice-bergs from arctic waters and Greenland. The sea water on the northern side of Newfoundland is therefore often frozen, and accordingly cold air masses coming from north to northeast will often not be warmed by heat transfer from open sea water.

Another aspect which may influence the local climate along the western side of Long Range Mountains is the Gulf of St. Lawrence and the Strait of Belle Isle. There is a very strong tidal current through the strait. The inflow of cold water from the NE may bring drifting ice and ice bergs into the gulf, and the outflow of water from the SW is relatively warm and will increase the humidity in the air along the coasts. The net current is the latter, with relatively warm water from the Gulf of St. Lawrence through the Strait of Belle Isle (ref.: K. Tucker, Nalcor). This means that humid air and fog will prevail along the western coast of the Northern Peninsula during winter.

Environment Canada has published very detailed climate normal's or averages 1971-2000 for all available weather stations in the area on their web site (http://climate.weatheroffice.gc.ca/climate_normals/index_e.html), averages are for stations with less than 30 years and more than 15 years of observation during the period. In addition to average values, extremes of maximum and minimum temperatures and maximum daily precipitation are given as well. For some stations (e.g. Daniel's Harbour, St. John's) also prevailing wind speeds and extreme values of both hourly wind speeds and gust wind speeds are given, with associated wind directions.

A selected extract of these data are given in Table 14.

Table 14. *Some climatic data for weather stations along the line route*.

Station	Elevation (m asl)	Absolute min temp (°C)	Max daily precipitation Oct-Mar (mm)	Highest wind gust (m/s) (Dir)
Daniel's Harbour	19	-39.4	88.2	42 (SE)
Corner Brook	5	-31.7	79.8	
Deer Lake	11	-37.2	85.1	
St. John's A	140.5	-23.8	100.8	54 (NW)

The data from Daniel's Harbour and Corner Brook show that the temperatures can go low, almost down to -40 °C during the winter (Daniel's Harbour, January-February).

8.3 Some comments on relevant icing processes

8.3.1 General

The basic concepts of the various forms of atmospheric icing are described in /Ref. 16/, Annex A. Below some further aspects on wet snow and freezing rain or drizzle are included in this chapter. Rime ice is discussed in

chapter 3. The comments and discussion here are meant as some background information to the preliminary load assessments in chapter 8.

8.3.2 Wet snow

As a "rule of thumb" indicator for wet snow the extremes for daily precipitation during winter months is often used. For Daniel's Harbour the values drop from 88.2 mm in November (5th, 1982) to 45 mm in February. Similar values apply for Corner Brook and Deer Lake. St. John's has measured about 100 mm. It is reasonable that the highest values are measured. We can therefore draw a preliminary conclusion that wet snow is hardly a dominant loading case along this line route. However, wet snow is always analyzed during the WRF simulations. Some information may therefore be developed during the case studies.

8.3.3 Freezing rain or drizzle

Freezing rain is a frequent phenomenon in Newfoundland. Several reports tell about devastating damages on overhead power line networks, a summary is given by A. Haldar, Nalcor, in (Haldar, 2007). Probably the biggest event appeared in St. John's on 11 April 1984 and lasted three days. An ice layer of almost 15 cm disrupted electrical power to 200 000 people.

In addition to Haldar's overview (Haldar, 2007) there are several studies of freezing rain and freezing drizzle in Canada and the US. A good overview is found in (Stuart and Isaac, 1999). Also, a more recent survey for both the US and Canada is shown in (Cortinas et.al., 2004).

Freezing rain depends on the vertical distribution of the air temperature, requiring an inversion layer where the temperature increases with height. At the top of the inversion the temperature must be well above 0 ºC to form a melting layer where falling snow melts into raindrops that in turn becomes supercooled in the freezing layer near ground, see Figure 75.

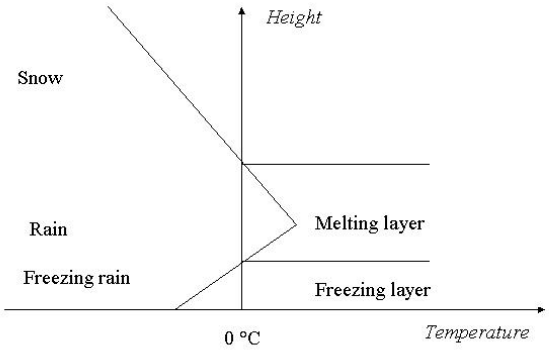

Figure 75. *Temperature conditions for freezing rain.*

Since freezing rain is a phenomenon that occurs at ground level and up through the freezing layer, it is of interest to know how deep such inversions can be in the region. This is unfortunately not known, but it is anticipated that little freezing rain will occur above 300-400 m.

Freezing drizzle is another process to create glaze ice, mostly known from aircraft icing. Freezing drizzle is formed in a separate way as freezing rain. Normally, droplets are formed in clouds by nucleation on so-called "condensation nuclei". These are very small hygroscopic particles (aerosols) in the atmosphere, mostly from sea salt, volcanic ash, soil dust, etc. Water vapor will then condense on these to form droplets. When these droplets become large enough they start to fall through the air and collide with other droplets and merge with them (coalesce), and may then grow to form drizzle. This process takes place even if the temperature is well below the freezing point.

A parallel process may take place when so-called "ice nuclei" are available in sufficient numbers. Then the water vapor goes directly into the ice phase and form ice crystals. Ice nuclei are activated at lower temperatures, below about -15 °C, than condensation nuclei which are activated around -10 °C. If ice crystals

and liquid droplets appear within the same cloud ice crystals will grow and the droplets evaporate, due to difference in saturation vapor pressure over ice and water surface. Eventually, the cloud will consist of only ice crystals (glaciated cloud).

Normally there is an abundance of condensation nuclei, while nuclei may occur in more limited numbers. However, if the number of ice nuclei is very low, then there will be little or no glaciations of clouds and droplets of liquid water will continue to grow by collision and coalescence. Hence, then freezing drizzle will eventually be formed.

As pointed out by several authors (Cortinas et al., 2004 /Ref. 8 /), (Stewart et al., /Ref. 7/), (Stuart and Isaac, 1999 /Ref. 44/), freezing drizzle occurs especially frequent over the East coast of the continent, with maxima over the north-eastern part of Newfoundland. A map showing contour lines for annual hours of freezing precipitation (rain + drizzle) is shown in Figure 76.

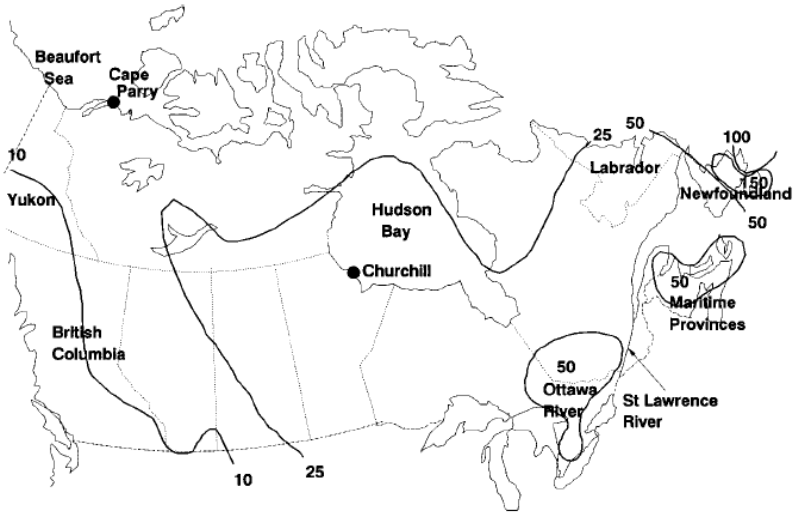

Figure 76. *Approximate contour lines for annual freezing precipitation hours for Canada. (Stuart and Isaac, 1999)*

It is anticipated that freezing rain occurs in connection with a low pressure system south of Newfoundland and a high pressure in the north. Cold air will be pushed southwards, especially around the eastern side of the island, and also through valleys and canals in the terrain in the NE-SW direction. If the low pressure brings a warm front northwards it is possible that a shallow layer with a temperature inversion will appear near the ground. With sub-freezing temperatures near the surface, and rain falling from above may be supercooled in the freezing layer.

This process supports the fact that freezing rain occurs mostly on the northern and eastern side of Newfoundland, especially on the Avalon Peninsula and Bonavista peninsula, as shown in Figure 76.

A special question is how deep the inversion layer may be in this area, and hence to which altitudes freezing rain may occur. From other experiences such inversion layers are often in the range of 200 – 300 m above ground or sea level.

Above this level we will have freezing drizzle. But still the intensities and amounts are unknown. It is therefore very important to include observations of the physical properties of the accreted ice in the observation scheme for the test sites. Such data are important also to compare with the WRF model results.

8.4 Ice loads vs radial ice concept

Generally there are two international concepts for assessing the action of ice on overhead line conductors, the *radial ice thickness* concept and the *mass (load) pr unit length (unit load)* of conductors. International codes are adapted according to the chosen concept in each country. In principle both concepts are equal as long as the ice density is unambiguous.

The *radial ice* concept is certainly unambiguous for icing due to freezing rain. In this case the ice density is always close to 900 kg/m^3, and there is always a relation between ice thickness and ice load on the conductor.

The concept represented by the terms *unit mass (kg/m)* or *unit load (N/m)* are often considered to be more suitable for other types of icing where the density varies within wider ranges, as demonstrated in Table 15. In these cases the ice mass or ice loads are often given with an associated density for the anticipated icing type in each case (may also vary between countries). Hence the diameter of the ice accretion is calculated from the load in order to establish the exposed area for wind pressure calculations. It is however always a question to define the appropriate density that will withstand the high winds for combined wind and ice loadings.

The densities in this project will be discussed along with the load assessments.

1 kg/m mass of ice corresponds to an ice load of 9.8 N/m. Often the factor 10 is used since the difference in resulting loads is well inside the intrinsic uncertainty of the values. The two notations are both commonly used internationally, somewhat imprecise however, for the same concept. This means that in many standards the term "load" is used, while the values are given as mass of ice per unit length of the conductor (kg/m).

To compare values of ice loadings with corresponding radial thicknesses for the traditional case of density equal to 900 kg/m^3 see Table 15. The conversion formula is:

$$m = \pi \cdot \rho \cdot R_{eq}(2r_0 + R_{eq}) \qquad \text{or} \qquad R_{eq} = \sqrt{r_0^2 + \frac{m}{\pi\rho}} - r_0$$

Where

m = unit ice mass on conductor (kg/m)

ρ = density of ice, 900 kg/m^3 is used in Table 15.

R_{eq} = equivalent ice thickness on conductor

r_0 = radius of conductor, here 15 mm.

Table 15. *Conversion table from unit ice mass, m (kg/m), to radial ice thickness. R_{eq} (mm). Density of ice: 900 kg/m^3. Conductor diameter is set here to 30 mm.*

m (kg/m)	1,1	2	3	4	5	6	7	8	10	12	15	20	25	30	40	50
R_{eq} (mm)	10	15.5	20.9	25.5	29.6	33.4	37.0	40.3	46.3	51.9	59.4	70.4	92.5	102	117	131

8.5 Ice loadings on existing lines on Northern Peninsula

The existing lines on the Northern Peninsula have a rather large dispersion in ice loadings, from 0.5 to 4.0 inches of radial ice. This corresponds from 13 mm to 102 mm. Table 15 shows that this again corresponds to a range of 1.5 – 30 kg/m load.

Table 16 gives a summary of these lines. It should be noted that the voltages of these lines are 69 kV, 138 and 230 kV. The two 230 kV lines are with steel towers, the others with wood poles. These lines are shown on the map in Figure 77.

It appears that all the lines along the western coast of the Northern Peninsula are designed according to the lowest loads, very probably due to the very low occurrence of freezing rain in this area. The highest ice load (r_{eq}=4", or m=30 kg/m) is for the 230 kV line from Deer Lake to Cat Arm. This line runs from SW towards NE up to White Bay. It is assumed that the lower load for this line (r_{eq}=1.75", or m≈10 kg/m) applies for this main direction of the line. A part of this line has however a NW-SE direction (see Figure 77) which is almost perpendicular to winds from the NE. It is assumed that this wind direction is the most critical for freezing rain in this area. Therefore this shift in design ice loading is logical.

The information here provided by Nalcor has been very useful for the further considerations of design ice loadings for the HVDC line.

Figure 77. *A map of the electric overhead line network in Newfoundland*.

Table 16. *Summary of loading assumptions for electric overhead power lines on Northern Peninsula (upper part) and Central Newfoundland (lower part)*

Line	Location	Voltage	Material	Loading				Percent decrease for Combined Condition	
				Max Ice	Max Wind	Combined			
		(kV)		(inch)	(mph)	Ice (inch)	Wind (mph)	Ice (%)	Wind (%)
TL 226	(Northern Peninsula) Deer Lake To Wiltondale	69	Wood	1	110	0.5	60	50	55
TL 227	(Northern Peninsula) Berry Hill To Daniel's Hr	69	Wood	1	110	0.5	60	50	55
TL 239	(Northern Peninsula) Berry Hill to Deer Lake	138	Wood	1	110	0.5	55	50	50
TL 241	(Northern Peninsula) Plum Point to Peter's Barren	138	Wood	0.5 - 2	110	1	55	50	50
TL 244	(Northern Peninsula) Plum Point to Bear Cove	138	Wood	1.5	95	0.5	55	33	58
TL 247**	(Northern Peninsula) Deer Lake To Cat Arm	230	Steel	1.75 - 4	110 - 130	1 - 2.5	50 - 60	60-65	50
TL 248	(Western Newfoundland) Deer Lake to Massey Drive	230	Steel	1.75	110	0.5	73	29	66
TL 251	(Northern Peninsula) Howley to Hampden	69	Wood	2	83	0.5	55	25	66
TL 252	(Northern Peninsula) Hampden to Jackson's Arm	69	Wood	2	83	0.5	55	25	66
TL 262	(Northern Peninsula) Daniel's Hr to Peters Barrens	69	Wood	1	110	0.5	60	50	55
TL 204	(Central Newfoundland) Stony Brook to Bay D'Espoir	230	Steel	1.75 - 2	110	0.5	73	30	66
TL 205	(Central Newfoundland) Stony Brook to Bay D'Espoir	230	Steel	1	110	0.5	73	50	66
TL 210	(Central Newfoundland) Grand Falls to Gander	138	Wood & Steel	1	110	0.5	73	50	66
TL 211	(Western Newfoundland) Massey Drive to Stephenville	230	Steel	1	110	0.5	73	50	66
TL 214	(Westcoast Newfoundland) Bottom Brook to Doyles	138	Steel & Alum.	1	117	0.5	55	50	47
TL 215	(Westcoast Newfoundland) Doyles to Grand Bay	69	Wood	1.5	150	1	73	67	49
TL 231	(Central Newfoundland) Stony Brook to Bay D'Espoir	230	Steel	1.75 - 2	110	0.5	73	30	66
TL 232	(Central Newfoundland) Buchans to Grand Falls	230	Wood & Steel	2	110	0.5	55	25	50
TL 233	(Western Newfoundland) Buchans to Bottom Brook	230	Wood & Steel	1.5	110	0.5	55	33	50
TL 248	(Western Newfoundland) Deer Lake to Massey Drive	230	Steel	1.75	110	0.5	73	29	66

8.6 Preliminary assessments of load categories

The ice loads in this report are classified as shown in Table 17. This classification is used for all three icing type: wet snow, freezing rain and rime ice.

Table 17. *Load categories (LC) for NFLD side.*

Level	Meaning
L	Low
M	Moderate
H	High
VH	Very high
E	Extreme

Details of the transmission route and local topography are presented in [Report April 2010]. The preliminary load classification for individual sections of the line route, after the results and discussions shown in this report, are shown in Figure 20. The individual sections refer to angle points marked for the line in Figure 78. This load classification must be considered as a first approach towards final load assessments that will depend on future studies.

Table 18. *Load categories for transmission line between angle points PI 19 and PI41*

From	To	Wet snow	Freezing rain	Rime ice
PI 19	PI 20		L	
PI 20	PI 21		L	
PI 21	PI 22		L	
PI 22	PI 23		L	
PI 23	PI 24		M	
PI 24	PI 25	L		
PI 25	PI 26	L		H
PI 26	PI 27			E
PI 27	PI 28			E - VH
PI 28	PI 29			VH
PI 29	PI 30			VH
PI 30	PI 31	H		VH
PI 31	PI 32C	H		
PI 32C	PI 33C	H		
PI 33C	PI 34C	H		
PI 34C	PI 35C	H		
PI 35C	PI 36C	H		
PI 36C	PI 37C	H - M		
PI 37C	PI 37	M - L		
PI 37	PI 38	M – L		
PI 38	PI 39	M – L		
PI 39	PI 40		M – L	
PI 40	PI 41	M	L?	

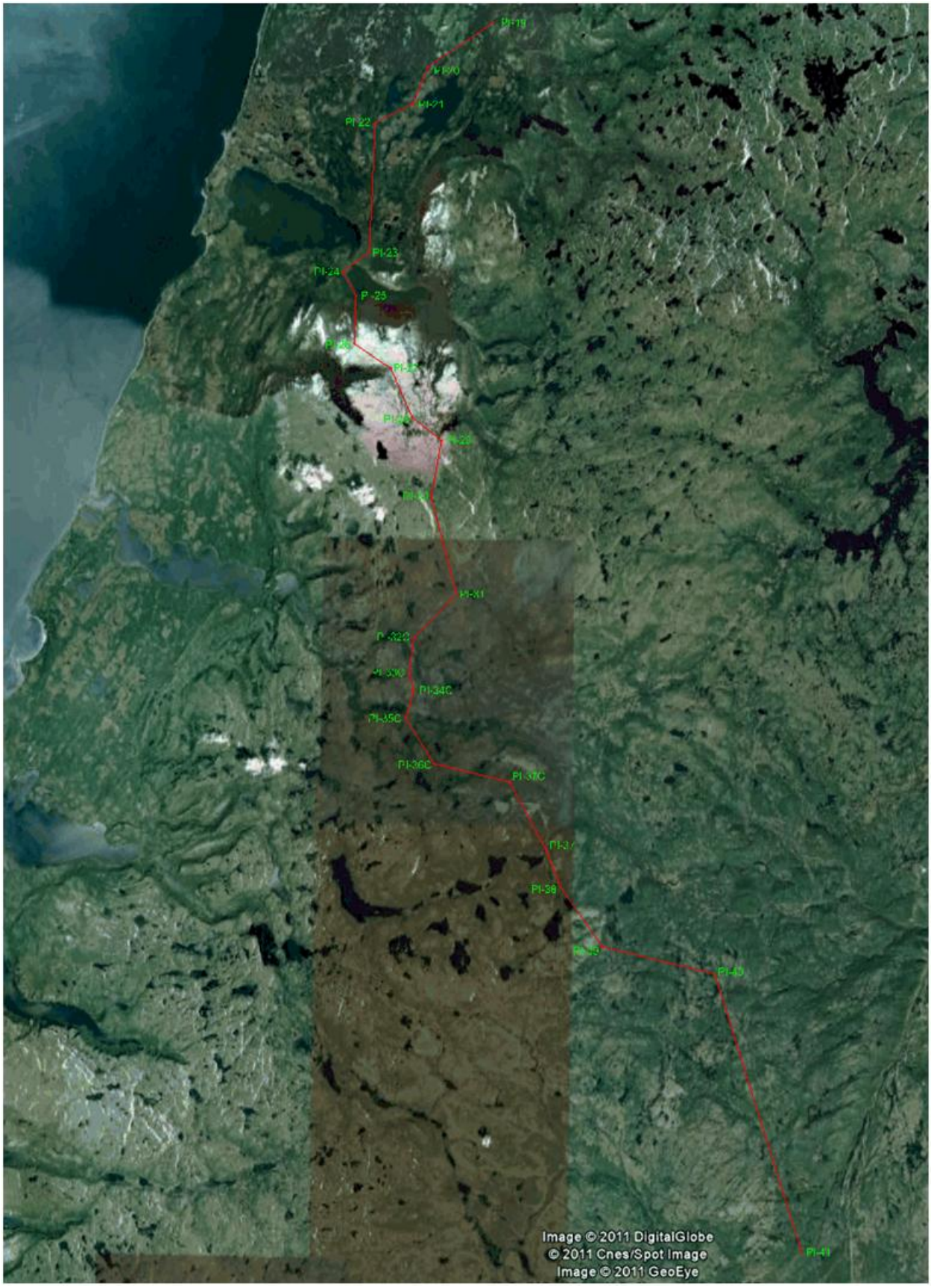

Figure 78. *Line route with angle points, PI, marked. Ref. to Table 18.*

9 Conclusion and proposed next steps

9.1 Conclusions from studies and measurements presented in this report

This study reveals that the risk of rime icing increases in the Long Range Mountains (LRM) above 300-400 m asl in areas open towards the SW-W on the western side of the mountain range and areas open towards the N-E on the eastern side. Above 500 – 600 m asl severe rime icing can occur with winds from both sectors, depending on the efficiency of sheltering terrain.

Measurements in test spans 2009-1 and 2009-2 confirm that icing is frequent in the area and that it is very site dependent. The test span 2009-1 is much more exposed to in-cloud icing than the test span 2009-2. In the period 2009-11-23 to 2010-06-14 there were 7 icing events with more than 1 kg/m in test span 2009-1 and 3 events in test span 2009-2. The highest ice load recorded on the test spans during the winter 2009-2010 was 7.2 kg/m on (15 January 2010) but the highest icing in test span 2009-2 was around 1.5 kg/m. The icing events recorded by the test spans during the winter 2009-2010 occurred with winds from both the SW-W and from the N-E.

The in-cloud icing in the area was studied in detail with icing models that used two different sources of input data: (i) WRF model (ii) WObs model. The WRF model is a state-of-the-art meso-scale numerical weather prediction system model that runs three dimensional analysis of the atmosphere; it does not need local weather information for the model. The WObs model is based on the Harstveit model but partly developed/modified for this study. The WObs model needs high quality routine weather observation from routine weather. It is to be expected that these icing models are most suitable to predict icing in range of 0 – 20 kg/m. Higher icing is related to large and irregular cross sections of ice and the estimate of collision coefficient is then less reliable. Higher icing is also often related to long duration of ice on conductors and ice shedding is not reliably assessed for any model.

Simulations of ice loadings with the WRF model are reasonably comparable for three test cases with the measured data from test span 2009-1 and test span 2009-2. The simulations give very useful information on relative icing risk in the area and how exposed each line section is.

The WObs model has been applied on weather observations from Daniel's Harbour for the period 1966 – July 2010. Comparison between the model and measurement shows that the model identifies almost all accumulation periods and gives acceptable estimation of icing. Comparison between field observation of icing on test towers #2 and #2b in the period 1974 – 1987 shows very good correlation, i.e. the WObs model predicts icing to similar amount as observed.

All major icing events in the period of 1966 – July 2010 were predicted by the WObs model, and it was found that some of the most significant icing events are within the period when the icing data collection program was operated during 1974-1987. Field visits and observations have been taken during some of the most important events, among them is the highest event and the third highest event. The winter 2009-2010 was found to have small icing events compared to the more severe winters.

The significant icing from February 1977 at test tower #4 in Labrador was modeled. The WObs model with data from Battle Harbour predicted a maximum icing of 25 kg/m in February. Icing was not reliably identified by the WRF model studies in the periods that were analyzed.

Review was made on the previous estimation of in-cloud icing in the LRM area. The conclusion was that it seems to be an overestimation of ice loading.

The main conclusions that can be drawn from studies presented in this report are:

- The icing measurements in test spans (2009-1 and 2009-2) give very important input for the study of in-cloud icing in the area. Especially to verify icing models that predict long term icing data.
- Icing is very frequent and may remain on conductors for some weeks in the most severe events in the exposed areas.

- The WObs model study indicates that in-cloud icing with a 50 year return period may be of the order of magnitude of 50 kg/m where conductors may approach local terrain levels on the western side of the Long Range Mountains (test span 2009-1). Loading predicted in test span 2009- 2 may be as low as 10 kg/m for the given line route.
- The winter 2009-2010 was found to have small icing events compared to the more severe winters.
- The Climatologically Monitoring Program that was operated from 1973-1987 has been useful since it contains visit to test towers in some of the most severe icing events that are predicted by icing models. The towers were visited in two of the three most severe cases.
- Previously defined ice loading in the area seems to be an overestimation and it does not take into account sheltering effects for many line sections in the Long Range Mountains.
- The most severe icing can be expected both from SW and NE directions.

9.2 Recommendations for continued studies

The following recommendations are made for the continued studies for the Long Range Mountains area

- Significant icing events for the winter 2010-2011 should be analyzed and compared with the WRF and WObs studies.
- Make a proposal of the final line route within available corridor in the Long Range Mountains with respect to ice loading.
- Provisional ice loading may be proposed for the final route in the Long Range Mountains area when measurements during the 2010-2011 season are studied. The final load assessments should be made at the latest possible stage before the final line design is to be made, in order to have all information updated at this stage.
- Wind measurements at test site 2009-1 (and perhaps 2009-2) should be operated. The state-of-the-art cameras and camera housing in harsh environments should be checked. Options for telecommunication of data and pictures should also be checked.
- Combination of wind and ice for the final route in the LRM area should be proposed.
- The vertical extension of risk zones for freezing rain should be better quantified.

The following recommendations are made for continued studies in the Labrador area

- A field study of the line route on the Labrador side is recommended before any further plans are specified for this part, both considering model studies and possible test sites.
- Further study with WRF and WObs icing models should be made if the final line route will pass in-cloud icing areas.

10 Reference list

Ref. 1 Boomer R.J., Richmond (Meteorology Research) M.C. A Meteorological Evaluation of the Combined Wind and Ice Loadings for a Portion of the Gull Island Transmission Line. MRI 74 R-1255. 20 September 1974.

Ref. 2 Brown R., Krishnasamy S., et,al. Climatological ice accretion modeling. Canadian climate centre Report No. 84-10. Ontario 1984.

Ref. 3 Butt Desmond. Ice Observations in Newfoundland and Labrador. 3rd IWAIS, Vancouver 1986.

Ref. 4 Cigré WG. B2.16, TF 03 Guidelines for Meteorological Icing Models, Statistical Methods and Topographical Effects. WG. B2.16, Task Force 03. Brochure 291, April 2006

Ref. 5 Cigré WG. B2.29, Systems for prediction and monitoring of ice shedding, anti-icing and de-icing for power line conductors and ground wires. Brochure 438, December 2010.

Ref. 6 COST 727 Atmospheric Icing on structures Measurements and data collection on icing: State of the Art. ISSN: 1422-1361. MeteoSchweiz 2007.

Ref. 7 Cober S.G. Isaac G., Strapp W. Characterizations of Aircraft Icing Environments that Include Supercooled Large Drops. JOURNAL OF APPLIED METEOROLOGY.

Ref. 8 Cortinas J.V., Bernstein B., Robbins.C, Strapp J.W. An Analysis of Freezing Rain, Freezing Drizzle, and Ice Pellets across the United States and Canada: 1976–90: WEATHER AND FORECASTING, Nov. 2001.

Ref. 9 Drage M., Atmospheric icing and meteorological variables – Full scale experiment and testing of models, Ph.D. dissertation, Reports in Meteorlogy and Oceanography, Report No. 4, 2005, University of Bergen, Norway, 2005.

Ref. 10 Drage, M. and Hauge, G., 2008: Atmospheric icing in a coastal mountainous terrain. Measurements and numerical simulations. Cold Regions Science and Technology 53, 150-161.

Ref. 11 Eliasson Á.J., Thorsteins E. Ice load measurements in test spns for 30 years. 12th IWAIS, Yokohama, October 2007.

Ref. 12 Eliasson Á.J., Gunnlaugsson P.Þ., Thorsteins E. Ice accumulation at measuring site Hallormsstadahals. 13 IWAIS 2009, Andermatt September 2009

Ref. 13 Fikke S.M. Modern Meteorology and Atmospheric Icing. 11th IWAIS, 2005.

Ref. 14 Finstad K., Lozowski E.P. and Gates E.M., A computational investigation of water droplets trajectories, J.Oceanic Atmos. Technol., 5, 160-170, 1988.

Ref. 15 Gudmundsson A., Thorsteins E., Bergmundsson J., HVDC Labrador – Island Transmission Link. Review of In-cloud icing on the Long Range Mountain Ridge. LVP and EFLA Cons. Eng. Reykjavík, May 2009.

Ref. 16 Gudmundsson A., Fikke S., Eliasson Á.J.,HVdc Labrador – Newfoundland Transmission Link. Ice loadings on HVdc line crossing Long Range Mountains. Report #1: General conditions, preliminary inspection, selection of test sites and proposals for further procedures. LVP 2009.

Ref. 17 Haldar Asim Twenty Years of Ice Monitoring Experience On Overhead Lines In Newfoundland and Labrador. 12th IWAIS, Yokohama 2007.

Ref. 18 Harstveit K, In-cloud rime calculations from routine meteorological observations at airfields, in Proc. 10th Int. Workshop on Atmos. Icing of Structures, Brno, Czech Republic, 2002.

Ref. 19 Harstveit K., Using Metar – Data to calculate in-cloud icing on a mountain site near by the airport in Proc. 13th Int. Workshop on Atmos. Icing of Structures, Andermatt, Swiss, 2009.

Ref. 20 ISO/TC98/SC3/WG6, Atmospheric icing of structures, International Standard, ISO 12494, 2000.

Ref. 21 Leavengood, D.C., and T.B. Smith, Studies of transmission line icing. Rept. By MRI to Southern California Edison Company, L.A. California, Cont. No. L-2127, MRI 68 FR-801. 1968

Ref. 22 Makkonen, L., 2000: Models for the growth of rime, glaze, icicles and wet snow on structures. Phil. Trans. R. Soc. London, 358, 2913–2939.

Ref. 23 Mallory J.H., Leavengood, D.C. Extreme Glaze and rime ice loads in southern Calicornia. 1th International Workshop on Atmospheric Icing of Structures (IWAIS 1982), 1-3 June 1982, Hanover, New Hampshire.

Ref. 24 Meteorology Research „Meteorological Evaluation of Eastern Side of the Great Northern Peninsula, Newfoundland“ by Meteorology Research, Inc. In 1977.

Ref. 25 Mont Shaw. 1977 Review of HVDC Line Routing in the Great Northern Peninsula Region. Newfoundland limited in 1977.

Ref. 26 Newfoundland and Labrador Hydro. Report on 1977/78 Climatological Monitoring Program. October 1978.

Ref. 27 Newfoundland and Labrador Hydro. Report on 1978/79 Climatological Monitoring Program. June 1979.

Ref. 28 Newfoundland and Labrador Hydro. Report on 1979/80 Climatological Monitoring Program. Aug. 1980.

Ref. 29 Newfoundland and Labrador Hydro. Report on 1980/81 Climatological Monitoring Program. June 1981.

Ref. 30 Newfoundland and Labrador Hydro. Report on 1981/82 Climatological Monitoring Program. Dec. 1982.

Ref. 31 Newfoundland and Labrador Hydro. Report on 1982/83 Climatological Monitoring Program. August 1983.

Ref. 32 Newfoundland and Labrador Hydro. Report on 1983/84 Climatological Monitoring Program. Sept. 1984.

Ref. 33 Newfoundland and Labrador Hydro. Report on 1984/85 Climatological Monitoring Program. August 1985.

Ref. 34 Newfoundland and Labrador Hydro. Report on 1985/86 Climatological Monitoring Program. Oct. 1986.

Ref. 35 Newfoundland and Labrador Hydro. Report on 1986/87 Climatological Monitoring Program. Sept. 1987.

Ref. 36 Nygaard B.E. Evaluation of icing simulations for the “COST727 icing test sites in Europe” in Proc. 13th Int. Workshop on Atmos. Icing of Structures, Andermatt, Swiss, 2009.

Ref. 37 Nygaard B.E., J.E. Kristjansson, E. Berge and L. Makkonen,, 2007: Using NWP models to simulate in-cloud atmospheric icing episodes. 12th International Workshop on Atmospheric Icing of Structures (IWAIS 2007), 9-13 October 2007, Yokohama, Japan, 4 p.

Ref. 38 Nygaard B.E., Fikke S.M., Elvertø L., Harstveit K. Modeling Icing in Exposed Mountain Terrain. 12 th IWAIS, Yokohama, October 2007.

Ref. 39 Nygaard B.E., Kristjánsson J.E., Berge E., Makkonen L. Using NWP models to simulate in-cloud atmospheric icing events. 12th IWAIS, Yokohama, October 2007.

Ref. 40 Pilkington R., Hill C., Langford L., A Review of the Environmental Conditions on the West Coast of Newfoundland PERD/CHC Report 20-34, 1997-10.

Ref. 41 Richmond M.C., Fegley M.J. (Meteorology Research) Revised Combined Wind and Ice Loadings for a Portion of the Gull Island Transmission Line. Jan. 30, 1975.

Ref. 42 Richmond M.C., Fegley M.J. (Meteorology Research) The follow- on Meteorological Evaluation of the Proposed Gull Island Transmission Line Network. 31 October 1975.

Ref. 43 Richmond M.C., Fegley M.J. (Meteorology Research) Meteorological Study of the Gull Island-Stephenville-Holyrood Transmission Line Routes. 30 november 1973.

Ref. 44 Stuart R.A, Isaac G.A. Freezing Precipitation in Canada, ATMOSPHERE-OCEAN 37 (1) 1999, 87–102.

Ref. 45 Sundin E., and Makkonen L., Ice loads on a lattice tower estimated by weather station data, J.Appl. Meteor., 37, 523-529, 1998.

Ref. 46 Thompson G, Nygaard B.E., Makkonen. L, .Dierer S. Using the Weather Research and Forecasting (WRF) Model to Predict Ground/Structural Icing. ” in Proc. 13th Int. Workshop on Atmos. Icing of Structures, Andermatt, Swiss, 2009.

Ref. 47 Thorkildson, Ronald M., Kathleen F. Jones, Maggie K. Emery, 2009: In-Cloud Icing in the Columbia Basin. Mon. Wea. Rev., 137, 4369–4381.

Ref. 48 Weather Eng. Corp. of Canada. Study of Climatological Monitoring Program 1977-1981, Final Report. April 1982.

11 Appendix A – Detailed model information on selected icing events at test site 2009-1.

Note that wind in WObs model is defined as the orthogonal to span (i.e. depends on span direction) while wind at Daniel's Harbour and wind in WRF is not reduced according to the span direction.

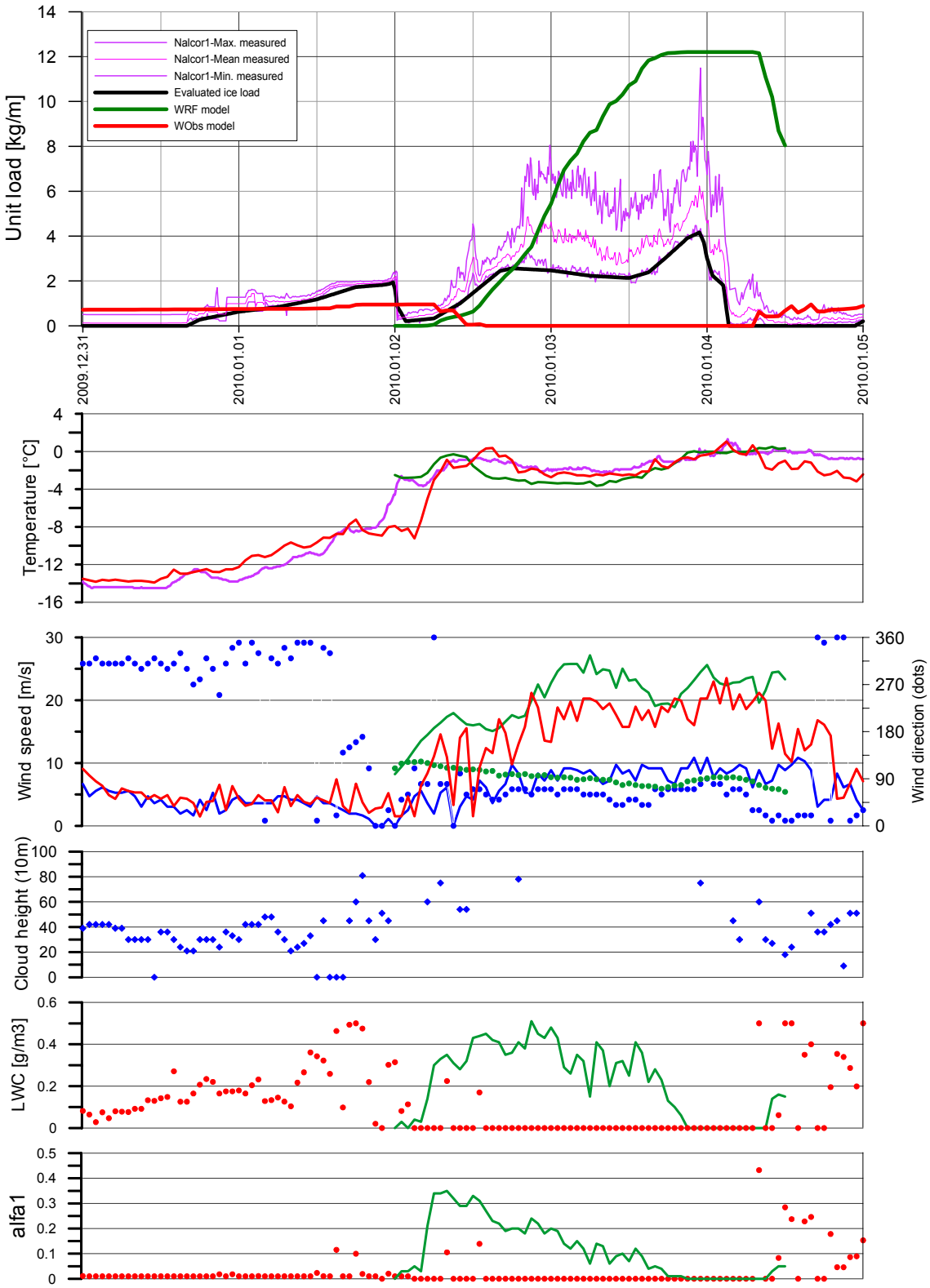

Figure 79. *Measurements from test site 2009-1 and Daniel's Harbour and results from WRF and WObs models.*

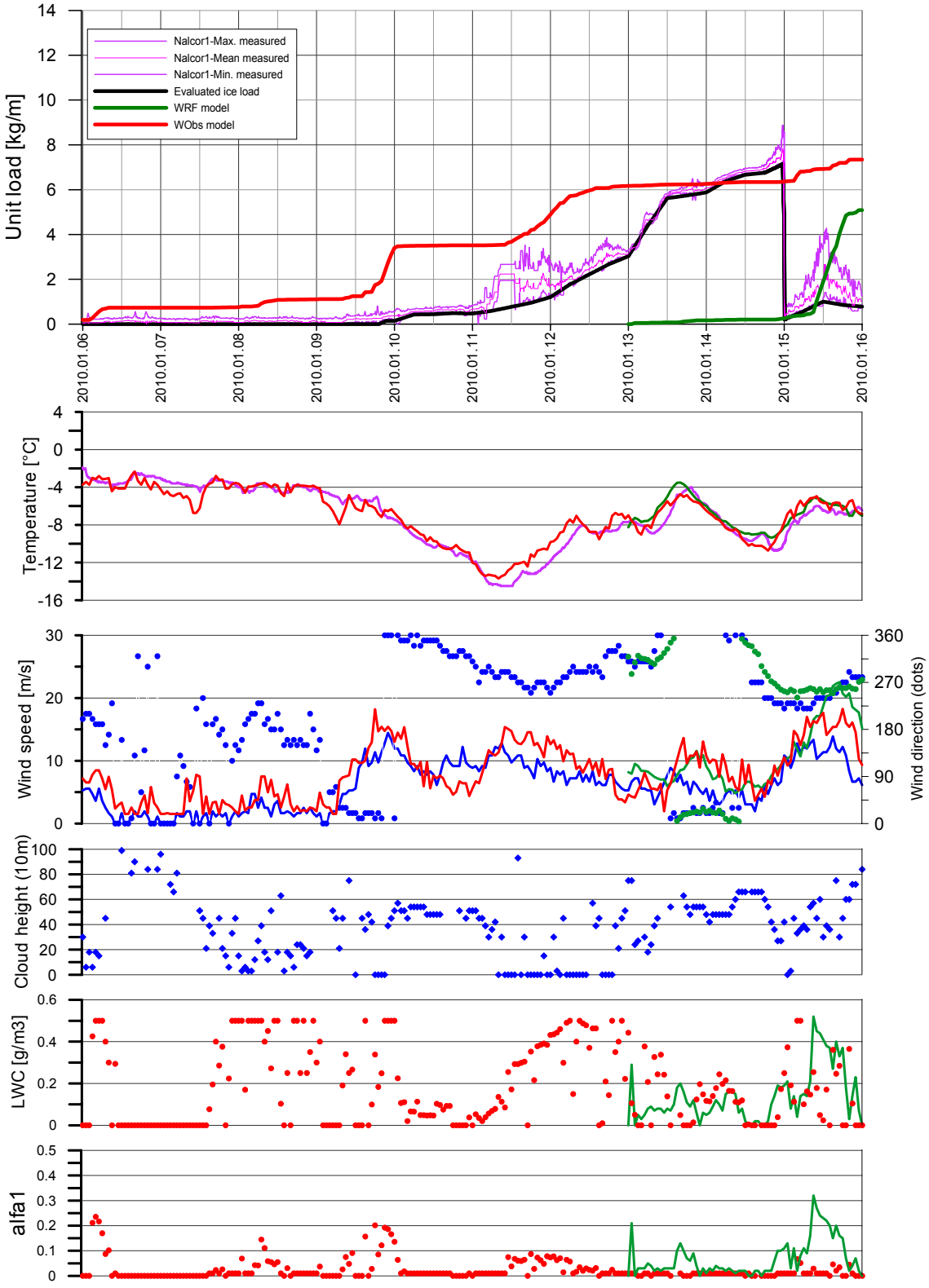

Figure 80. *Measurements from test site 2009-1 and Daniel's Harbour and results from WRF and WObs models.*

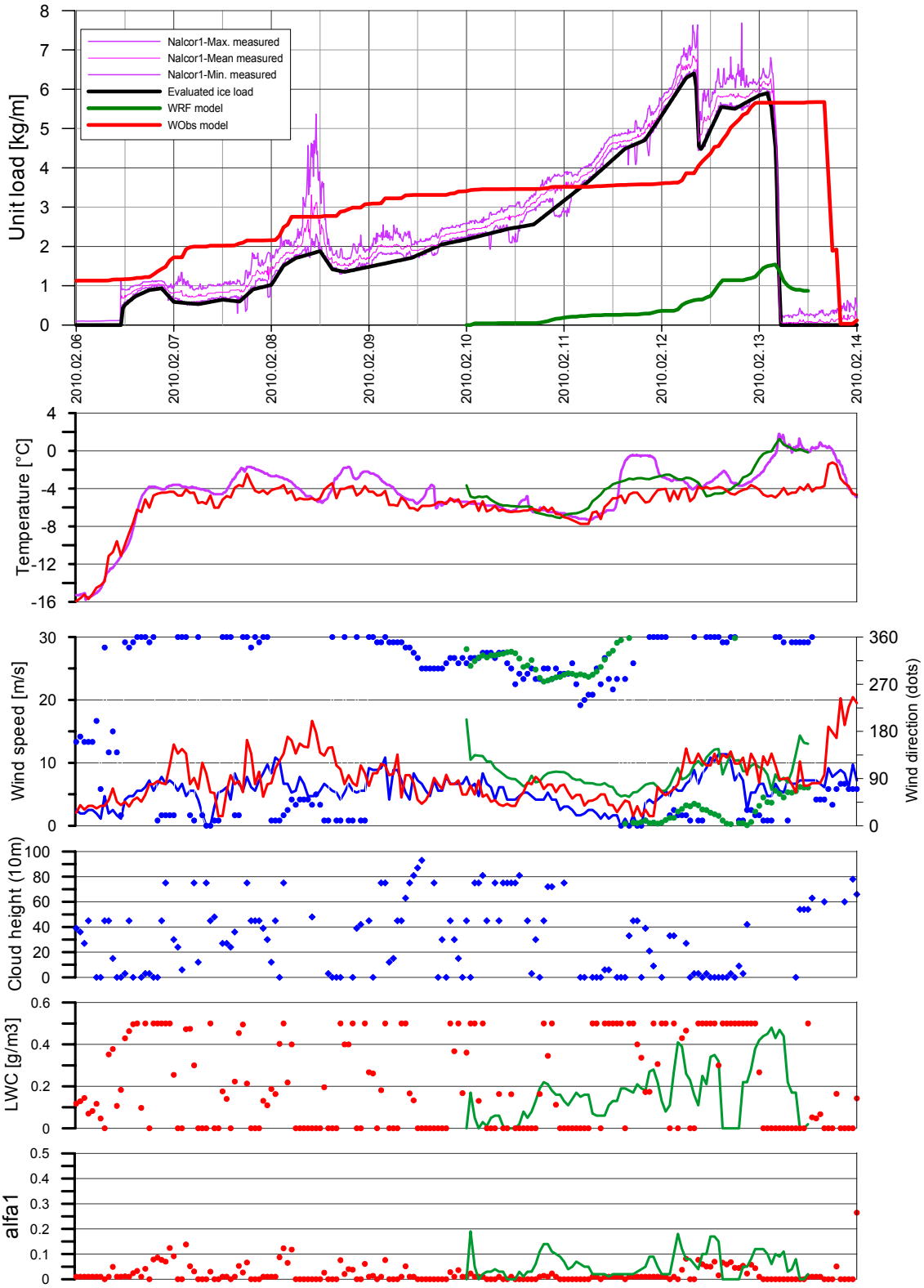

Figure 81. *Measurements from test site 2009-1 and Daniel's Harbour and results from WRF and WObs models.*

12 Appendix B – Test site 2009-1, comparison between measured icing and WObs

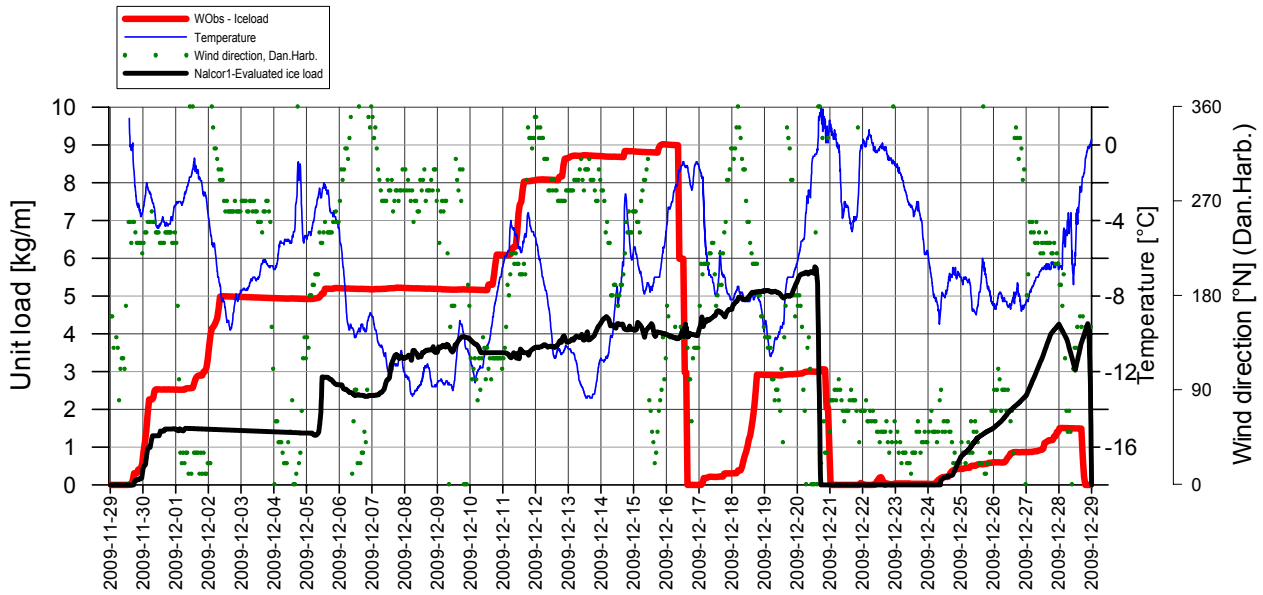

Figure 82. *Site 2009-1, comparison between measured icing (black) and icing predicted by WObs model (red).*

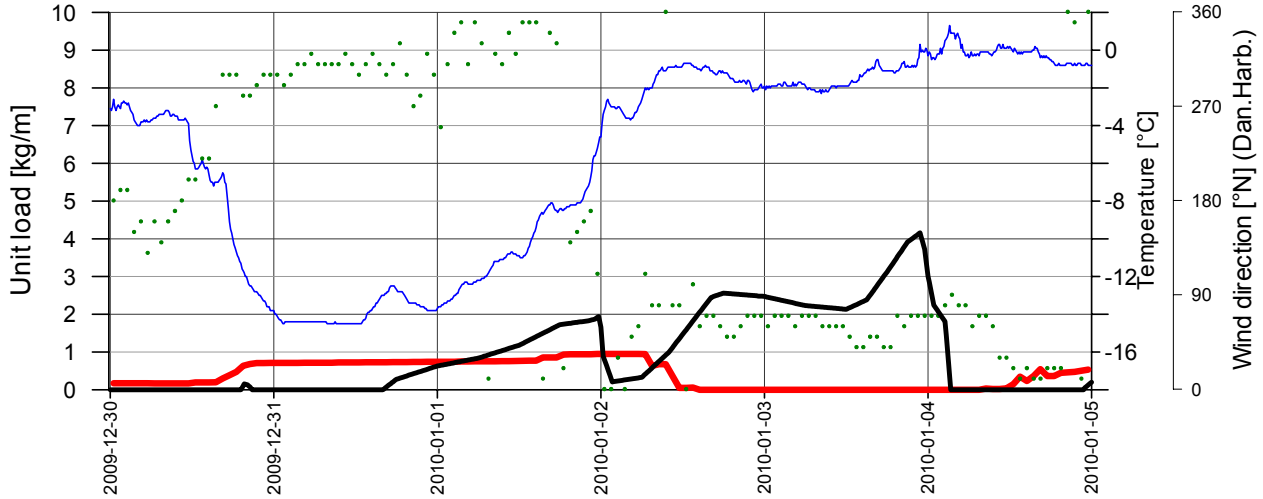

Figure 83. *Site 2009-1, comparison between measured icing (black) and icing predicted by WObs model (red).*

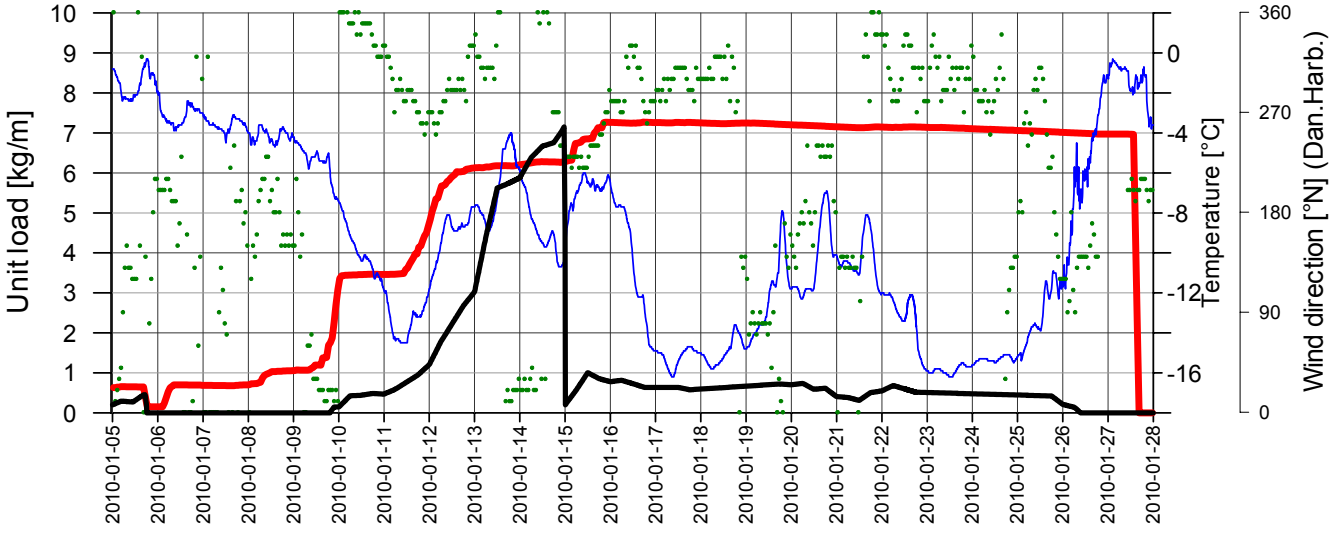

Figure 84. *Site 2009-1, comparison between measured icing (black) and icing predicted by WObs model (red).*

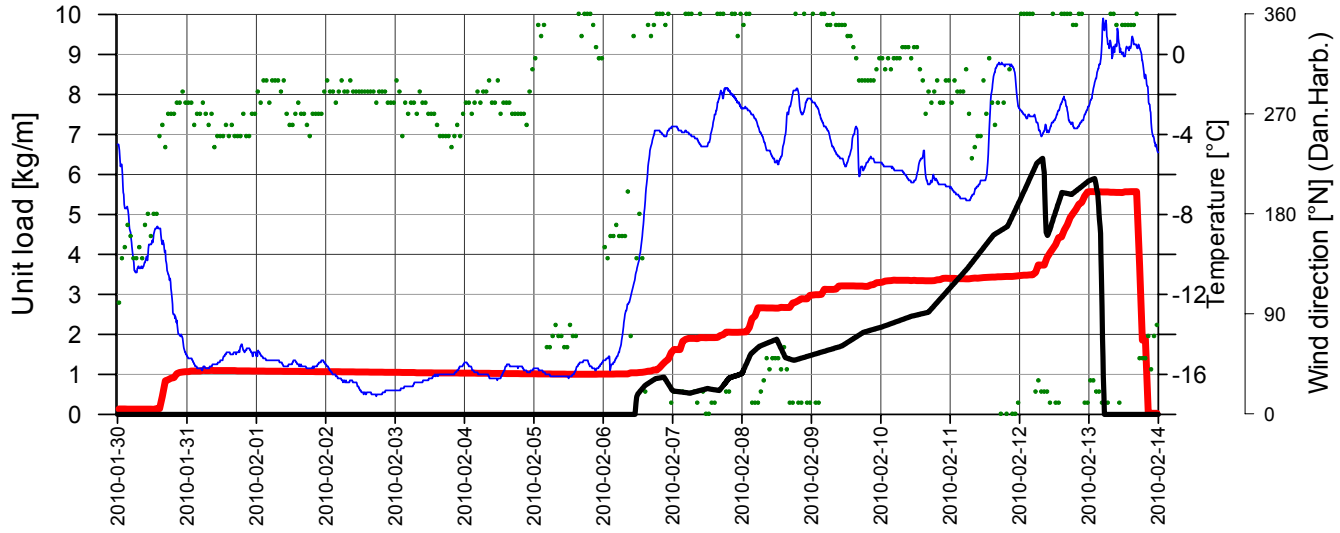

Figure 85. *Site 2009-1, comparison between measured icing (black) and icing predicted by WObs model (red).*

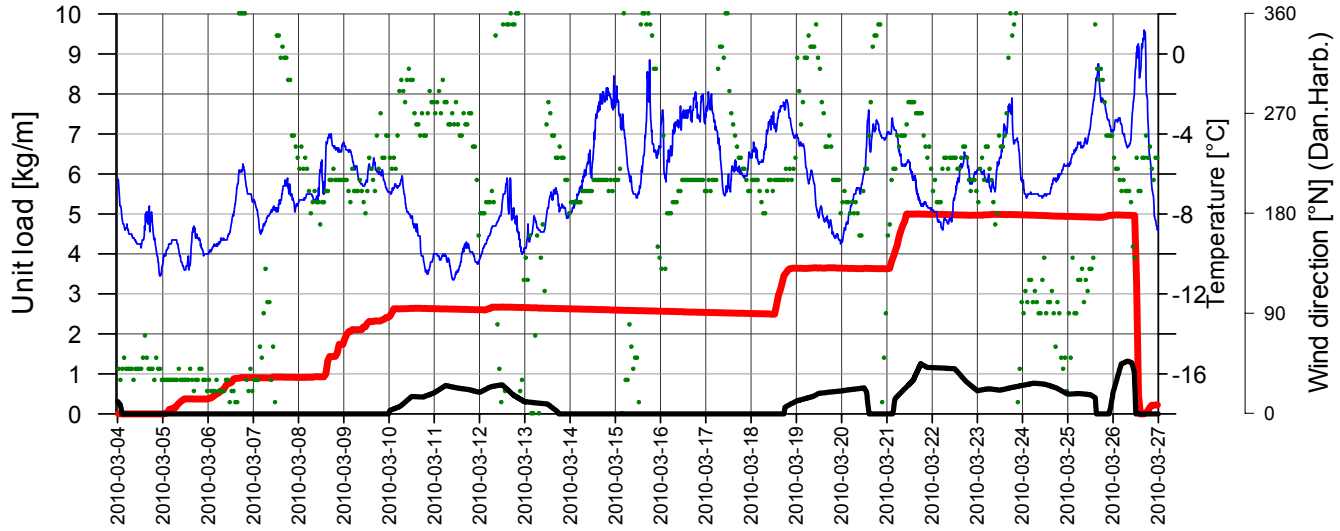

Figure 86. *Site 2009-1, comparison between measured icing (black) and icing predicted by WObs model (red).*

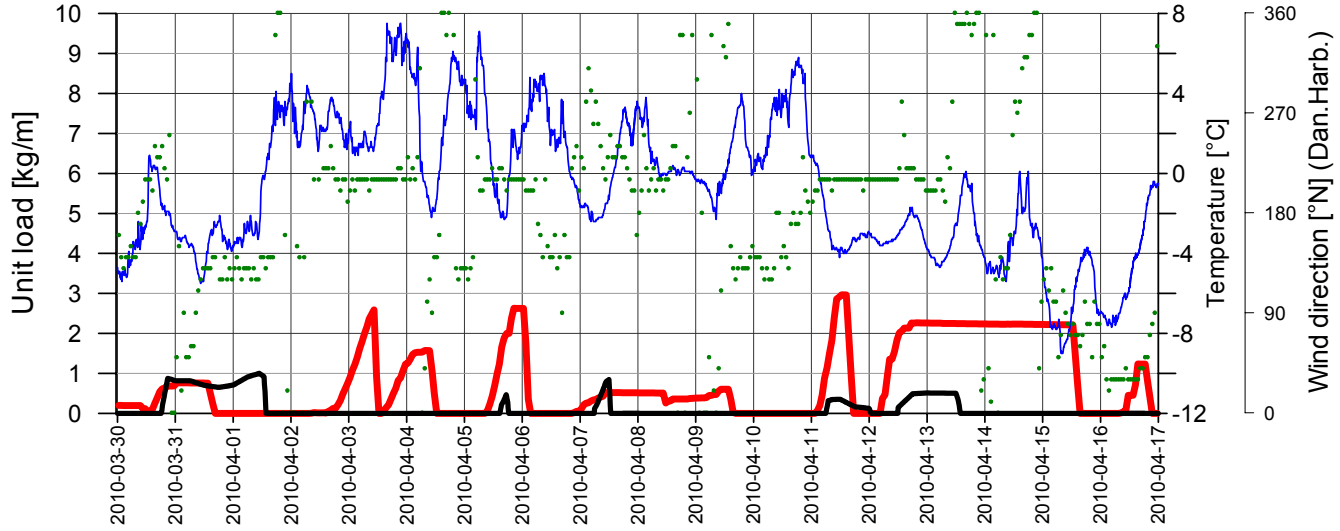

Figure 87. *Site 2009-1, omparison between measured icing (black) and icing predicted by WObs model (red).*

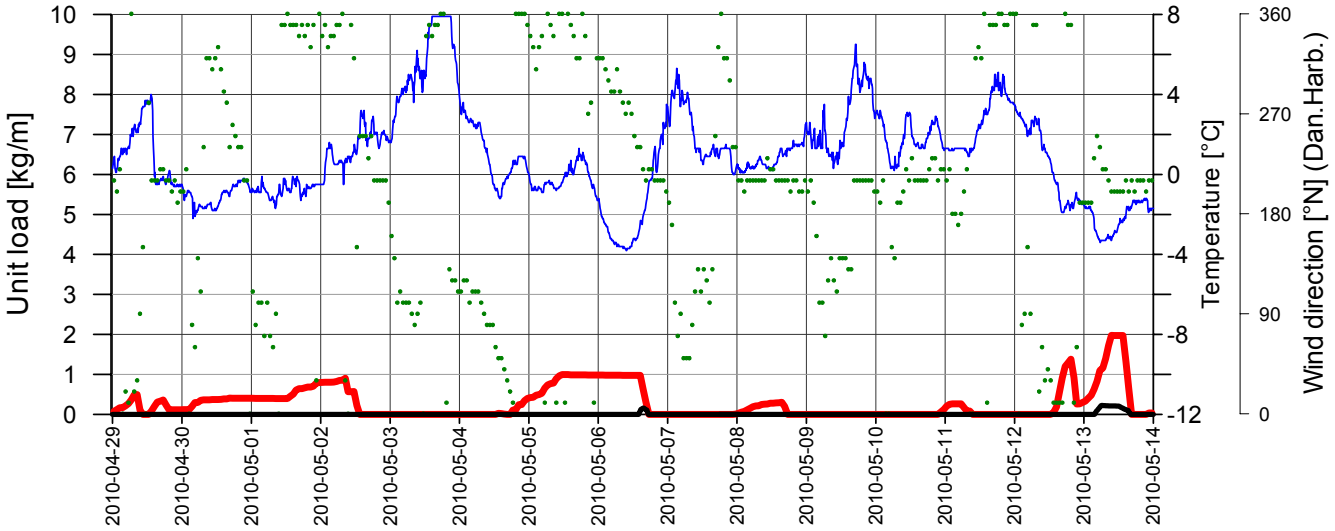

Figure 88. *Site 2009-1, comparison between measured icing (black) and icing predicted by WObs model (red).*

13 Appendix C – Test span 2009-2, comparison between measured icing and WObs

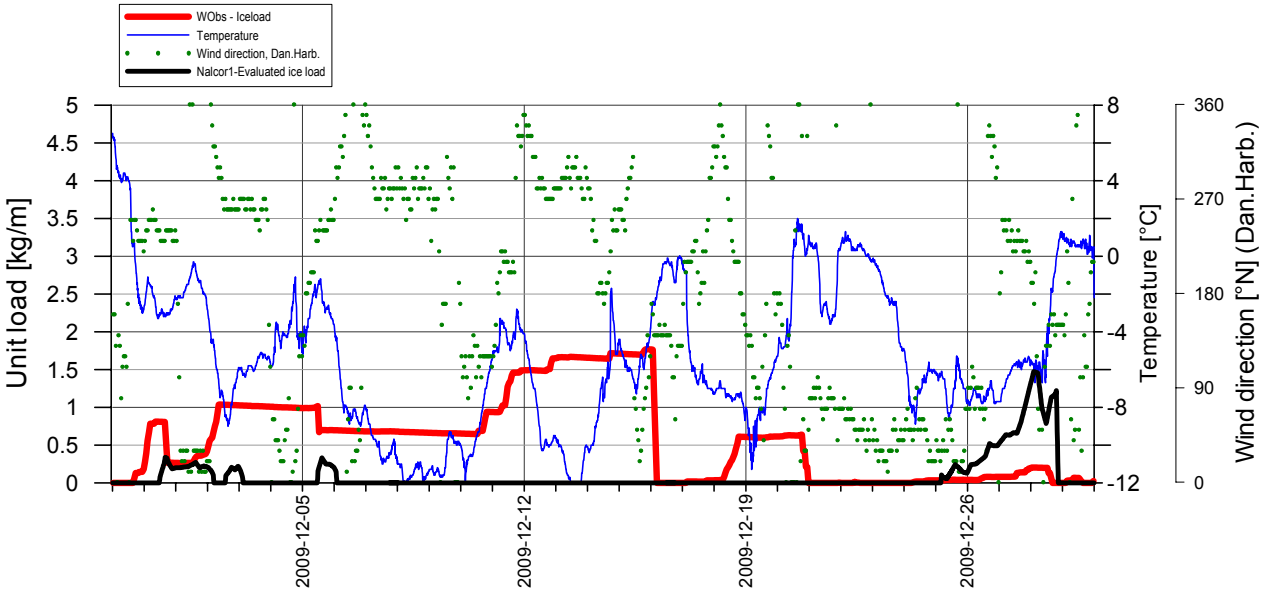

Figure 89. *Site 2009-2, comparison between measured icing (black) and icing predicted by WObs model (red).*

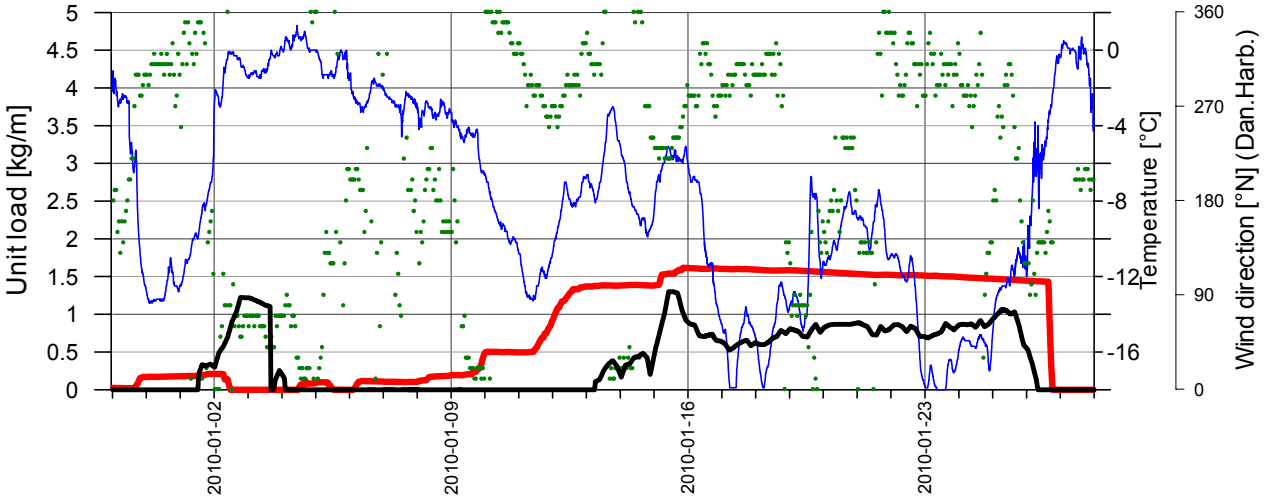

Figure 90. *Site 2009-2, comparison between measured icing (black) and icing predicted by WObs model (red).*

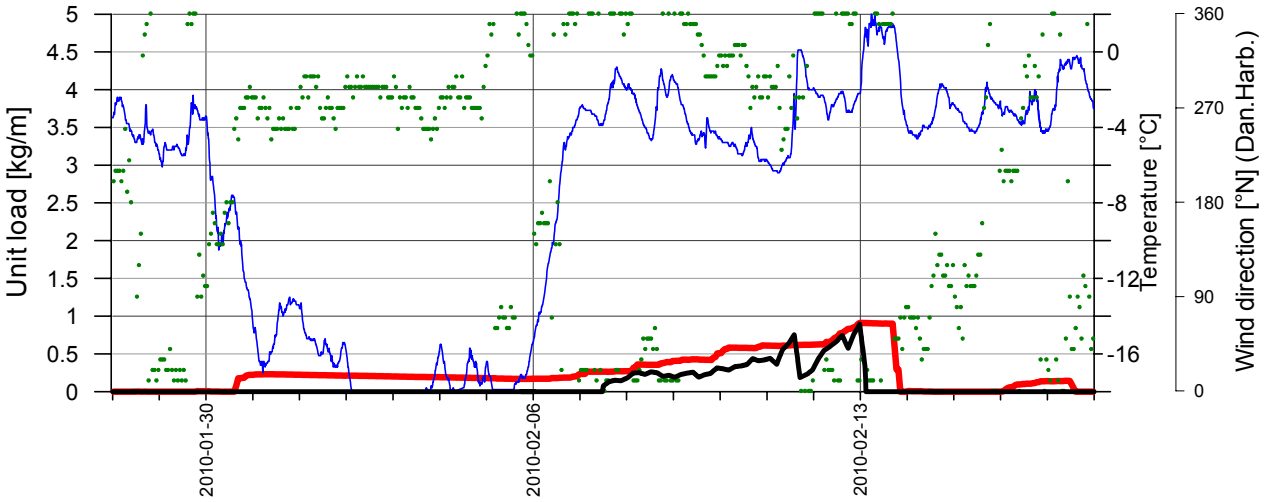

Figure 91. *Site 2009-2, comparison between measured icing (black) and icing predicted by WObs model (red).*

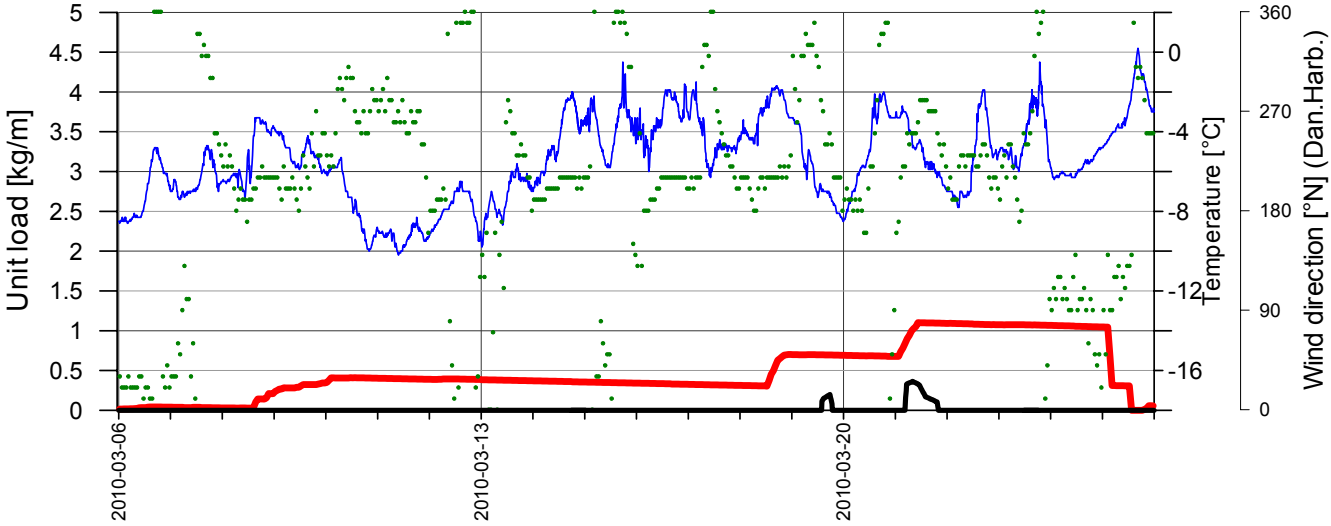

Figure 92. *Site 2009-2, comparison between measured icing (black) and icing predicted by WObs model (red).*

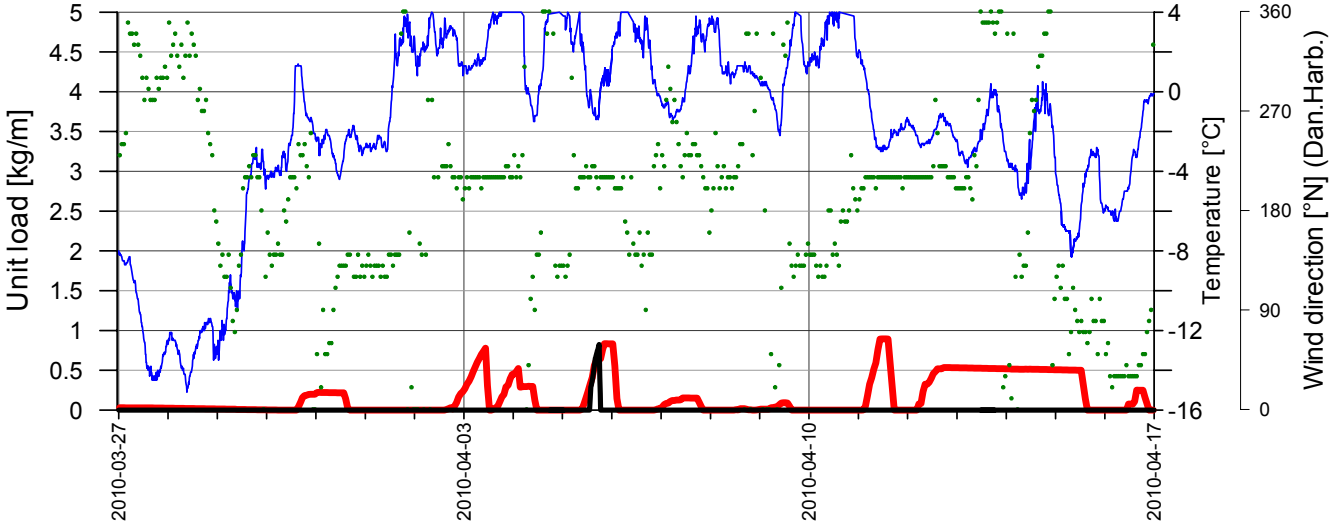

Figure 93. *Site 2009-2, comparison between measured icing (black) and icing predicted by WObs model (red).*

14 Appendix D – Wind statistic from the Transport Canada Wind and Wave Atlas

The following is information on wind statistics on the North east coast of Newfoundland and the West coast of Newfoundland. The data is obtained from the Transport Canada Wind and Wave Atlas and downloaded from the following sites:

http://www.meds-sdmm.dfo-mpo.gc.ca/alphapro/wave/TDCAtlas/TDCAtlasEC.htm#ECMap

http://www.meds-sdmm.dfo-mpo.gc.ca/alphapro/wave/TDCAtlas/TDCProducts.htm

Newfoundland – North east coast

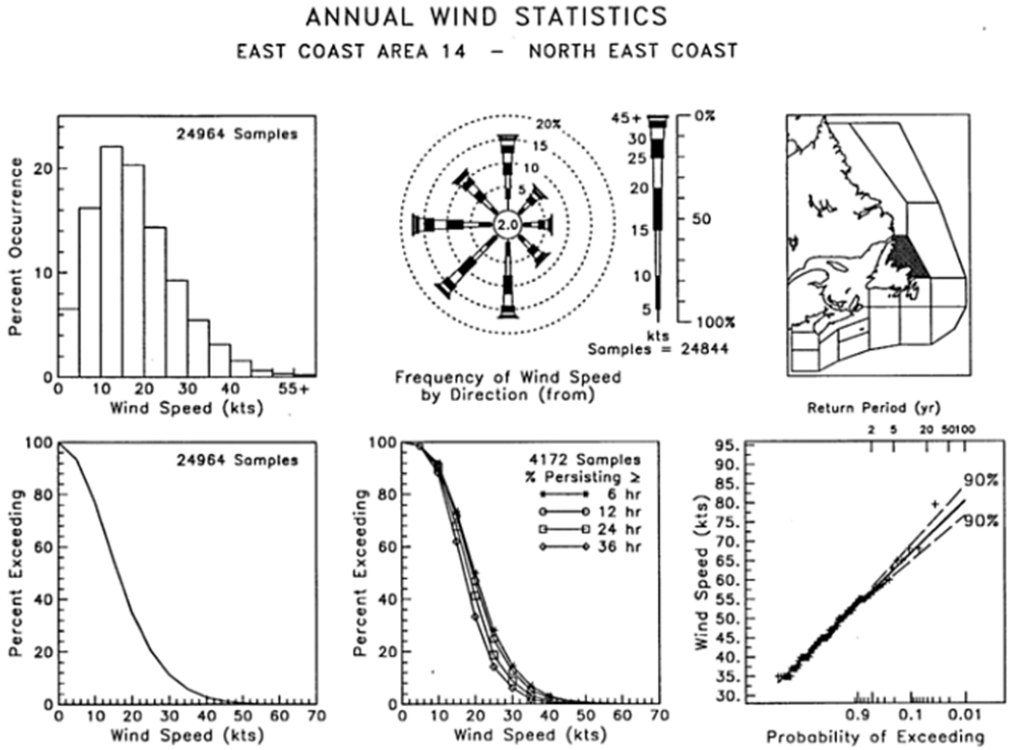

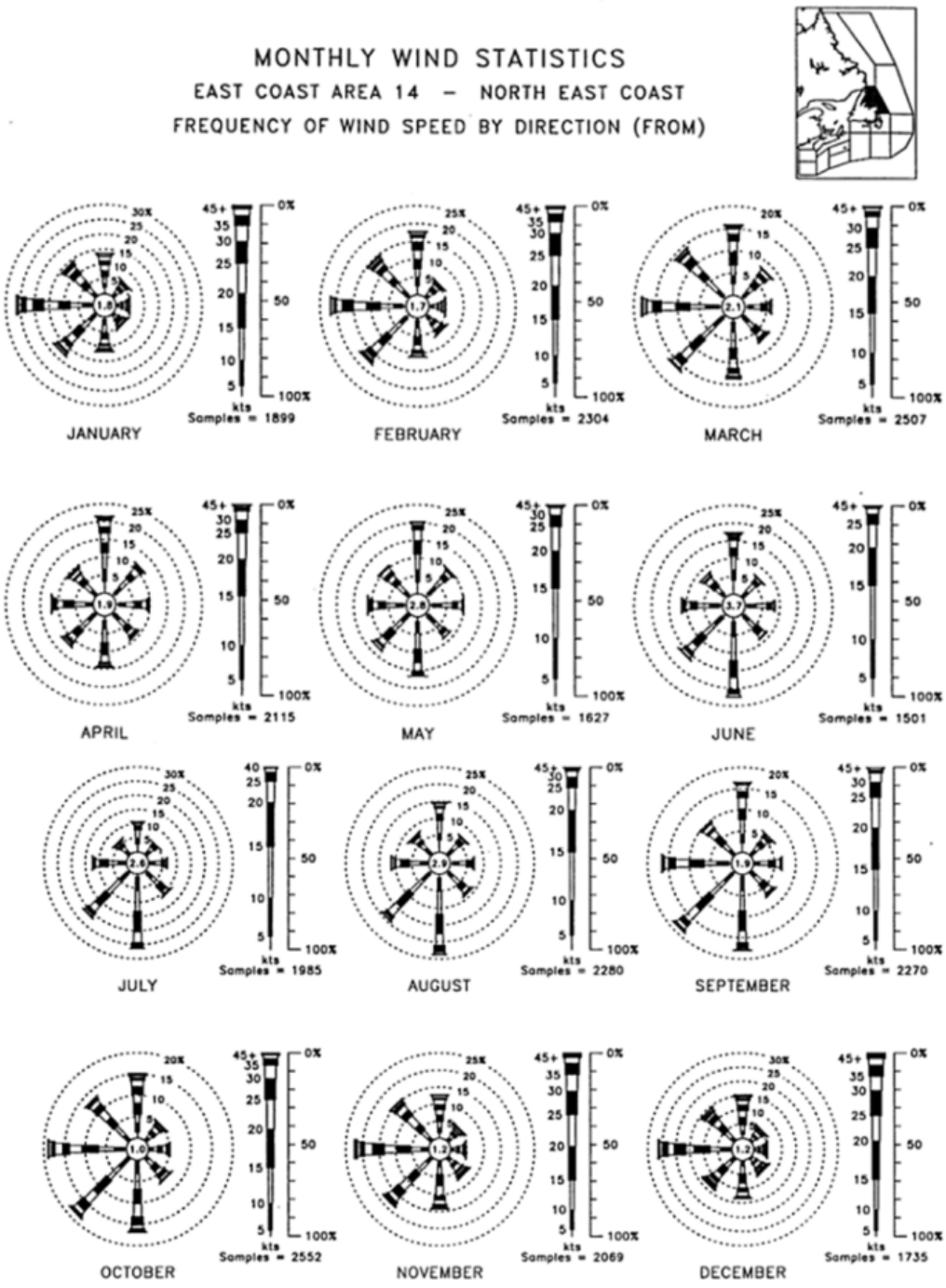
MONTHLY WIND STATISTICS
EAST COAST AREA 14 – NORTH EAST COAST
FREQUENCY OF WIND SPEED BY DIRECTION (FROM)
JANUARY
Samples = 1899
FEBRUARY
Samples = 2304
MARCH
Samples = 2507
APRIL
Samples = 2115
MAY
Samples = 1627
JUNE
Samples = 1501
JULY
Samples = 1985
AUGUST
Samples = 2280
SEPTEMBER
Samples = 2270
OCTOBER
Samples = 2552
NOVEMBER
Samples = 2069
DECEMBER
Samples = 1735
kts

Newfoundland – Gulf of St. Lawrence area

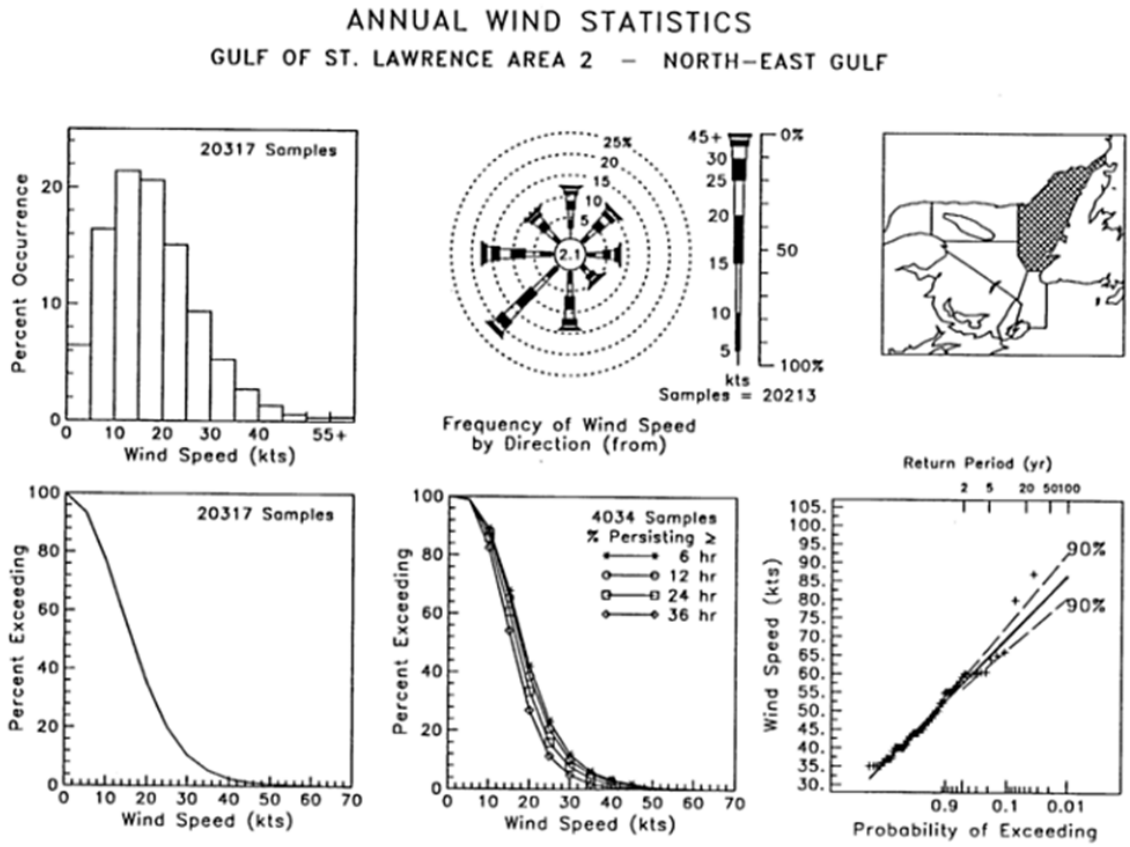

MONTHLY WIND STATISTICS

GULF OF ST. LAWRENCE AREA 2 – NORTH–EAST GULF

FREQUENCY OF WIND SPEED BY DIRECTION (FROM)